学位論文

Studies on the kidney function in cartilaginous fish by mapping of membrane transporting proteins

（膜輸送タンパク質のマッピングによる軟骨魚類腎機能に関する研究）

平成 27 年 12 月博士（理学）申請

東京大学大学院理学系研究科

生物科学専攻

長谷川　久美

Abstract

The ocean is a high-salt and high-osmolality environment, and adaptation strategies adopted by marine organisms can be categorized into three groups depending on the composition of their body fluids: 'osmotic and ionic conformer', 'osmotic and ionic regulator' and 'ionic regulator but osmotic conformer'. The third strategy is also known as 'urea-based osmoregulation' adopted by most cartilaginous fish (sharks, skates, rays and chimaeras). They maintain plasma NaCl concentration at approximately half of SW, while they retain a high concentration of urea to keep their plasma slightly hyperosmotic to the surrounding SW. Therefore, they are prevented from dehydration even in the SW environment.

Kidney is one of the most important organs for the unique osmoregulation of cartilaginous fish. The nephron of cartilaginous fish has a complicated structure compared to other vertebrates. The precise mechanisms of nephron function still remain to be clarified. The final aim of my study is to deduce how urine is produced in cartilaginous fish. To achieve this, I tried to determine the functions of each tubular segment of the nephron by mapping of membrane transporting molecules. I chose the holocephalan elephant fish (*Callorhinchus milii*) as a model fish, because elephant fish is one of the few species of cartilaginous fish with genome sequence data.

This thesis is comprised of two chapters. In chapter 1, I focused on the excretion of excess materials, SO_4^{2-} that is contained at high concentration in seawater. In chapter 2, I investigated on reabsorption of urea, a key molecule of cartilaginous fish osmoregulation. In chapter 1, I first determined the cDNA sequences encoding solute carrier family 26, member 1 (Slc26a1) and member 6 (Slc26a6), which are important SO_4^{2-} transporters reported in the mammalian and teleost kidneys. Elephant fish Slc26a1 (cmSlc26a1) and cmSlc26a6 mRNAs were co-expressed in the proximal II (PII) segment of the nephron, which comprises the second loop in the sinus zone. Results of functional analyses using *Xenopus* oocytes and of immunohistochemistry revealed that cmSlc26a1 is a basolateral electroneutral SO_4^{2-} transporter, while cmSlc26a6 is an apical electrogenic Cl^-/SO_4^{2-}

exchanger. In addition, I found that SO_4^{2-} was highly concentrated in a bladder-like structure in elephant fish embryos. Both cmSlc26a1 and cmSlc26a6 mRNAs were abundantly expressed in the kidney of embryos. These results suggest that the PII segment of the nephron contributes to the secretion of excess SO_4^{2-} in the kidney of elephant fish. Possible mechanisms for SO_4^{2-} secretion in the PII segment are discussed in this chapter.

Previous studies implied that urea is reabsorbed from the collecting tubule via a facilitative urea transporter. I therefore predicted that a low-urea environment must be generated around the collecting tubule for passive urea reabsorption. In chapter 2, to identify water reabsorption segment involved in the generation of a low-urea environment, I searched for all possible water channel aquaporins (AQPs) available at present in the database. Eleven putative AQPs were found in the elephant fish genome database and five AQPs (AQP1, 3-1, 3-2, 4 and 10-1) were abundantly expressed in the kidney. Among them, cmAQP4 mRNA was highly expressed in the basolateral membranes of the tubules in the bundle zone. Results of functional analysis using *Xenopus* oocytes showed that cmAQP4 is a mercury insensitive water channel. The 3-D reconstruction of the cmAQP4-immunoreactive tubules revealed that cmAQP4 is intensely localized in the descending and ascending limbs of the first loop, and weakly expressed in the collecting tubule. These results implied that the first loop and the collecting tubule are segments for water reabsorption, which create a low-urea environment around the collecting tubule. An updated model for urea reabsorption is discussed in this chapter.

In the last part of this thesis, I depict a whole picture of the urine production in cartilaginous fish kidney. The function of cartilaginous fish kidney is discussed from the viewpoints of comparative anatomy and comparative physiology, by comparing with other vertebrates inhabiting diverse aquatic and terrestrial environments.

Contents

General Introduction

For all living organisms, maintenance of body fluids at a stable condition is essential for their life. Volume and concentrations of solutes in their body fluids are thus maintained within rather narrow ranges, irrespective of diverse habitats on the earth, such as in ocean, fresh waters, and in land. Living organisms have developed and adopted diverse adaptation strategies even in the same environment.

The ocean covers 70 % of the surface of the earth, and is a high-salt and high-osmolality environment. Adaptation strategies of marine organisms can be categorized into three groups according to the composition of the body fluids. The first group is 'osmotic and ionic conformers' and their plasma osmolality and ionic composition are almost the same as that of seawater (SW) (Marshall and Grosell 2006). This group includes marine invertebrates and hagfish. Another strategy of SW adaptation is 'osmotic and ionic regulator' as represented by ray-finned fish. They maintain their body fluid concentration approximately one-third that of SW regardless of environmental salinities. They excrete excess ions from the gills and kidney, and obtain water by drinking SW (Marshall and Grosell 2006).

The third strategy is a urea-based osmoregulation represented by cartilaginous fishes (sharks, skates, rays and chimaeras). They regulate plasma NaCl concentration to a level approximately half that of SW, while they store high concentrations of nitrogenous compounds, such as urea and methylamine, as osmolytes to increase their plasma osmolality (Smith 1929). As a result, their body fluid is slightly hyperosmotic to the surrounding SW. Therefore, they are not dehydrated even in the high-salinity marine environment; rather absorbing water into the body due to the slight osmotic gradient. They can be called 'ionic regulator but osmotic conformer'. Although this ureosmotic strategy was considered to be unique in cartilaginous fish, it is known that coelacanths also possesses urea-based osmoregulation (Griffith et al. 1974). In tetrapods, the crab-eating frog can survive in brackish or marine environment by accumulating urea in the body (Gordon et al. 1961). Although mammals do not accumulate urea in plasma, the

mammalian kidney accumulates urea in the inner medulla, resulting in a high osmolality to help reabsorption of water from glomerular filtrate. Therefore, 'water retention by accumulating urea' is considered to be a widely adopted strategy in vertebrates.

Osmoregulatory organs of cartilaginous fish

In urea-based osmoregulation, various osmoregulatory organs, such as the rectal gland, gill, and kidney, work in harmony in the cartilaginous fish body. The rectal gland is a specialized salt-secreting organ, which secretes Na^+ and Cl^- actively against concentration gradients (Burger and Hess 1960). Rectal gland secretes a fluid nearly iso-osmotic to plasma; the concentration of Na^+ and Cl^- in the secretion is approximately twice to that in plasma, while the concentration of urea in the secretion is twenty times lower than that in plasma. In elephant fish (*Callorhinchus milii*) and other chimaeras, a discrete rectal gland was not observed. Instead, unique tubular structures were embedded in the wall of the post-valvular intestine, and it was shown that these structures are the equivalent of rectal gland in elasmobranchs (Leydig 1851; Crofts 1925; Fange and Fugelli 1963; Lagios and Stasko-Concannon 1979; Hyodo et al. 2007). On the other hand, gills of marine cartilaginous fish do not appear to contribute to NaCl secretion (Shuttleworth 1988; Tresguerres et al. 2004; Choe et al. 2007), unlike the marine teleost gills that excrete excess Na^+ and Cl^- via ionocytes. Rather, the gills of cartilaginous fish are considered to be involved in the regulation of acid-base balance. The gill has a large surface area with a huge concentration gradient of urea between internal and external environments. To avoid urea loss from the body, cartilaginous fish gills have low permeability to urea (Boylan 1967; Wood et al. 1995; Pärt et al. 1998; Walsh and Smith 2001).

Kidney: an important organ for urea-based osmoregulation in cartilaginous fish

The major function of kidney is excretion of waste product via urine, such as nitrogenous waste products. In freshwater teleosts, excretion of excess water is an

important function of the kidney. The production of urine is basically accomplished by three steps: filtration, reabsorption, and secretion. Ultrafiltration takes place at the renal corpuscle and filters small molecules (molecular weight: <70000) from the blood to produce a primary urine (glomerular filtrate). Then, while the fluid passing through the renal tubules, reabsorption of vital molecules from the filtrate occurs. Kidneys of most vertebrates, including mammals, teleosts, and cartilaginous fish, share these common characteristics, but variations in morphological and functional features exist depending on lineages and their habitats. For instance, marine teleosts cannot produce concentrated urine that is hyperosmotic to plasma. To avoid loss of water, the glomerular filtration rate of marine teleost kidneys is considerably lower than that of freshwater teleost kidneys (Hickman and Trump 1969; Brown and Dantzler 1997; Baustian and Beyenbach 1999). Some species of marine teleosts, such as toadfish and pipefish, have lost the renal corpuscle, and thereby they lack glomerular filtration (Beyenbach and Liu 1996; Beyenbach 2004). Excretion of excess divalent ions is the major function of the marine teleost kidneys.

Urea retention is one of the most important roles in the cartilaginous fish kidney. Although urea is freely filtered by the glomerulus, more than 90% of filtered urea is reabsorbed from the filtrate to the circulation (Clarke and Smith 1932; Kempton 1953). Thus, renal urea loss accounts for only 4 to 20% of total urea loss. Perhaps reflecting its important function, the nephron of cartilaginous fish kidney shows a complicated structure among vertebrates. The kidney of cartilaginous fish consists of multiple lobules, and each lobule is separated into two regions, a sinus zone and a bundle zone (Lacy and Reale 1985b). A single nephron traverses repeatedly between the two zones and has an elaborate four-loop configuration, and consists of at least 10 morphologically distinguishable segments (Fig. I, Lacy and Reale 1985a; Hentschel et al. 1998; Kakumura et al. 2015). In the bundle zone, the resulting five tubules of a single nephron are enclosed in a sac-like peritubular sheath. The cells composing the sheath are connected to each

other by tight junctions, suggesting that the sheath acts as a barrier separating the microenvironment inside the sheath from the outside (Lacy and Reale 1986). Furthermore, Hentschel et al. (1998) described a single lymph capillary-like central vessel. The central vessel originates as a few blind-ended branches at the distal end of the bundle, runs along the entire bundle, and merges with the large venous sinusoid capillaries of the renal portal system (Hentschel et al. 1998).

Although a mechanism for urea reabsorption has not been clarified yet in the cartilaginous fish kidney, the above anatomical features have been considered essential in the urea reabsorption. Anatomical evidence was observed in the kidney of stenohaline river stingray (family Potamotrygonidae) of Rio Negro in the Amazon. Unlike the four-loop nephron, the nephron of freshwater stingrays has only two loops and lacks the structures found in the bundle zone of marine cartilaginous fish kidney (Lacy et al. 1989). Coincidently, freshwater stingrays do not retain urea in their plasma (Wood et al. 2002), suggesting that the complicated kidney structure of marine cartilaginous fish is involved in the urea reabsorption.

Mapping of membrane transporting proteins

To understand the function of each nephron segment, renal micropuncture and microperfusion studies were performed (Schmidt-Nielsen et al. 1966; Deetjen et al. 1972; Schmidt-Nielsen et al. 1972; Stolte et al. 1977; Friedman and Hebert 1990). In spiny dogfish (*Squalus acanthias*), urea concentrations of fluid obtained from various puncture sites along the proximal tubule were not significantly different from those of plasma (Schmidt-Nielsen et al. 1966). Deetjen et al. (1972) indicates that the urea concentration in the tubular fluid flowing into the collecting duct has already reached a low concentration for excretion. These studies suggest that segment(s) contributing to urea reabsorption exist in the distal tubule. The third loop has been considered to be a segment for NaCl reabsorption as result of microperfusion of the third loop showed high rates of

Cl^- absorption in spiny dogfish. Furosemide, an inhibitor of Na^+-K^+-$2Cl^-$ cotransporter (NKCC), abolished the Cl^- absorption when added to the luminal perfusate (Friedman and Hebert 1990). Electrophysiological properties of the third loop imply that the NaCl absorption is NKCC2-dependent, which is similar to those observed in the mammalian diluting segment (Hebert and Friedman 1990). These physiological methods, however, have limitation to determine detailed characteristics of each nephron segment due to the complicated anatomical and morphological features as described above.

Recently, a growing body of information has been accumulated on the membrane transporting molecules. The distribution patterns of membrane transporters provide valuable information on the transcellular movement of small molecules including water, ions and urea. Mapping of membrane transporters has become one of the important techniques to reveal the function of nephron segments in cartilaginous fish (Swenson et al. 1994; Biemesderfer et al. 1996; Hyodo et al. 2004; 2014; Althoff et al. 2006; Kakumura et al. 2009; 2015; Yamaguchi et al. 2009; Nakada et al. 2010; Cutler et al. 2012a; 2012b; Li et al. 2013). Regarding urea reabsorption, facilitative urea transporter (UT), which shares high homology to mammalian UT-A2, has been identified in several cartilaginous fish species including spiny dogfish (Smith and Wright 1999), Atlantic stingray (*Dasyatis sabina*) (Janech et al. 2003; 2006), little skate (*Raja erinacea*) (Morgan et al. 2003), houndshark (*Triakis scyllium*) (Hyodo et al. 2004), and elephant fish (Kakumura et al. 2009). In houndshark and elephant fish, the UT protein is localized in both apical and basolateral membranes of the collecting tubule, which is the final segment of the nephron (Hyodo et al. 2004; Kakumura et al. 2015). Furthermore, salinity acclimation significantly changed the cellular distribution of UT protein in the apical membrane of the collecting tubule in houndshark (Yamaguchi et al. 2009). The collecting tubule is thus considered to be important for urea reabsorption in cartilaginous fish kidney.

Elephant fish as a research model

Limited genome and transcriptome information has hindered progress in molecular physiological studies in cartilaginous fish, when compared to mammals and teleosts. The major impediment to the genome and transcriptome analyses in cartilaginous fish is the large size of their genomes. For instance, spiny dogfish, nurse shark (*Ginglystoma cirratum*), horn shark (*Heterodontus francisi*), and little skate, which are all popular species for biological researches, have genome sizes that range from 3,500 to 7,000 Mb (Schwartz and Maddock 2002). Among cartilaginous fish, elephant fish is known to have a small genome size relatively (Venkatesh et al. 2005). Because of this reason, Venkatesh et al. (2007; 2014) started a genome project, and now elephant fish is the only species of cartilaginous fish with a well-assembled genome database.

The natural habitats of *C. milii* are on the continental shelves of southern Australia and New Zealand. During the spawning season (autumn in the Southern Hemisphere), mature adult fish migrate into large estuaries and inshore bays to lay eggs. In collaboration with Deakin University and University of Tasmania, Australia, the Laboratory of Physiology at Atmosphere and Ocean Research Institute (AORI) has established an experimental system for elephant fish using adult fish and developmental embryos in captive condition (Hyodo et al. 2007; Kakumura et al. 2009; 2015; Takagi et al. 2012; 2014). With these advantages, elephant fish has become an excellent experimental model to investigate kidney function by mapping of membrane transporter proteins on the nephron.

'Secretion' and 'reabsorption' in the cartilaginous fish nephron

The concentrations of divalent ions, such as Mg^{2+} and SO_4^{2-}, in SW is >40-fold higher than those in plasma of marine teleosts. To avoid hypermagnesemia and hypersulfatemia, marine teleosts concentrate divalent ions in the kidney to excrete them into the urine. It is now known that excretion of divalent ions is accomplished by a "secretion" process in the renal tubule, in addition to the filtration by the glomerulus. The molecular mechanisms

of divalent ion secretion have been investigated in some teleosts. In mammals, Slc26 family is known as sulfate transporters (Alper and Sharma 2013). Katoh et al. (2006) identified Slc26a1 gene expression in the proximal tubule of SW-acclimated rainbow trout. Kato et al. (2009) identified another Slc26 protein, Slc26a6A, in the proximal tubule of pufferfish (*Takifugu obscurus*) nephron. Furthermore, Watanabe and Takei (2011) found that multiple Slc26a6 proteins are localized in the proximal tubule, and that their expressions are dynamically regulated during the transfer from FW (low SO_4^{2-}) to SW (high SO_4^{2-}) environments. In pufferfish, a Mg^{2+} transporter, Slc41a1, was discovered to be localized in intracellular vacuoles of the proximal tubule, and this implies vesicular Mg^{2+} accumulation and excretion (Islam et al. 2013). Furthermore, the cyclin M 3 (Cnnm3), which is homologous to the bacterial Mg^{2+} and Co^{2+} efflux protein, CorC (Gibson et al. 1991; Wang et al. 2003; 2004), is involved in paracellular Mg^{2+} excretion by the proximal tubule (Islam et al. 2014). Taken together, it is likely that the proximal tubule is involved in divalent ion secretion in teleost kidneys.

Concentrations of Mg^{2+} and SO_4^{2-} in urine were higher than those in plasma in cartilaginous fishes. A micropuncture study suggested that secretion of divalent ions occurred in the second loop of nephron (Stolte et al. 1977). These results suggest that a "secretory" segment(s) is present in the four-loop nephron of cartilaginous fish. However, the detailed mechanisms of divalent ion secretion, including the identity of the secretory segment(s), remain unclear in the kidney of cartilaginous fish.

It is reasonable to consider that most segments of the four-loop nephron contribute to "reabsorption" of many valuable molecules, including urea and nutrients. Thus far, the collecting tubule that express the facilitative UT was considered to be a segment for urea reabsorption (Hyodo et al. 2004; Kakumura et al. 2015). Early distal tubule has been suggested to be a diluting segment (active reabsorption of NaCl) (Friedman and Hebert 1990; Hebert and Friedman 1990; Kakumura et al. 2015). With respect to the urea reabsorption, the concentration of urea in urine is lower than that in plasma, the

phenomenon suggested that there must be a specific mechanism for 'uphill' transport of urea from the filtrate to the circulation. To achieve this, an existence of secondarily-active transporting system, such as a sodium-coupled urea cotransporter and/or antiporter, was suggested in the cartilaginous fish kidney (Walsh and Smith 2001). However, such sodium-coupled urea transporters have not been discovered in vertebrate kidney. In the collecting tubule, Na^+/K^+-ATPase signal was hardly detected, suggesting that reabsorption of urea in the collecting tubule occurs transcellularly by facilitated diffusion. As described previously, the collecting tubule expressing facilitative UT is wrapped together with the first and third loops by impermeable peritubular sheath in the bundle zone. Based on these anatomical, morphological and molecular evidence, Hyodo et al. (2014) hypothesized a urea reabsorption model in the cartilaginous fish nephron. They predicted the presence of three functionally distinguishable segments in the bundle zone: urea reabsorption, NaCl active reabsorption, and water reabsorption. In this model, 1) high osmotic environment is generated in the peritubular sheath by NaCl active reabsorption and 2) water is reabsorbed from undefined segments to the interstitial fluid in bundle by osmotic gradient. 3) Concentration of urea in the interstitial fluid within the peritubular sheath is lower than that in plasma, and 4) urea is passively reabsorbed from the filtrate in the collecting tubule to the interstitial fluid via the facilitative UT.

Aim of the study

The final goal of my study is to demonstrate the whole picture of urine production in cartilaginous fish. To achieve this, I tried to determine function of each tubular segment of the elephant fish nephron by molecular mapping of membrane transporting molecules.

In **Chapter 1**, I focused on the 'secretory' function. As described previously, excess SO_4^{2-} is secreted from a particular segment of the nephron. I first determined cDNA sequences encoding Slc26a1 and Slc26a6 from the kidney of elephant fish. Elephant fish Slc26a1 (cmSlc26a1) and cmSlc26a6 mRNAs were abundantly expressed in the kidney.

These mRNAs were co-expressed in the proximal II (PII) segment of the nephron, which comprises the second loop in the sinus zone. Functional analyses using *Xenopus* oocytes and the results of immunohistochemistry revealed that cmSlc26a1 is a basolateral electroneutral SO_4^{2-} transporter, while cmSlc26a6 is an apical electrogenic Cl^-/SO_4^{2-} exchanger. I found that the embryo had bladder-like structure filled with urine containing extremely high concentrations of Mg^{2+} and SO_4^{2-}. Both cmSlc26a1 and cmSlc26a6 were abundantly expressed in the kidney of embryos. My results demonstrated that the PII segment of the nephron contributes to the secretion of excess SO_4^{2-} in the kidney of elephant fish.

In **Chapter 2**, I focused on the urea 'reabsorption'. To test the hypothesis for urea reabsorption proposed by Hyodo et al. (2014), I tried to identify the segments for water reabsorption. I searched aquaporin (AQP) genes in the elephant fish genome database and obtained sequences encoding eleven AQP genes, including six AQPs identified previously (Kakumura, 2013). Among the eleven cmAQPs, cmAQP4 was strongly expressed in the segments in the tubular bundle. The tracking of immunoreactive segments revealed that cmAQP4 is located in the first loop and the collecting tubule. Taken together with the information on segments for NaCl and urea reabsorption, I propose a model for urea reabsorption in the elephant fish kidney.

In the **General Discussion**, I discuss the whole picture of urine production in cartilaginous fish kidney, from the viewpoints of vertebrate evolution and adaptation to diverse environments.
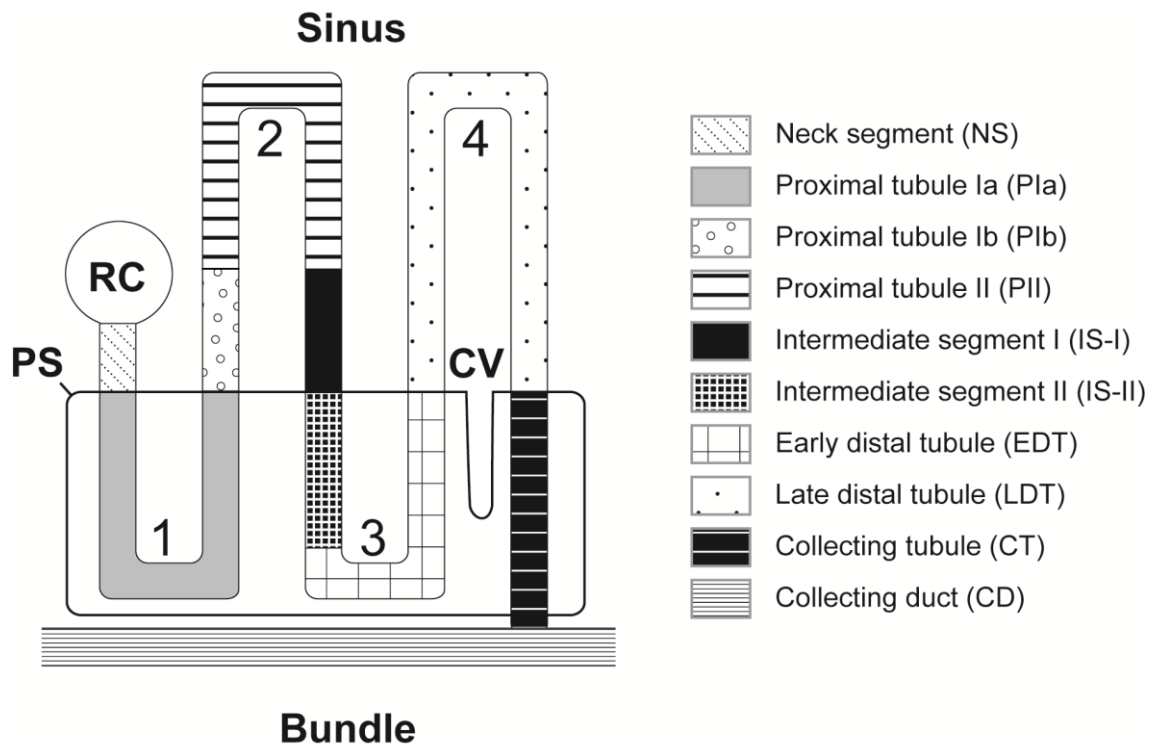
Fig. I. Schematic diagrams of marine cartilaginous fish nephron. CV, central vessel; PS, peritubular sheath; RC, renal corpuscle.

Chapter 1

Sulfate transporters involved in sulfate excretion in the kidney are localized in the renal proximal tubule II of the elephant fish (*Callorhinchus milii*)

Abstract

Most vertebrates, including cartilaginous fishes, maintain their plasma SO_4^{2-} concentration ($[SO_4^{2-}]$) within a narrow range between 0.2-1.0 mM. The kidneys of marine teleost fishes have a major role of excreting SO_4^{2-} to maintain a plasma concentration 40 times less than external seawater. It was known that cartilaginous fishes also excrete excess SO_4^{2-} via the kidney. However, little is known about the underlying mechanisms for SO_4^{2-} regulation in cartilaginous fish, largely due to the extraordinarily elaborate four-loop configuration of the nephron, which consists of at least 10 morphologically distinguishable segments. In Chapter 1, I determined the cDNA sequences encoding solute carrier family 26, member 1 (Slc26a1) and member 6 (Slc26a6), which are SO_4^{2-} transporters reported in mammalian and teleost kidneys, in the kidney of holocephalan elephant fish (*Callorhinchus milii*). Elephant fish Slc26a1 (cmSlc26a1) and cmSlc26a6 mRNAs were co-expressed in the proximal II (PII) segment of the nephron, which comprises the second loop in the sinus zone. Results of functional analyses using *Xenopus* oocytes and immunohistochemistry, revealed that cmSlc26a1 is a basolaterally-located electroneutral SO_4^{2-} transporter, while cmSlc26a6 is an apically-located, electrogenic Cl^-/SO_4^{2-} exchanger. In addition, I found that SO_4^{2-} was highly concentrated in a bladder-like structure of elephant fish embryos. Both cmSlc26a1 and cmSlc26a6 were abundantly expressed in the kidney of embryos. The results demonstrated that the PII segment of the nephron contributes to the secretion of excess SO_4^{2-} in the kidney of elephant fish. Possible mechanisms for SO_4^{2-} secretion in the PII segment are discussed.

Introduction

Sulfate (SO_4^{2-}) is essential for various biological processes including production of highly sulfated proteoglycans by chondrocytes, detoxification of many endogenous and exogenous compounds, and maintenance of cell membranes (Markovich 2001). Most vertebrates maintain the plasma SO_4^{2-} concentration ($[SO_4^{2-}]$) within a narrow range (0.2-1.0 mM), and the kidney plays a pivotal role in SO_4^{2-} homeostasis. Terrestrial and freshwater (FW) habitats are SO_4^{2-}-deficient environments, and the kidneys of mammals and FW-teleost fishes reabsorb SO_4^{2-} from the filtrate in order to retain SO_4^{2-} in the body (Nakada et al. 2005; Markovich and Aronson 2007). In contrast, the $[SO_4^{2-}]$ in seawater (SW) is >40-fold higher than that in the plasma of marine teleost fish. To avoid hypersulfatemia, marine teleost actively excrete SO_4^{2-} via the kidney (Renfro et al. 1999; Pelis and Renfro 2004; Kato et al. 2009), and in stenohaline marine teleosts, SO_4^{2-} secretion from the proximal segment is one of the major roles of the kidney (Beyenbach et al. 1986).

Most cartilaginous fishes (sharks, skates, rays and chimaeras) inhabit a marine environment and a comparison between the composition of plasma and urine revealed that the concentration of divalent ions in the urine (26-182 mM) is 10 to 100 times higher than that in plasma (0.5-8 mM) (Smith 1929; Smith 1931; Burger 1967; Read 1971). This suggests that divalent ions, including SO_4^{2-}, are excreted by the cartilaginous fishes kidney similar to marine teleost fish. However, the complexity of nephron configuration of marine cartilaginous fishes is higher than that of marine teleost fish. The kidneys of marine cartilaginous fishes are divided into a sinus zone and a bundle zone. Each nephron has an elaborate four-loop configuration and traverses repeatedly between the two zones (Lacy and Reale 1985a; Hentschel et al. 1998; Kakumura et al. 2015) and can be divided at least into 10 morphologically distinguishable segments. A micropuncture study showed the existence of a secretory segment of divalent ions in the second loop of the little skate

nephron (Stolte et al. 1977). However, the functional characteristics of these diverse nephron segments are still largely unknown.

Recently a growing body of information has been accumulated on the membrane transporting molecule. The distribution patterns of membrane transporters on the transcellular transport of small molecules such as ions and urea in osmoregulatory organs (Swenson et al. 1994; Biemesderfer et al. 1996; Piermarini et al. 2002; Hyodo et al. 2004; 2007; 2014; Choe et al. 2005; 2007; Althoff et al. 2006; Kakumura et al. 2009; 2015, Yamaguchi et al. 2009; Nakada et al. 2010; Cutler et al. 2012a; 2012b; Takabe et al. 2012; Li et al. 2013). The distal segments and the collecting tubule are important for urea reabsorption shown by the mapping of membrane transporters in the renal tubules of cartilaginous fishes (Hyodo et al. 2004; 2014; Yamaguchi et al. 2009; Kakumura et al. 2015). To clarify the nephron segment involved in the excretion of SO_4^{2-}, I cloned putative SO_4^{2-} transporters solute carrier family 26, member 1 (Slc26a1) and member6 (Slc26a6) from the cartilaginous fish kidney, and examined their SO_4^{2-} transporting activities *in vitro* using a *Xenopus* oocyte expression system. Slc26a1 and Slc26a6 are anion transporters, which belong to the *Slc26* gene family. Ten Slc26 genes have been identified in mammals (Alper and Sharma 2013). Slc26a1 and Slc26a6 proteins were shown to be localized in the proximal tubules of mammalian and marine teleost kidneys, where they play a role in the SO_4^{2-} regulation (Karniski et al. 1998; Knauf et al. 2001; Petrovic et al. 2003; Nakada et al. 2005; Katoh et al. 2006; Kato et al. 2009; Watanabe and Takei 2011). I chose the holocephalan elephant fish (elephant shark, *Callorhinchus milii*) as a model cartilaginous fish, as its genome sequence is available (Venkatesh et al. 2007; 2014). I found that the proximal II segment of the second loop is most probably the position contributing to the SO_4^{2-} secretion in the elaborate cartilaginous fish nephron. In addition, Slc26a1 and Slc26a6 mRNAs were expressed in the kidney of embryos; urine containing high concentrations of Mg^{2+} and SO_4^{2-} was found in a bladder-like structure.

Materials and methods

Adult fish and embryos

Elephant fish (*Callorhinchus milii*; Bory de Saint-Vincent, 1823) of both sexes were collected in Western Port Bay, Victoria, Australia, using recreational fishing equipment, and transported to Primary Industries Research Victoria, Queenscliff, using a fish transporter. The fish were kept in a 10,000 l round tank with running seawater (SW) under a natural photoperiod for at least three days before sampling (Hyodo et al. 2007). To obtain developing embryos, mature female fish were kept in 10,000 l round tanks under a natural photoperiod from March to May, and fed daily with frozen pilchard. During that period, newly laid eggs were collected from the tanks, and maintained in 1,000 l tanks with running SW. Embryos at stage 36 of the development were sampled at the end of September (Takagi et al 2014). The developmental stages were identified by using an established staging scheme (Didier et al. 1998).

Fish were anaesthetized in 0.1% (w/v) 3-amino benzoic acid ethyl ester (Sigma-Aldrich, St. Louis, MO, USA) before sampling. Blood samples were obtained from the caudal vasculature with a syringe in adult fish or a heparin-coated hematocrit capillary in embryos (Terumo, Tokyo, Japan), and centrifuged at $2,250 \times g$ for 10 min to obtain plasma. Urine that was present in bladder-like structure of stage 36 embryos was collected with a syringe and fine gauge needle. The urine and plasma were stored at $-20°C$. After the fish were sacrificed by decapitation, tissues were dissected out and snap frozen in liquid nitrogen, and kept at $-80°C$ until use. For mRNA and protein localization, tissues were fixed in 4% paraformaldehyde in 0.1 M phosphate buffer (pH 7.4) containing 350 mM urea, or Bouin's solution without acetic acid at $4°C$ for 2 days, and then stored in 70% ethanol at $4°C$. All animal experiments were conducted according to the Guideline for Care and Use of Animals approved by the committees of University of Tokyo and Deakin University.

cDNA cloning

Total RNA was extracted from the kidney with Isogen (Nippon Gene, Toyama, Japan). Two micrograms of total RNA was treated using a TURBO DNA-free kit (Life Technologies, Carlsbad, CA, USA) and reverse-transcribed to first-strand cDNA using High Capacity cDNA Reverse Transcription Kit (Life Technologies), according to the manufacturer's instructions. The amino acid sequences of Slc26a1 and Slc26a6 of frog (*Xenopus laevis*) were used as BLAST queries to search for candidate genes in the Elephant Shark Genome Database (http://esharkgenome.imcb.a-star.edu.sg/). The cDNA sequence encoding the entire open reading frame (ORF) of elephant fish (cm) Slc26a1 (cmSlc26a1) and Slc26a6 (cmSlc26a6) were determined by 3´- and 5´-RACE methods using the SMARTer RACE cDNA Amplification Kit (Clontech, Mountain View, CA, USA), according to the manufacturer's instructions. cDNAs were amplified with high-fidelity KOD-Plus DNA polymerase (Toyobo, Osaka, Japan), ligated into pGEM T-easy (Promega, Madison, WI, USA), and the nucleotide sequence was determined by an automated DNA sequencer (3130*xl* Genetic Analyzer; Life Technologies) and BigDye® Terminator v3.1 Cycle Sequencing Kit (Applied Biosystems, Foster City, CA, USA). All primers used are listed in Table 1-1. The possible conserved domains of cmSlc26a1 and cmSlc26a6 were predicted by online software of InterPro Scan (Jones et al. 2014).

Tissue distribution of cmSlc26a1 and cmSlc26a6 mRNAs

The tissue distribution of cmSlc26a1 and cmSlc26a6 mRNAs was examined by quantitative real-time PCR (qPCR) using a 7900HT Sequence Detection System (Life Technologies) and KAPA SYBR FAST ABI Prism qPCR Kit (Kapa Biosystems, Boston, MA, USA), as previously described in detail (Yamaguchi et al. 2009). Total RNA was extracted from twelve tissues (brain, gill, heart, liver, spleen, pancreas, spiral intestine, kidney, rectal gland, skeletal muscle, gonad and uterus) of four adult fish (two males and two females), and ten tissues (brain, gill, heart, liver, spleen, spiral intestine, kidney, rectal

gland, urinary bladder and skeletal muscle) of six stage 36 embryos using Isogen. To generate a standard curve for mRNA quantification, partial DNA sequences were amplified by PCR with specific primer sets, which were subsequently purified with QIAquick PCR purification kit (Qiagen, Hilden, Germany). The standard DNA were then serially diluted, and used as the known amount of transcript for absolute quantification in qPCR analyses. The copy numbers of the standard DNAs were calculated with BioMath Calculators (http://www.promega.com/techserv/tools/biomath/calc01.htm). For internal controls, elephant fish β-actin (cmACTB, NM_001292743) was used for adult fish. For stage 36 embryos, elephant fish elongation factor 1α (cmEF1α, AB622989) was used, because previous study has demonstrated that the expression level of the β-actin was unstable during development when compared to that of ef 1α in zebrafish (McCurley and Gallard, 2008). Primer sets for qPCR were designed using Primer Express software, and their sequences are shown in Table 1-1.

Molecular phylogenetic analysis

The translated amino acid sequences of cmSlc26a1 and cmSlc26a6 were aligned with those of other vertebrate Slc26 proteins using Clustal W 2.1 program (Thompson et al. 1994). The sequences of Slc26 family proteins were obtained from the DDBJ and Ensembl databases. Molecular phylogenetic trees were constructed by a Bayesian Metropolis coupled Markov chain Monte Carlo method in the MrBayes 3.1.2 program (http://mrbayes.sourceforge.net/). I ran four separate Marcov chains for 1,000,000 generations and sampled them every 100 generations to create a posterior probability distribution of 10,000 trees. The first 2,500 trees were discarded as burn-in before stabilization, and then a 50% majority-rule tree was constructed from the subsequent trees. The reliability of the generated tree was shown by posterior probabilities in the Bayesian analysis.

In situ hybridization

Kidneys fixed in Bouin's solution without acetic acid were dehydrated by serial alcohol/xylene and embedded in Palaplast (McCormick Scientific, Richmond, IL, USA). Serial sections at 6 μm were cut and mounted onto MAS-coated slides (Matsunami Glass, Osaka, Japan). The DNA fragments of cmSlc26a1 (1361 bp), cmSlc26a6 (1383 bp), Na^+-K^+-$2Cl^-$ cotransporter-2 (cmNKCC2 [AB769493], 1337 bp) were amplified by PCR using gene-specific primers listed in Table 1-1, and then purified for the synthesis of cRNA probes, sense and anti-sense, using the digoxigenin (DIG)- Labeling Kit (Roche Applied Science, Mannheim, Germany), according to the manufacturer's protocols. Deparaffinized sections were treated with 5 mg/ml proteinase K (Sigma-Aldrich) in Tris-EDTA buffer [100 mM tris(hydroxymethyl)aminomethane and 50 mM ethylenediaminetetraacetic acid, pH 7.5], post-fixed in 4% paraformaldehyde, and then hybridized with 1 μg/ml DIG-labeled cRNA probes in hybridization buffer [50% formamide, 5 ×Saline Sodium Citrate Buffer (SSC), 40 μg/ml bovine calf thymus DNA] at 58°C for 40 h. After hybridization, sections were washed in $2 \times$ SSC (0.3 M NaCl and 33.3 mM sodium citrate, pH 7.0) for 30 min at room temperature, followed by $1 \times$ SSC for 1 h at 65°C, and finally $0.1 \times$ SSC for 1 h at 65°C. Hybridized probes were detected by immunohistochemical reaction using alkaline phosphatase-conjugated anti-DIG antibody (Roche Applied Science), and hybridization signals were developed with 4-nitro blue tetrazolium chloride (450 mg/ml) and X-phosphate/5-bromo-4-chloro-3-indolyl-phosphate (175 mg/ml) incubation for 16-48 h at room temperature. Stained sections were mounted with Aquamount (BDH Laboratory Supplies, Poole, England). Micrographs were taken using a digital camera (DXM1200; Nikon, Tokyo, Japan) attached to an upright microscope.

Immunohistochemistry

Polypeptides IYIERTEREKPKVK+C of cmSlc26a1 and C+MEQPGSGPEKHTLE of

cmSlc26a6, corresponded to the NH_2- and COOH-terminal of cytoplasmic domains respectively, were synthesized and conjugated to keyhole limpet hemocyanin via the cysteine residue. These conjugated peptides were emulsified with complete Freund's adjuvant and injected into Japanese white rabbits to produce antibodies specific for cmSlc26a1 and cmSlc26a6 (Eurofins Genomics, Tokyo, Japan).

Kidney sections were prepared as described in the previous section. Immunohistochemical staining for cmSlc26a1 and cmSlc26a6 was performed with the avidin-biotin-peroxidase complex kit or *Elite* avidin-biotin-peroxidase complex kit (Vector, Burlingame, CA, USA). After rehydration, tissue sections were incubated sequentially with: (1) 2% normal goat serum in phosphate buffered saline (pH 7.4; PBS-NGS) for 30 min at room temperature, (2) cmSlc26a1 (1:2000) or cmSlc26a6 (1:20000) antiserum diluted with PBS-NGS for 48 h at 4°C, (3) biotinylated, goat anti-rabbit IgG for 30 min at room temperature, (4) avidin-biotin-peroxidase complex for 45 min or 30 min at room temperature, and (5) 0.05% diaminobentizine tetrahydrochloride (Sigma-Aldrich) with 0.01% hydrogen peroxide in 50 mM Tris buffer (pH 7.2) for 10 min at room temperature. The specificity of immunoreactive signals for cmSlc26a1 and cmSlc26a6 was confirmed by preabsorption of antibodies with the synthetic antigens (2.5×10^{-6} M) for 24 h at 4°C prior to incubation. Developed sections were counterstained with haematoxylin.

Measurement of osmolality and ion concentrations

Plasma and urine osmolality was measured using a vapor pressure osmometer (Wescor 5520; Logan, UT, USA). Anions (Cl^- and SO_4^{2-}) in the plasma and urine were measured using ion chromatography (Shimadzu AV10; Kyoto, Japan). Cations (Na^+, Mg^{2+} and Ca^{2+}) were measured by an atomic absorption spectrophotometer (Hitachi 180-50; Tokyo, Japan). Urea concentration was measured using a Wako Urea NB test kit (Wako Pure Chemical Industries, Osaka, Japan).

Characterization of SO$_4^{2-}$ transporting activities of cmSlc26a1 and cmSlc26a6 using [^{35}S]SO$_4^{2-}$

The entire coding regions of cmSlc26a1 and cmSlc26a6 cDNAs were inserted into the pGEMHE *X. laevis* expression vector. The constructs were linearized with *Nhe* I, and cRNAs were transcribed *in vitro* using the T7 mMESSAGE mMACHINE kit (Ambion, Austin, TX, USA). Oocytes were surgically collected from *X. laevis* and incubated for 20 min with shaking in Modified Barth solution (MBS) without calcium [MBS(-); in mM: 88 NaCl, 1 KCl, 2.4 NaHCO$_3$, 0.82 MgSO$_4$, HEPES , pH 7.4], and were manually defolliculated after the treatment with 1 mg/ml collagenase (Sigma-Aldrich). Defolliculated oocytes were incubated in MBS with calcium [MBS(+); in mM: 88 NaCl, 1 KCl, 2.4 NaHCO$_3$, 0.3 Ca(NO$_3$)$_2$, 0.41 CaCl$_2$, 0.82 MgSO$_4$] for 24 h, and then injected with 50 nl of water or cRNA at 1 μg/μl (50 ng/oocyte). The injected oocytes were incubated at 18°C in MBS(+) supplemented with 100 units/ml Penicillin and 10 mg/ml Streptomycin Sulfate for 48-72 h. The incubation medium was changed every 24 h, including the day of the uptake experiment.

On the day of assay, the injected oocytes were incubated in a preincubation buffer (in mM: 94 NaCl, 4.5 KCl, 1.8 CaCl$_2$, 1 MgCl$_2$, 10 HEPES-Tris, and 1 Na$_2$SO$_4$, pH 7.5) for 30 min at 18°C. Oocytes were then placed in one of the following four uptake buffers (Na$^+$ buffer, Cl$^-$-free Na$^+$ buffer, K$^+$ buffer and Cl$^-$-free K$^+$ buffer) containing 10 μCi/ml [^{35}S]Na$_2$SO$_4$ (NEX041H; PerkinElmer, Waltham, MA, USA) for 1 h at 18°C. The composition of each buffer is as follows: Na$^+$ buffer (in mM: 94 NaCl, 4.5 KCl, 1.8 CaCl$_2$, 1 MgCl$_2$, 10 HEPES-Tris, and 1 Na$_2$SO$_4$, pH 7.5), Cl$^-$-free Na$^+$ buffer (in mM: 94 Na-gluconate, 4.5 K-gluconate, 1.8 Ca-gluconate, 1 Mg-gluconate, 10 HEPES-Tris, and 1 Na$_2$SO$_4$, pH 7.5), K$^+$ buffer (in mM: 98.5 KCl, 1.8 CaCl$_2$, 1 MgCl$_2$, 10 HEPES-Tris, and 1 Na$_2$SO$_4$, pH 7.5), and Cl$^-$-free K$^+$ buffer (in mM: 98.5 K-gluconate, 1.8 Ca-gluconate, 1 Mg-gluconate, 10 HEPES-Tris, and 1 Na$_2$SO$_4$, pH 7.5). 4,4'-Diisothiocyanatostilbene-2,2'-disulfonic acid (DIDS; Sigma-Aldrich) at 1 mM was used to inhibit anion exchanger

activities. The uptake was terminated by washing oocytes in ice-cold buffer that they had been incubated in without [^{35}S]Na$_2$SO$_4$. Oocytes were dissolved in 10 % sodium dodecyl sulfate (SDS), and the radioactivity was measured using a liquid scintillation counter (Tri-carb™ 3100 TR; PerkinElmer, MA, USA).

Characterization of cmSlc26a1 and cmSlc26a6 by electrophysiology using Cl$^-$-selective microelectrodes

The cmSlc26a1 and cmSlc26a6 cRNAs were prepared as described above. Defolliculated *X.* oocytes were injected with 50 nl of water or of the cRNA at 0.5 μg/μl (25 ng/oocyte). Oocytes were incubated at 16°C in oocyte recipe 3 (OR3) media (Romero et al. 1998), and examined 3-6 days after injection.

Intracellular free Cl$^-$ concentration was measured as intracellular Cl$^-$ activity (aCl$_i$) using Cl$^-$-selective microelectrodes prepared with Cl$^-$-ionophore I, cocktail A (Fluka Chemical, Ronkonkoma, NY, USA) as described previously (Romero et al. 2000). aCl$_i$ was measured from the difference in potential between the Cl$^-$ electrode and a KCl reference electrode impaled into the oocyte, and membrane potential (V_m) was measured as the difference between the KCl microelectrode and an extracellular calomel. Cl$^-$ electrodes were calibrated using 10 and 100 mM NaCl, followed by a test of the specificity by using 100 mM NaHCO$_3$ and a point calibration in ND96 [in mM: 96 NaCl, 2 KCl, 1 MgCl$_2$, 1.8 CaCl$_2$, and 5 HEPES (pH 7.5)]. For Cl$^-$-free buffer (0Cl-ND96), Cl$^-$ was replaced with gluconate. For solutions containing SO$_4^{2-}$, 10 mM NaCl or Na-gluconate was replaced with 5 mM Na$_2$SO$_4$ and 2.5 mM choline chloride or choline gluconate (Kato et al. 2009).

All *Xenopus* experiments were conducted according to the Guideline for Care and Use of Animals approved by the committees of University of Tokyo and Mayo Clinic College of Medicine.

Statistical analysis

Data are presented as means ± SEM. Data from the radioisotope assay were analyzed by one-way analysis of variance (ANOVA) followed by Tukey-Kramer's multiple comparison test. Unpaired t-tests were used for all other data analysis. *P* values less than 0.05 were considered statistically significant.

Results

Identification of SO$_4^{2-}$ transporters, Slc26a1 and Slc26a6, in elephant fish

Using the amino acid sequences of Slc26a1 and Slc26a6 proteins from frog (*Xenopus laevis*) as queries, I found a number of fragmented sequences that shared high homology to Slc26a1 and Slc26a6 in the elephant fish genome database. Then, cDNA sequences encoding the entire ORF of Slc26a1 and Slc26a6 were cloned. The elephant fish Slc26a1 (cmSlc26a1) and Slc26a6 (cmSlc26a6) mRNAs encoded putative ORFs of 720 and 769 amino acid residues, respectively. Molecular phylogenetic analysis with other vertebrate Slc26 proteins showed that cmSlc26a1 (accession: LC089740) and cmSlc26a6 (accession: LC089741) clustered in the clades of Slc26a1 and Slc26a6, respectively (Fig. 1-1). In teleosts, three Slc26a6 genes (*slc26a6a*, *slc26a6b*, and *slc26a6c*) have been identified and the three Slc26a6 isoforms clustered in the Slc26a6 clade in the teleost lineage (Fig. 1-1). Both cmSlc26a1 and cmSlc26a6 contain 12 putative membrane spanning domains with intracellular amino and carboxyl termini. A Slc26/Sulfate Permease (SulP) transporter domain (PF00916) and a Sulfate Transporter and Ant-Sigma factor antagonist (STAS) domain (PF01740), which are the signature features of the Slc26 transporter family (Alper and Sharma 2013), were found in both cmSlc26a1 and cmSlc26a6.

Tissue distribution of cmSlc26a1 and cmSlc26a6 mRNAs in adult fish

The tissue distribution of cmSlc26a1 and cmSlc26a6 mRNAs was quantitatively examined in four adult elephant fish (Fig. 1-2). The cmSlc26a1 mRNA was almost exclusively expressed in the kidney. The expression of cmSlc26a6 mRNA was also highest in the kidney, but moderate levels of expression were found in the brain, intestine, and gonad.

Functional properties of cmSlc26a1 and cmSlc26a6: radioisotope assay

The SO_4^{2-} transporting activities of cmSlc26a1 and cmSlc26a6 were examined using *Xenopus* oocytes and [^{35}S]-labeled SO_4^{2-} (Fig. 1-3). In response to exposure to Cl$^-$-free Na$^+$ buffer (0 mM Cl$^-$, open bars in Fig. 1-3) containing SO_4^{2-}, the oocytes expressing cmSlc26a6 had significantly higher SO_4^{2-} uptake (405.8 ± 39.1 pmol/oocyte) than water-injected control oocytes (8.2 ± 3.2 pmol/oocyte) (Fig. 1-3A). Exposure to Na$^+$ buffer (100 mM Cl$^-$, black bars in Fig. 1-3) did not induce SO_4^{2-} uptake in the oocytes expressing cmSlc26a6 (1.5 ± 0.1 pmol/oocyte in cmSlc26a6 cRNA-injected oocytes and 1.7 ± 0.3 pmol/oocyte in water-injected oocytes). The observed SO_4^{2-} uptake in the Cl$^-$-free Na$^+$ buffer was abolished (2.1 ± 0.4 pmol/oocyte) by the addition of 1 mM DIDS, an inhibitor for anion transporters (Fig. 1-3A). Depolarization of oocytes by replacing Na$^+$ with K$^+$ in the Cl$^-$-free assay medium resulted in twofold increase in SO_4^{2-} uptake (Cl$^-$-free K$^+$ buffer; 845 ± 131.2 pmol/oocyte) (Fig. 1-3A). K$^+$ depolarization of oocytes moderately increased SO_4^{2-} uptake in the K$^+$ buffer containing 100 mM Cl$^-$, however, the increase was not statistically significant.

Injection of cmSlc26a1 cRNA into oocytes also induced SO_4^{2-} uptake (Fig. 1-3B). In contrast to the results in cmSlc26a6-expressing oocytes, significantly SO_4^{2-} transport was observed when 100 mM Cl$^-$ (black bars in Fig. 1-3) was added in the Na$^+$ buffer (260.8 ± 34.0 pmol/oocyte) (Fig. 1-3B). Exposure to Cl$^-$-free (open bars in Fig. 1-3) Na$^+$ buffer moderately increased SO_4^{2-} uptake (34.9 ± 2.2 pmol/oocyte); however, the level was 7 times lower than that of Na$^+$ buffer. The observed SO_4^{2-} uptake in both assay media was abolished by the addition of 1 mM DIDS. No significant difference was observed in SO_4^{2-} uptake between exposure to Na$^+$ buffer and K$^+$ buffer (Fig. 1-3B).

Functional properties of cmSlc26a1 and cmSlc26a6: electrophysiological assay

The Cl$^-$/SO_4^{2-} exchanging activity was examined by monitoring the intracellular Cl$^-$ activity (aCl$_i$) and membrane potential (V_m) of oocytes in response to exposure to Cl$^-$-free

medium containing SO_4^{2-} (Fig. 1-4). Initial aCl$_i$ values were 47.3 ± 3.2 mM for cmSlc26a6-injected oocytes (n = 10), 45.1 ± 2.7 mM for cmSlc26a1-injectied oocytes (n = 3), and 46.3 ± 4.6 mM for water-injected oocytes (n = 5). Initial V_m values were −30.5 ± 2.6 mV for oocytes expressing cmSlc26a6 (n = 14), −39.1 ± 4.9 mV for oocytes expressing cmSlc26a1 (n = 3), and −50.8 ± 7.9 mV for water-injected oocytes (n = 9). Exposure of 5 mM SO_4^{2-} elicited a moderate hyperpolarization (−18.2 ± 3.7 mV, n = 10, p<0.01) in cmSlc26a6-injected oocytes. In oocytes expressing cmSlc26a6, Cl$^-$ removal from the assay medium reduced aCl$_i$ (−1.03 ± 0.23 mM/min, n = 10, p<0.01, for cmSlc26a6; 0.03 ± 0.03 mM/min, n = 5, for control) and hyperpolarized (−58.4 ± 8.0 mV, n = 10, p<0.01, for cmSlc26a6; −4.1 ± 0.8 mV, n = 5, for control). Reintroduction of Cl$^-$ depolarized and recovered aCl$_i$ to the initial level. Control oocytes did not respond to sequential removal and supplementation of Cl$^-$.

For cmSlc26a1 cRNA-injected oocytes, no change was observed in aCl$_i$ or V_m in response to exposure to SO_4^{2-} containing medium or Cl$^-$-free medium (Fig. 1-4).

In situ hybridization

As described in other marine elasmobranchs, the elephant fish kidney consists of multiple, irregular lobules, and each lobule is separated into two zones, a sinus zone and a bundle zone (Fig. 1-5A). A single nephron makes four loops within the lobule. Beginning at the renal corpuscle, the first and third loops are situated in the bundle zone, and the second and fourth loops are in the sinus zone (Fig. 1-5M). *In situ* hybridization signals of cmSlc26a1 and cmSlc26a6 mRNAs were observed in the sinus zone but not in the bundle zone (Figs. 1-5D and 1-5G). In the sinus zone, two major nephron segments are distinguishable: a proximal II (PII) segment and a late distal tubule (LDT). PII is characterized a relatively large tubular diameter with an extensive brush border on the apical membrane (white arrows in Fig. 1-5B), while the LDT has a relatively small diameter and thin epithelial cells without a brush border on the apical membrane (white

arrowheads in Fig. 1-5B). The hybridization signals of both cmSlc26a1 and cmSlc26a6 mRNAs were detected in the PII segment (black arrows in Figs. 1-5E and 1-5H), but not in the LDT (black arrowheads in Figs. 1-5E and 1-5H). The signal intensity of cmSlc26a1 mRNA was considerably higher than that of cmSlc26a6 mRNA. This difference is consistent with the results of the qPCR experiment, in which the expression level of cmSlc26a1 mRNA in the kidney was about 10 times higher than that of cmSlc26a6 mRNA (Fig. 1-2). For comparison, cmNKCC2 mRNA signal was used for the markers of LDT (black arrowheads in Fig. 1-5K) and the early distal tubule in the bundle zone (Fig. 1-5L) as previously described (Kakumura et al. 2015). No colocalization was observed between the hybridization signals of cmNKCC2 mRNA (black arrowheads) and cmSlc26a1 and cmSlc26a6 mRNAs (black arrows). No signal was observed in the negative controls in which sections were incubated with sense probes (data not shown).

Localization of cmSlc26a1 and cmSlc26a6 by immunohistochemistry

The subcellular localization of cmSlc26a1 and cmSlc26a6 was examined using antisera raised against synthetic polypeptides of the corresponding transporters. Consistent with the *in situ* hybridization results, immunoreactive signals for cmSlc26a1 and cmSlc26a6 were observed in the PII segments of the nephron (arrows in Fig. 1-6). Immunoreactive cmSlc26a1 was found on the basolateral membrane (Fig. 1-6A), while cmSlc26a6 was detected on the apical, brush border membrane (Fig. 1-6C). Preabsorption of the anti-cmSlc26a1 (Fig. 1-6B) and anti-cmSlc26a6 (Fig. 1-6D) sera with the synthetic polypeptides resulted in the disappearance of the immunoreactive signals on the membranes, respectively. Sections treated with pre-immune sera showed no specific signals (data not shown).

Expression in embryos

I discovered a urinary bladder-like structure in the peri-hatching embryos (stage 36

and hatched embryos) of elephant fish, and measured the ion concentrations in the plasma and urine of stage 36 embryos. The plasma concentration of Na^+ in embryos was significantly lower than that in adult fish, while plasma urea concentration was higher in embryos compared to adult fish (Table 1-3). Other plasma parameters in embryos were similar to those of adult fish. The urine osmolality of embryos was nearly equal to the plasma osmolality. However, divalent ions, such as Mg^{2+} and SO_4^{2-} in the embryonic urine were >100 times higher than those in plasma. Although the Ca^{2+} concentration in the embryonic urine was significantly higher than that of plasma, the concentration factor of Ca^{2+} (cf = 3.3) was considerably lower than those of Mg^{2+} (cf = 228) and SO_4^{2-} (cf = 194). The concentrations of monovalent ions, Na^+ and Cl^-, in the urine of embryos were significantly lower than those in plasma.

Quantitative real-time PCR showed that cmSlc26a1 and cmSlc26a6 mRNAs were abundantly expressed in the kidney of embryos (Fig. 1-7). Furthermore, the tissue distribution pattern of cmSlc26a1 and cmSlc26a6 mRNAs in embryos (Fig. 1-7) was similar to that in adult fish (Fig. 1-2).

Discussion

Since seawater is a SO_4^{2-}-rich environment, marine fishes excrete SO_4^{2-} with their kidneys to avoid hypersulfatemia. In Chapter 1, I determined cDNA sequences encoding ORF of SO_4^{2-} transporters, Slc26a1 and Slc26a6, from the kidney of holocephalan elephant fish (*Callorhinchus milii*). Results of functional and immunohistochemical investigations revealed that the cmSlc26a1 is a basolateral SO_4^{2-} transporter, while the cmSlc26a6 is an electrogenic Cl^-/SO_4^{2-} exchanger on the apical membrane. The cmSlc26a1 and cmSlc26a6 were co-localized in PII segment of the nephron, suggesting that the PII segment is the site for the secretion of excess SO_4^{2-} in the highly elaborated nephron of cartilaginous fish.

cmSlc26a6 is an electrogenic Cl^-/SO_4^{2-} exchanger

In teleosts, three types of Slc26a6 (Slc26a6A, Slc26a6B and Slc26a6C) have been found (Nakada et al. 2005; Kato et al. 2009). The Slc26a6A is expressed only in the seawater (SW) environment, suggesting that Slc26a6A is a candidate for the major apical SO_4^{2-} transporter that mediates SO_4^{2-} secretion in the kidneys of marine teleosts (Kato et al. 2009; Watanabe and Takei 2011). In the eel, Slc26a6A and Slc26a6B were expressed in the separate segments of the proximal tubule (Watanabe and Takei 2011). In elephant fish, however, I found only a single gene encoding Slc26a6 from the genome database. Molecular phylogenetic result revealed that the three Slc26a6 genes were duplicated in the teleost lineage, supporting the finding that only single Slc26a6 gene exists in elephant fish.

The functional features of cmSlc26a6 are highly similar to those of teleost and tetrapod Slc26a6. In mammals and teleosts, Slc26a6 mediates electrogenic exchange of various anions including SO_4^{2-}/Cl^- (Xie et al. 2002; Kato et al. 2009), Cl^-/oxalate, $Cl^- \text{-} OH^-/HCO_3^-$, and electroneutral Cl^-/formate (Alper and Sharma 2013). In the present *in vitro* assay with

radio-labeled SO_4^{2-}, SO_4^{2-} uptake by the oocytes expressing cmSlc26a6 was induced only when Cl^- was removed from the assay medium. The SO_4^{2-} uptake was abolished by the use of Cl^--containing assay buffer or the addition of DIDS, an inhibitor of anion transporter. These results suggest that cmSlc26a6 acts as a Cl^-/SO_4^{2-} exchanger that relies on a Cl^- concentration gradient as the driving force. Furthermore, depolarization of oocytes by replacing Na^+ with K^+ significantly facilitated SO_4^{2-} uptake, suggesting that cmSlc26a6 is an electrogenic SO_4^{2-} transporter. These conclusions were further supported by the electrophysiological data. Specifically, presence and absence of extracellular SO_4^{2-} and Cl^-, respectively, reduced intracellular Cl^- activity and hyperpolarized. These observed characteristics of cmSlc26a6 indicate that SO_4^{2-} is secreted against the concentration gradient by using a negative membrane potential and extracellular Cl^- that act as the driving force.

cmSlc26a1 is an electroneutral SO_4^{2-} transporter

The ion transport characteristic of cmSlc26a1 is distinct from that of cmSlc26a6 as a significant SO_4^{2-} uptake activity was only detected in the presence of Cl^- in the assay buffer. When Cl^- was removed from the assay medium, only a minor SO_4^{2-} uptake was observed. These results imply that cmSlc26a1 is a SO_4^{2-} transporter but not a Cl^-/SO_4^{2-} exchanger, and that Cl^- is required to exert SO_4^{2-} transporting activity. These conclusions were supported by the results of the electrophysiology experiments in which no change was observed in intracellular Cl^- activity in response to exposure to the medium containing SO_4^{2-}, irrespective of Cl^- concentration in the assay medium. A similar effect of extracellular Cl^- on SO_4^{2-} transport was reported in the Slc26a1 of mammals and teleosts (Satoh et al. 1998; Xie et al. 2002; Lee et al. 2003; Regeer et al. 2003; Nakada et al. 2005). In rats, SO_4^{2-} uptake by Slc26a1 expressing oocytes increase only in the presence of extracellular Cl^- (Satoh et al. 1998). However, in mouse and eel, moderate levels of SO_4^{2-} are transported by Slc26a1 even in the absence of extracellular Cl^- (Xie et

al. 2002; Nakada et al. 2005). Other monovalent anions, such as other halides, formate, and lactate, were reported to enhance SO_4^{2-} transport via Slc26a1 (Xie et al. 2002). However, the mechanism of SO_4^{2-} uptake activated by monovalent anions remains unknown.

Depolarization of oocytes had no effect on SO_4^{2-} uptake in the oocytes expressing cmSlc26a1, suggesting that cmSlc26a1 is an electroneutral SO_4^{2-} transporter. In the electrophysiological assay, the result of unchanged membrane potential in oocytes expressing cmSlc26a1 in the presence of extracellular SO_4^{2-} also supports the electroneutral nature of the transporter. Currently, without knowing the exchanged anion or cotransported cation, the mode of SO_4^{2-} transport by cmSlc26a1 is not clarified. In mammalian nephron, earlier studies demonstrated that SO_4^{2-} transport in basolateral membrane vesicles occurs via a SO_4^{2-}/HCO_3^- exchanger (Pritchard and Renfro 1983; Kuo and Aronson 1988). Furthermore, rat Slc26a1 was shown to be localized on the basolateral membrane and functions as an electroneutral $SO_4^{2-}/2HCO_3^-$ or oxalate^{2-}/$2HCO_3^-$ exchanger (Karniski et al. 1998; Krick et al. 2009). Further investigation is needed to clarify the ion(s) exchanged by cmSlc26a1 for SO_4^{2-}.

Identification of the SO_4^{2-} secretory segment in the elephant fish nephron

Elasmobranch kidneys are unusually complicated structures compared to other vertebrate kidneys, as they are comprised of multiple lobules, and each lobule is divided into two zones: a sinus zone and a bundle zone. Each nephron has an elaborate four-loop configuration (Fig. 1-5M) and traverses repeatedly between the two zones (Lacy and Reale 1985b; Hentschel 1987; Kakumura et al. 2015). The *in situ* hybridization experiments of this study revealed that the expression of both cmSlc26a1 and cmSlc26a6 mRNAs was in the sinus zone, but not in the bundle zone. The sinus zone of the elephant fish kidney is mostly comprised of two nephron segments: the PII (the second loop of nephron) and the late distal tubule (LDT; the fourth loop of nephron) (Kakumura et al.

2015). The PII and LDT are easily distinguishable by their morphological characteristics; the PII segment has the largest tubular diameter with an extensive brush border on the apical membrane, while the LDT shows a relatively small diameter and thin epithelial cells without a brush-bordered apical membrane (Lacy and Reale 1985a; Kakumura et al. 2015). The morphological features of the tubule that showed both cmSlc26a1 and cmSlc26a6 mRNA expressions were those of the PII segment and not the LDT. This assessment was further confirmed by the comparison with cmNKCC2 mRNA signals, as a previous research has shown that cmNKCC2 mRNA is expressed in two separate diluting segments: the early distal tubule (EDT) in the bundle zone and the posterior half of the LDT in the sinus zone (Kakumura et al. 2015). A comparison using serial sections clearly showed that the cmSlc26a1 and cmSlc26a6 mRNA hybridization signals did not overlap with the cmNKCC2 signal, suggesting that the PII segment is the secretory segment of SO_4^{2-} in the elephant fish kidney. The present result is consistent with the previous micropuncture study, which showed a secretory segment of divalent ions in the second loop of the little skate nephron (Stolte et al. 1977).

In Figure 1-8, I propose a hypothetical model for the secretion of SO_4^{2-} in the elephant fish kidney. In the PII segment, cmSlc26a1 (an electroneutral SO_4^{2-} transporter) and cmSlc26a6 (an electrogenic Cl^-/SO_4^{2-} exchanger) are localized on the basolateral and apical membranes, respectively (Fig. 1-6A, Fig. 1-6B). A negative membrane potential drives SO_4^{2-} secretion via apically-located cmSlc26a6 into the primary urine. Consistent with my notion, intense Na^+-K^+-ATPase (NKA) signals were detected in several nephron segments including the PII segment in the elephant fish kidney (Kakumura et al. 2015). The resulting decrease in intracellular $[SO_4^{2-}]$ then drives SO_4^{2-} uptake into the PII cells from blood sinus via the basolaterally-located cmSlc26a1. A similar system for SO_4^{2-} secretion was proposed in the proximal tubule of marine teleost fishes (Kato et al. 2009; Watanabe and Takei 2011).

In addition to the negative membrane potential, the concentration gradient for Cl^- is

considered to be an important driving force for SO_4^{2-} secretion via cmSlc26a6. For secretion of SO_4^{2-} into the filtrate via the apically-located cmSlc26a6 to occur, a high concentration of Cl^- in the filtrate is required to facilitate Cl^-/SO_4^{2-} exchange. In this regard, the PII segment is well-located to contribute to SO_4^{2-} secretion for the following reason. In the mammalian kidney, it is well recognized that the apical NKCC2 and the basolateral NKA contribute to active reabsorption of Na^+ and Cl^- in the thick ascending limb of the loop of Henle (Gamba et al. 1994; Hebert et al. 2004). In elephant fish, cmNKA α1 and cmNKCC2 mRNAs were co-expressed in the EDT and posterior half of the LDT, implying that these distal segments contribute to Na^+ and Cl^- reabsorption and the resulting dilution of filtrate (Kakumura et al. 2015). Since the filtrate passes through the PII segment of the nephron prior to the diluting segments, it is highly probable that the concentration of Cl^- is still high in the PII segment, which would facilitate SO_4^{2-} secretion.

In Table 1-4, I estimated a driving force for SO_4^{2-} efflux via cmSlc26a6 as the ratio $[SO_4^{2-}]_{out}/[SO_4^{2-}]_{in}$, following the calculation by Kato and colleagues in SW mefugu (Kato et al. 2009). The calculation was performed using the following equation (Table 1-4).

$$\Delta\mu_{Slc26a6} = \Delta\mu_{Cl-SO4} = \Delta\mu_{Cl} - \Delta\mu_{SO4}$$

$$= RT \times \ln([Cl^-]_{in}/[Cl^-]_{out}) + (-1) \times FV_m -$$

$$\{RT \times \ln([SO_4^{2-}]_{in}/[SO_4^{2-}]_{out}) + (-2) \times FV_m\}$$

where R is the gas constant, T is the absolute temperature, F is the Faraday constant, ln is the natural log, V_m is the membrane potential, and $\Delta\mu_{ion}$ is the electrochemical potential difference (Joules/mole). At the point of equilibrium, the calculated $[SO_4^{2-}]_{out}/[SO_4^{2-}]_{in}$ values are 366.3, 246.5, and 165.9 when V_m is -80, -70, and -60 mV, respectively, under the following assumptions: 1) the stoichiometry of Cl^-/SO_4^{2-} exchange is 1:1; 2) $[Cl^-]_{out}$ is 308.2 mM, which is the plasma $[Cl^-]$ of adult elephant fish; 3) $[Cl^-]_{in}$ is 20 mM, which is similar to the cytosolic $[Cl^-]$ of mammalian proximal tubular cells (Cassola et al. 1983; Ishibashi et al. 1988; Krapf et al. 1988); and 4) the temperature is 293 K (20°C). These values were approximately two-times higher than those calculated for SW mefugu (Kato

et al. 2009). The ratio was >100, even when I assumed a higher cytosolic [Cl^-]. Although it will be necessary to measure the ion concentration profiles of the intracellular fluid of the PII cells and of the filtrate flowing into the PII segment, the estimated values of the driving force suggest that cmSlc26a6 has the ability to secrete SO_4^{2-} under conditions that are relevant to the predicted composition of the fluid in the PII segment.

As mentioned above, the localization of cmSlc26a1 and cmSlc26a6 in the PII segment was similar to that of Slc26a1 and Slc26a6A in the proximal tubule of marine teleost fishes, implying that the mechanisms by which elephant fish secrete SO_4^{2-} is similar to those of teleost fishes. Meanwhile, basolateral Slc26a1 and apical Slc26a6 have also been found in the mammalian proximal tubule (Markovich and Aronson 2007), but in the mammalian kidney, net absorption of SO_4^{2-} occurs. An investigation using Slc26a6-null mice revealed that Slc26a6 is important for Cl^-/base exchange in the apical membrane of the proximal tubule (Wang et al. 2005). Instead of Slc26a6, another apically-located sulfate transporter, Slc13a1, is considered to contribute to SO_4^{2-} reabsorption in the mammalian kidney (Markovich 2012) and in the FW teleost kidney (Nakada et al. 2005; Kato et al. 2009; Watanabe and Takei 2011).

Environmental adaptation during development is an important research in the field of animal homeostasis (Kaneko et al. 2008). In oviparous cartilaginous fish, including elephant fish, the embryos are enclosed in a tough and fibrous egg capsule in SW for the entire developmental period (~6 months). Although the egg capsule is important for protection from predation, it does not separate the intracapsular ionic environment from that of the external SW. Previous study demonstrated that the osmolality and ionic composition of the egg capsule fluid are similar to those of SW throughout the development of elephant fish (Takagi et al. 2014). Despite these findings, I found that the concentration of plasma Mg^{2+} and SO_4^{2-} of embryos were maintained at levels 10 times lower than those of SW (Mg^{2+}, 50 mM; SO_4^{2-}, 30 mM), implying that embryos, like adult

fish, must regulate plasma Mg^{2+} and SO_4^{2-}. In addition, I discovered a urinary bladder-like structure in the peri-hatching embryos (this study) which contained highly concentrated $MgSO_4$. Interestingly, Mg^{2+} and SO_4^{2-} concentrations in the urine (Mg^{2+}, 396.4 ± 17.7 mM; SO_4^{2-}, 310.3 ± 9.3 mM) were more than 100 times higher than those of plasma (Mg^{2+}, 1.3 ± 0.1 mM; SO_4^{2-}, 1.6 ± 0.1 mM). The concentration of Ca^{2+} in the urine (12.8 ± 1.9 mM) was also higher than that in the plasma of embryos (3.9 ± 0.1 mM), but the concentration factor for Ca^{2+} was much lower than that of Mg^{2+} and SO_4^{2-}, suggesting an existence of particular mechanism for excretion of Mg^{2+} and SO_4^{2-}. Given I found that the kidney of elephant fish embryos were expressing cmSlc26a1 and cmSlc26a6 mRNA, the tubular secretion of SO_4^{2-} may already be functional in embryos.

Perspectives and Significance

In the 1960s, it was described that the cartilaginous fish nephron had an extraordinarily, elaborate four-loop configuration (Borghese 1966). However, over the past half a century, the precise mechanisms of nephron function have not been clarified, largely due to the complex architecture of the kidney. To further our understanding on the functioning of the cartilaginous fish kidney, detailed mapping of some membrane transporters was carried out in the nephron of the elephant fish. This molecular anatomical approach has revealed the possible functions of each nephron segment, including urea reabsorption, NaCl reabsorption, glucose reabsorption, and urea synthesis (Hyodo et al. 2014; Kakumura et al. 2015). I have further shown that the PII in the sinus zone of the elephant fish kidney is important for excretion of SO_4^{2-}. Future research will ascertain if the PII segment is also important in the secretion of other divalent ions such as Mg^{2+} (Islam et al. 2013; 2014).

In euryhaline teleost fish, the kidneys switch their role of SO_4^{2-} homeostasis from reabsorption to excretion, depending on the salinities of their habitats (Watanabe and Takei 2011). Although most cartilaginous fishes inhabit marine environments, some

cartilaginous fish, e.g., bull shark and Atlantic stingray, are euryhaline. Thus, it would be interesting in future investigations to consider the role of the kidney in divalent ion homeostasis in the euryhaline cartilaginous fish species.

Table 1-1. Primer sets used in the present study

Primers for 5'-RACE		
Gene name	Primer sequence 5' to 3'	
cmSlc26a1	AS	CAAGGCAACTGCAATACTAGC
cmSlc26a6	AS	CCCGAATGTAAAGTAAATCAGC
Primers for 3'-RACE		
cmSlc26a1	S	ACAATGAAGTCAGTCCTGAAGG
cmSlc26a6	S	AGATGTCCTCCTCAATTATTGG
Primer sets for cloning		
cmSlc26a1	S	(same with the tissue distribution primer)
	AS	GGTCTGAGAAATCTTAAATGGAAG
cmSlc26a6	S	(same with the tissue distribution primer)
	AS	(same with the tissue distribution primer)
Primer sets for real-time qPCR assay		
cmSlc26a1	S	GGAGAAATCCCCACAGGATTC
	AS	(same with the tissue distribution primer)
cmSlc26a6	S	CTCCACTGCCTGGCGAAA
	AS	AGTGAAGGGTGTCCATTCATGAG
Primer sets for *in situ* hybridization		
cmSlc26a1	S	GAGAAGTGGAACGCCAGTGT
	AS	GTTTTCTTGCATGTTGCCACT
cmSlc26a6	S	(same with the 3'-RACE primer)
	AS	(same with the tissue distribution primer)
Primer sets for radioisotope assay and electrophysiological assay		
cmSlc26a1	S	(same with the tissue distribution primer)
	AS	(same with the cloning primer)
cmSlc26a6	S	(same with the tissue distribution primer)
	AS	(same with the tissue distribution primer)

S and AS mean sense and antisense, respectively.

Table 1-2. The accession numbers of genes used in the analysis

Gene name	Accession number
cmSlc26a1	LC089740
cmSlc26a6	LC089741
Eel Slc26a1	AB111927
Eel Slc26a3	AB111930
Eel Slc26a6A	AB084425
Eel Slc26a6B	AB111928
Eel Slc26a6C	AB111929
Zebrafish Slc26a1	NM_001080667
Zebrafish Slc26a2	XM_680022
Zebrafish Slc26a3	FJ170816
Zebrafish Slc26a4	NM_001165915
Zebrafish Slc26a5	NM_201473
Zebrafish Slc26a6A	ENSDART00000149230
Zebrafish Slc26a6B	ENSDART00000045602
Zebrafish Slc26a6C	FJ170818
Zebrafish Slc26a11	NM_199767
Human Slc26A1	AF297659
Human Slc26a2	U14528
Human Slc26a3	NM_000111
Human Slc26a4	NM_000441
Human Slc26a5	AF523354
Human Slc26a6	AF279265
Human Slc26a7	AF331521
Human Slc26a8	AF331522
Human Slc26a9	AF314958
Human Slc26a11	AF345195
Mouse Slc26a2	NM_007885
Mouse Slc26a4	NM_011867
Mouse Slc26a5	NM_030727
Mouse Slc26a6	NM_134420
Mouse Slc26a7	NM_145947
Mouse Slc26a8	AF403499
Mouse Slc26a9	NM_177243
Mouse Slc26a11	NM_178743
Fugu Slc26a5	AB200327
Fugu Slc26a6A	AB200328
Fugu Slc26a6B	AB200329
Fugu Slc26a6C	AB200330
Fugu Slc26a11	AB200331
Tetraodon Slc26a1	ENSTNIT00000016422

Table 1-3. Plasma and urine parameters in elephant fish embryos and adult.

stage		Na$^+$	Cl$^-$	Ions (mmol L^{-1})			Urea (mmol L^{-1})	Osmolality (mOsm kg^{-1})
				Mg^{2+}	SO$_4^{2-}$	Ca^{2+}		
st.36	plasma	298.7 ± 4.2 (12)*	314.7 ± 8.5 (12)	1.3 ± 0.1 (12)	1.6 ± 0.1 (15)	3.9 ± 0.1 (12)	502.9 ± 7.5 (12)	1048.9 ± 3.1 (12)*
	urine	258.9 ± 43.0 (12)†	123.2 ± 22.9 (15)†	296.4 ± 17.7 (12)†	310.3 ± 9.3 (15)†	12.8 ± 1.9 (12)†	218.6 ± 15.2 (12)†	1055.8 ± 2.3 (12)
adult	plasma	394.0 ± 10.0 (5)‡	308.2 ± 4.3 (5)	2.3 ± 0.4 (5)	2.5 ± 0.4 (5)	3.6 ± 0.1 (5)	448.7 ± 8.8 (5)‡	1073.6 ± 3.4 (5)‡

*Data from Takagi et al. 2014. Values are means ± SEM. †A significant difference was observed between embryo plasma and urine (P <0.05). ‡A significant difference was observed between plasma of embryos and adult fish (P <0.05).

Table 1-4. Calculations of $[SO_4^{2-}]_{out}/[SO_4^{2-}]_{in}$ under various conditions of $[Cl^-]_{in}$, $[Cl^-]_{out}$, and V_m at the equilibria ($\Delta\mu_{cmSlc26a6} = 0$)

V_m (mV)	$[Cl^-]_{in}$ (mM)	$[Cl^-]_{out}$ (mM)	$([SO_4^{2-}]_{out}/[SO_4^{2-}]_{in})$
-50	20	308.2	111.6
-60	20	308.2	165.9
-70	20	308.2	246.5
-80	20	308.2	366.3
-90	20	308.2	544.3
-70	20	308.2	246.5
-70	30	308.2	164.3
-70	40	308.2	123.3
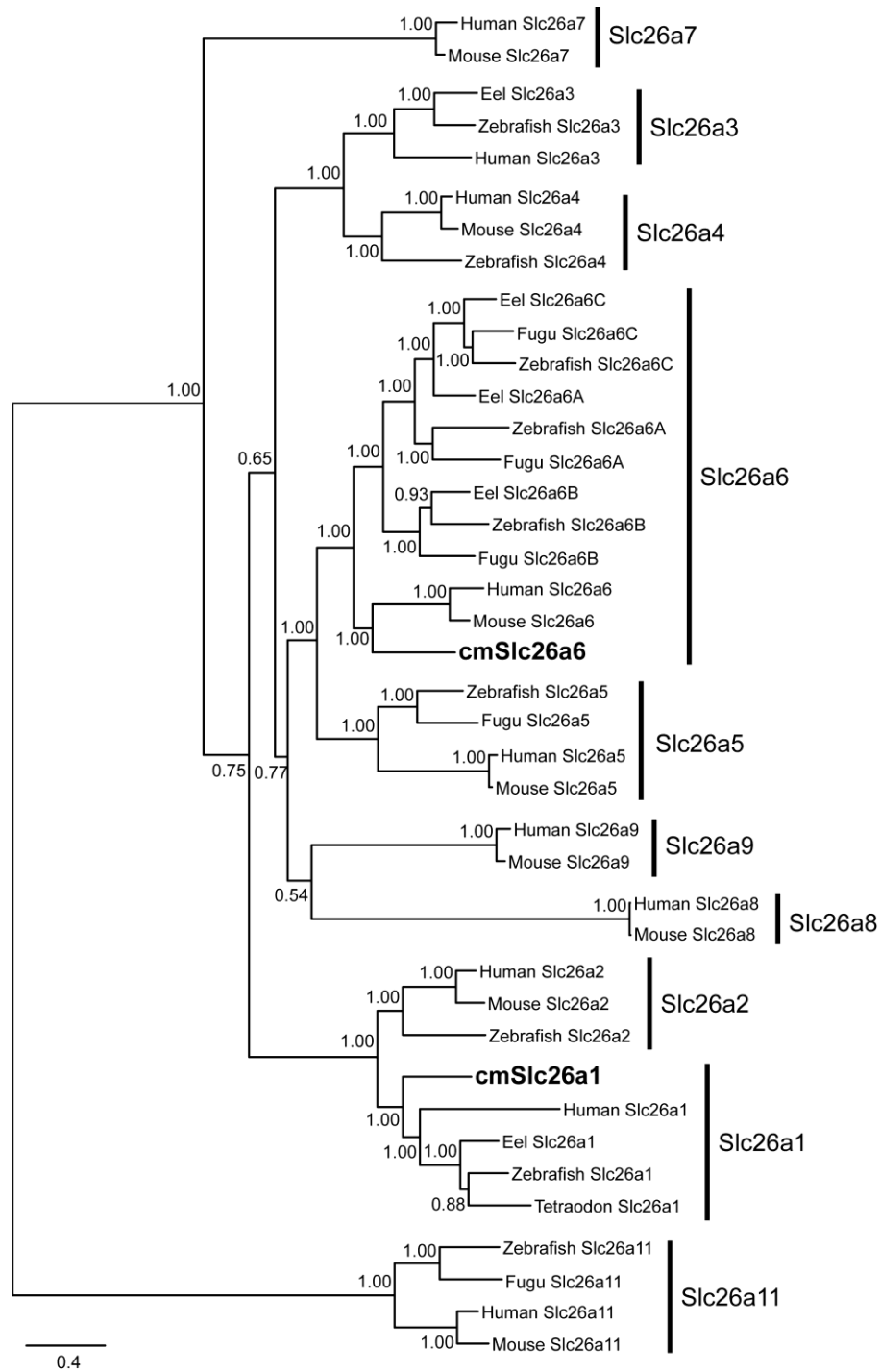
Fig. 1-1. Molecular phylogeny of vertebrate Slc26 family proteins. The elephant fish (holocephalan) sequences identified in Chapter 1 are shown in bold letters with select vertebrates (mammals and teleosts) indicated in normal font. The accession numbers of genes and mRNAs used in the analysis are listed in Table 1-2. Numbers at branch nodes represent Bayesian posterior probabilities.
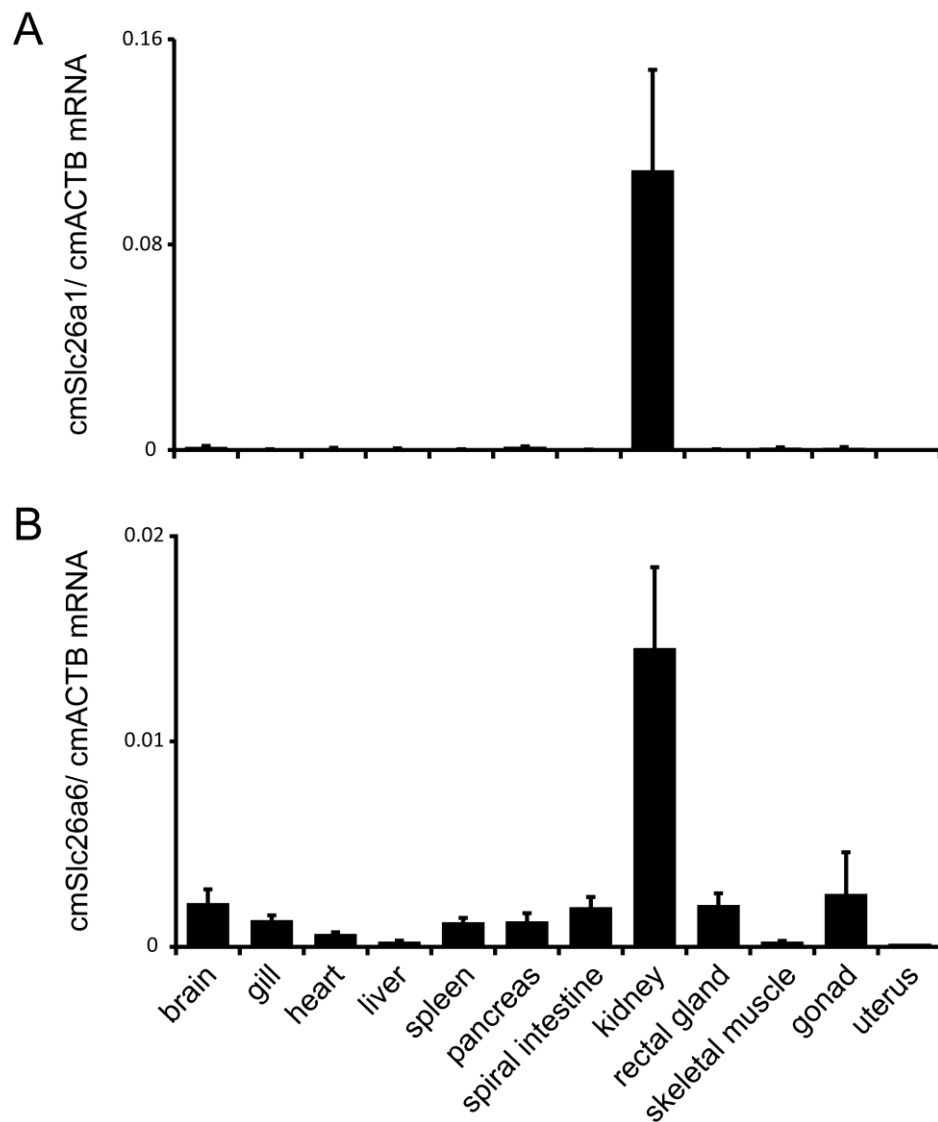
Fig. 1-2. Tissue distribution of mRNAs encoding (A) cmSlc26a1 and (B) cmSlc26a6 in adult elephant fish. Data are presented as means ± SEM. The values were normalized against those of cmACTB mRNA. $n = 4$ (two male and two female) for each tissue analysis, except for uterus which was $n = 2$.
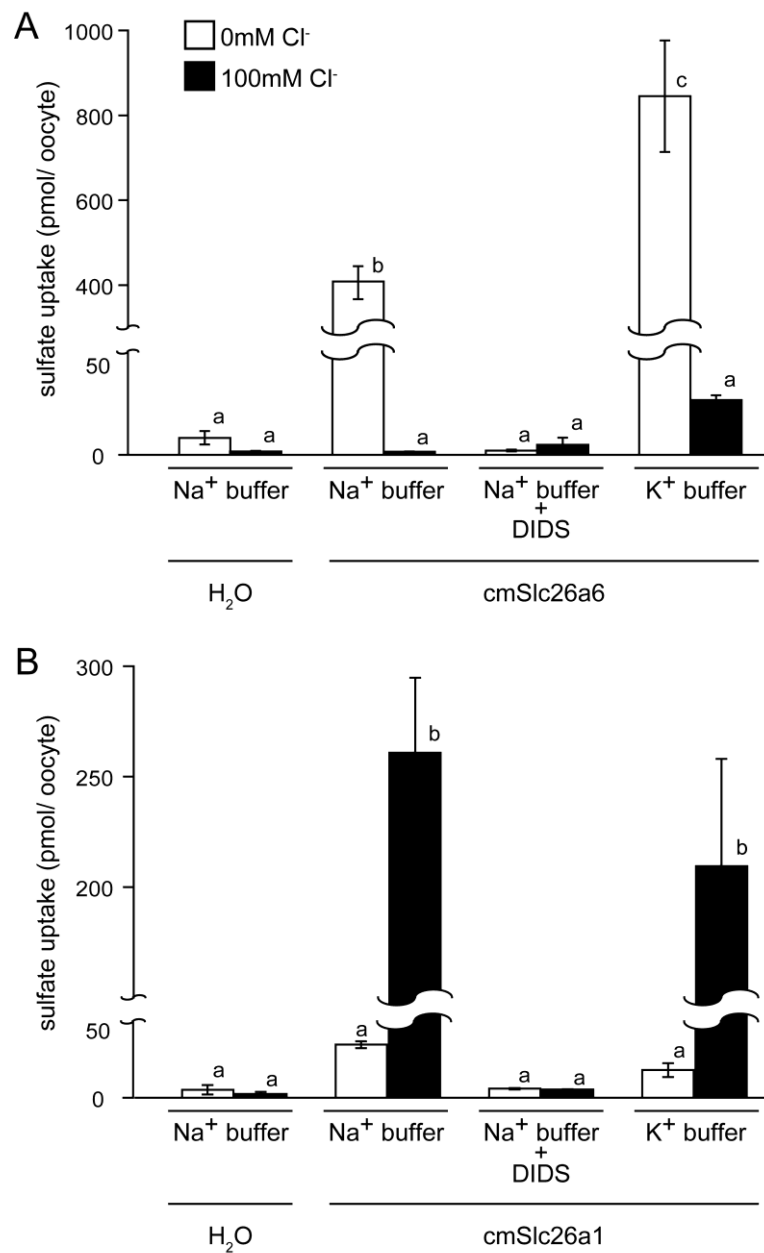
Fig. 1-3. Functional characterization of cmSlc26a1 and cmSlc26a6 using $[^{35}S]SO_4^{2-}$. A: $[^{35}S]SO_4^{2-}$ uptake mediated by water-injected or cmSlc26a6 cRNA-injected oocytes were examined in Na^+ buffer or K^+ buffer in the presence (closed bars) or absence (open bars) of 100 mM Cl^-. DIDS was used as a general anion exchanger inhibitor. Values not sharing the identical letter are significantly different ($p < 0.05$; "a", "b", or "c"). B: $[^{35}S]SO_4^{2-}$ uptake mediated by water-injected or cmSlc26a1 cRNA-injected *X. laevis* oocytes. Values not sharing the identical letter are significantly different ($p < 0.05$; "a" or "b").
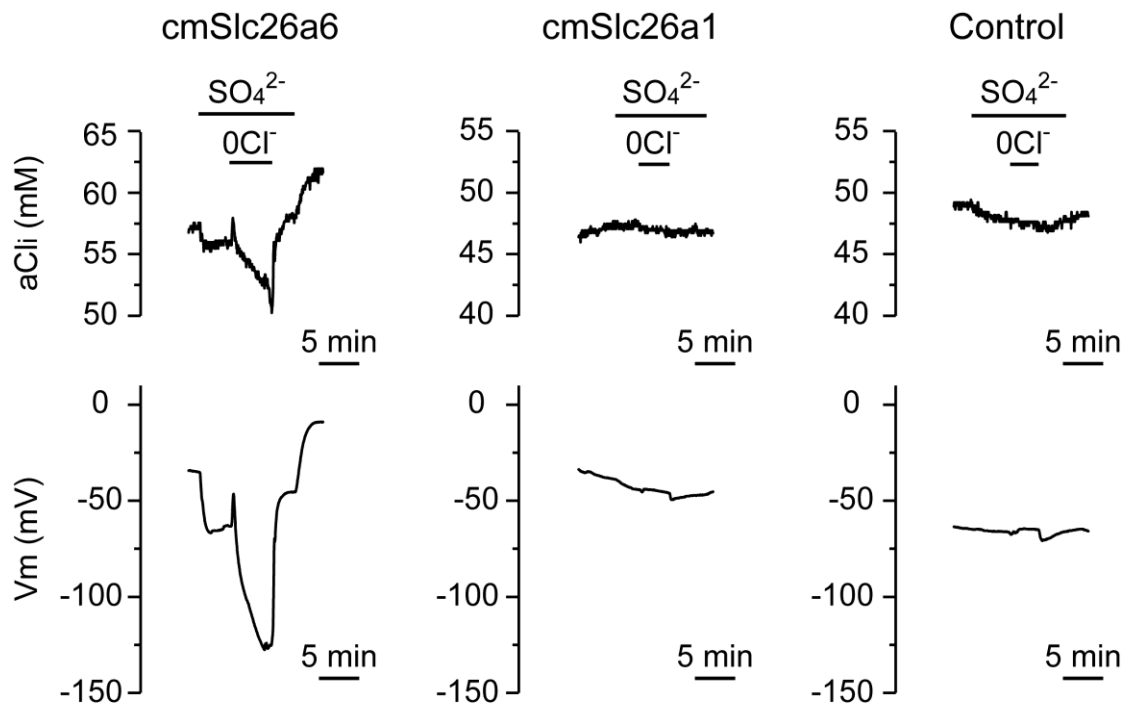
Fig. 1-4. Functional characterization of cmSlc26a1 and cmSlc26a6 using Cl⁻-selective microelectrodes**.** Representative traces are shown for intracellular Cl⁻ activity (aCl$_i$) and membrane potential (V_m) of oocytes expressing either cmSlc26a1 or cmSlc26a6, and control oocytes. In the continuous presence of 5 mM SO_4^{2-}, Cl^-/SO_4^{2-} exchanging activity was monitored as changes in aCl$_i$ and V_m after extracellular Cl⁻ was removed (0 Cl⁻) and replaced by gluconate.
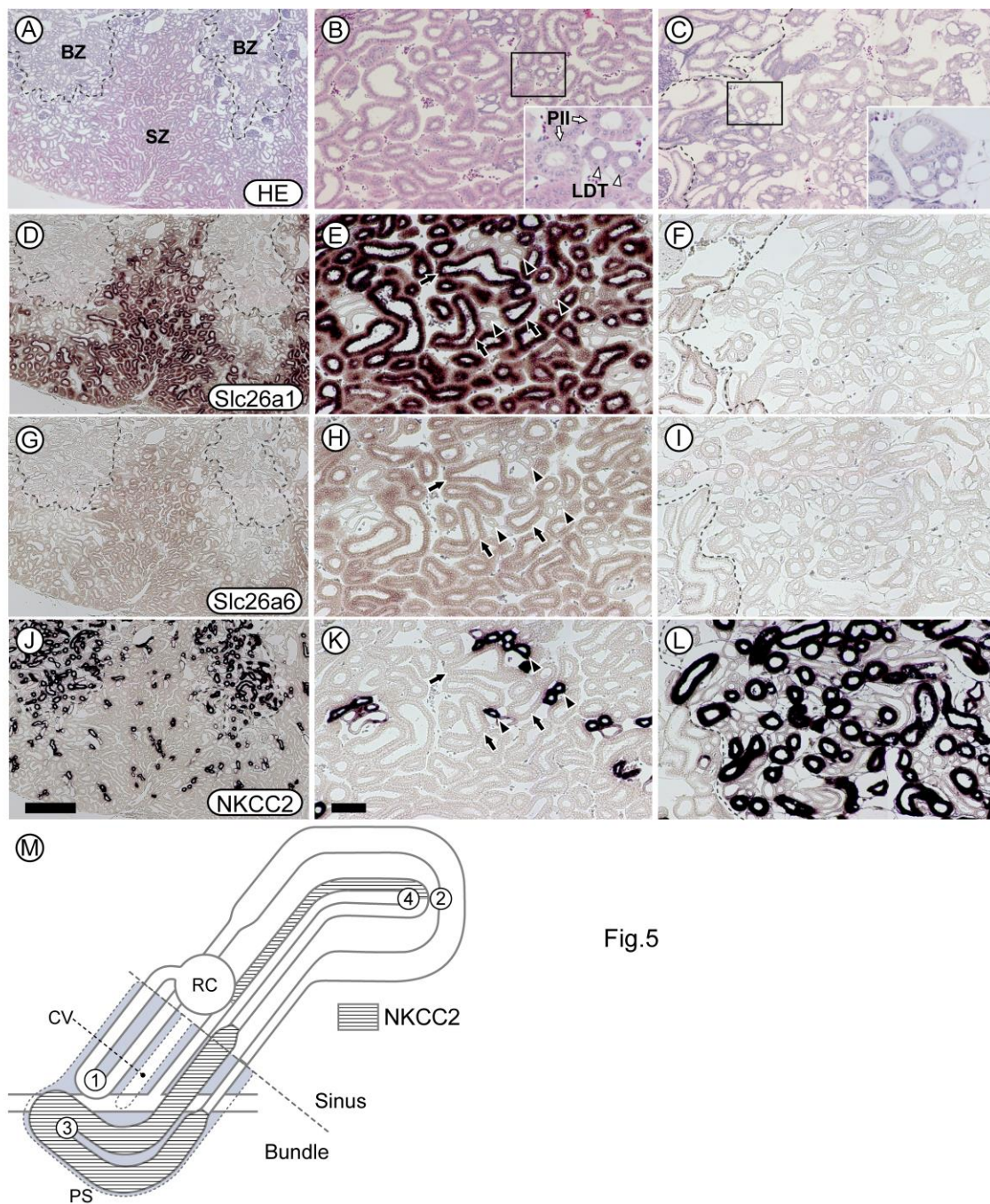
Fig. 1-5. Kidney sections subjected to either hematoxylin-eosin (HE) staining (A, B, C) or *in situ* hybridization with cRNA probes for cmSlc26a1 (D, E, F), cmSlc26a6 (G, H, I) or cmNKCC2 (J, K, L). A, D, G, and J are low power micrographs. The kidney lobule is separated into two zones, a sinus zone (SZ) and a bundle zone (BZ). Signals for cmSlc26a1 and cmSlc26a6 mRNAs were detected only in the sinus zone, while

cmNKCC2 mRNA was expressed in tubules in both the sinus and bundle zones. B, E, H, and K are magnified views of the sinus zone. In the sinus zone, two major nephron segments are identifiable: a proximal II (PII; arrows) segment and a late distal tubule (LDT; arrowheads). The signals for cmSlc26a1 and cmSlc26a6 mRNAs were colocalized in the PII segments, while cmNKCC2 mRNA was expressed in the LDT. C, F, I, and L are magnified views of the bundle zone. In the bundle zone, a cross-sectional view of the five tubular segments can be identified (inset in C). cmNKCC2 mRNA was expressed in the early distal tubule, while cmSlc26a1 and cmSlc26a6 mRNAs were not expressed in the bundle zone (F, I). (M) Schematic representation of the elephant fish nephron showing the localization of cmNKCC2 mRNA (modified based on Kakumura et al. 2015). The encircled numbers represent the number of loops. CV, central vessel; RC, renal corpuscle; PS, peritubular sheath. Scale bars, 500 μm (A, D, G, J) and 100 μm (B, C, E, F, H, I, K, L).
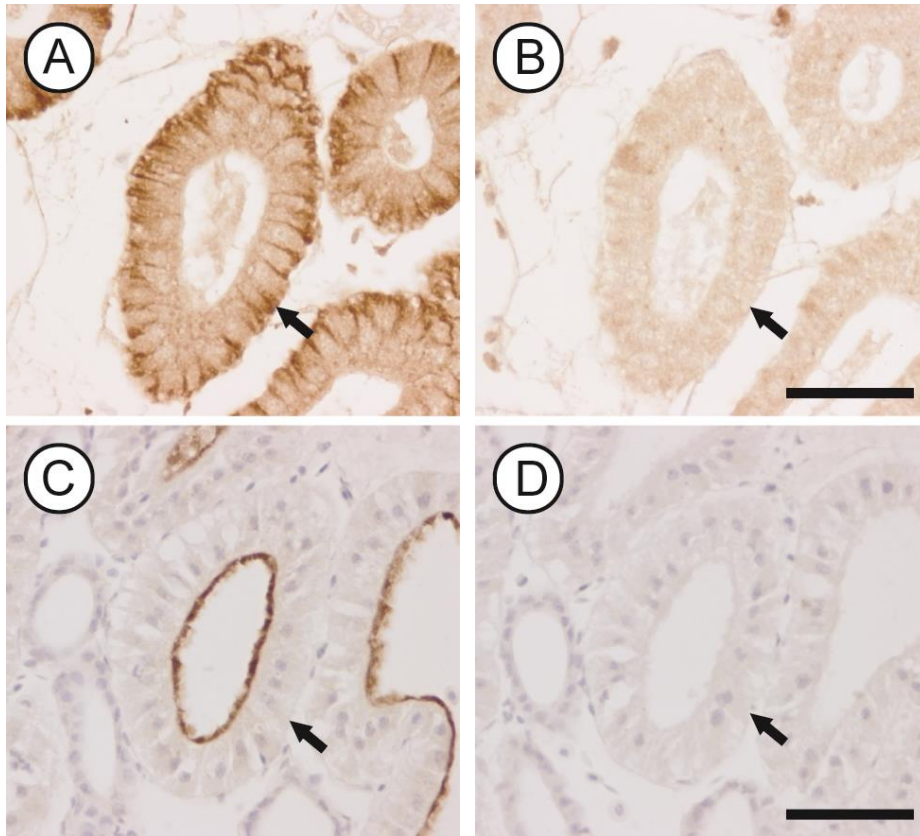
Fig. 1-6. Localization of immunoreactive cmSlc26a1 and cmSlc26a6 in the sinus zone of elephant fish kidney. Immunoreactive signals of Slc26a1 were detected in the basolateral membrane of PII cells (arrow in A). Signals of cmSlc26a6 were detected in the apical membrane of PII cells (C). Preabsorption of antibodies with the antigen peptides resulted in disappearance of the immunoreactive signals on the membranes (B, D, cmSlc26a1 and cmSlc26a6 respectively). Sections are counterstained with hematoxylin. Scale bars, 50 µm
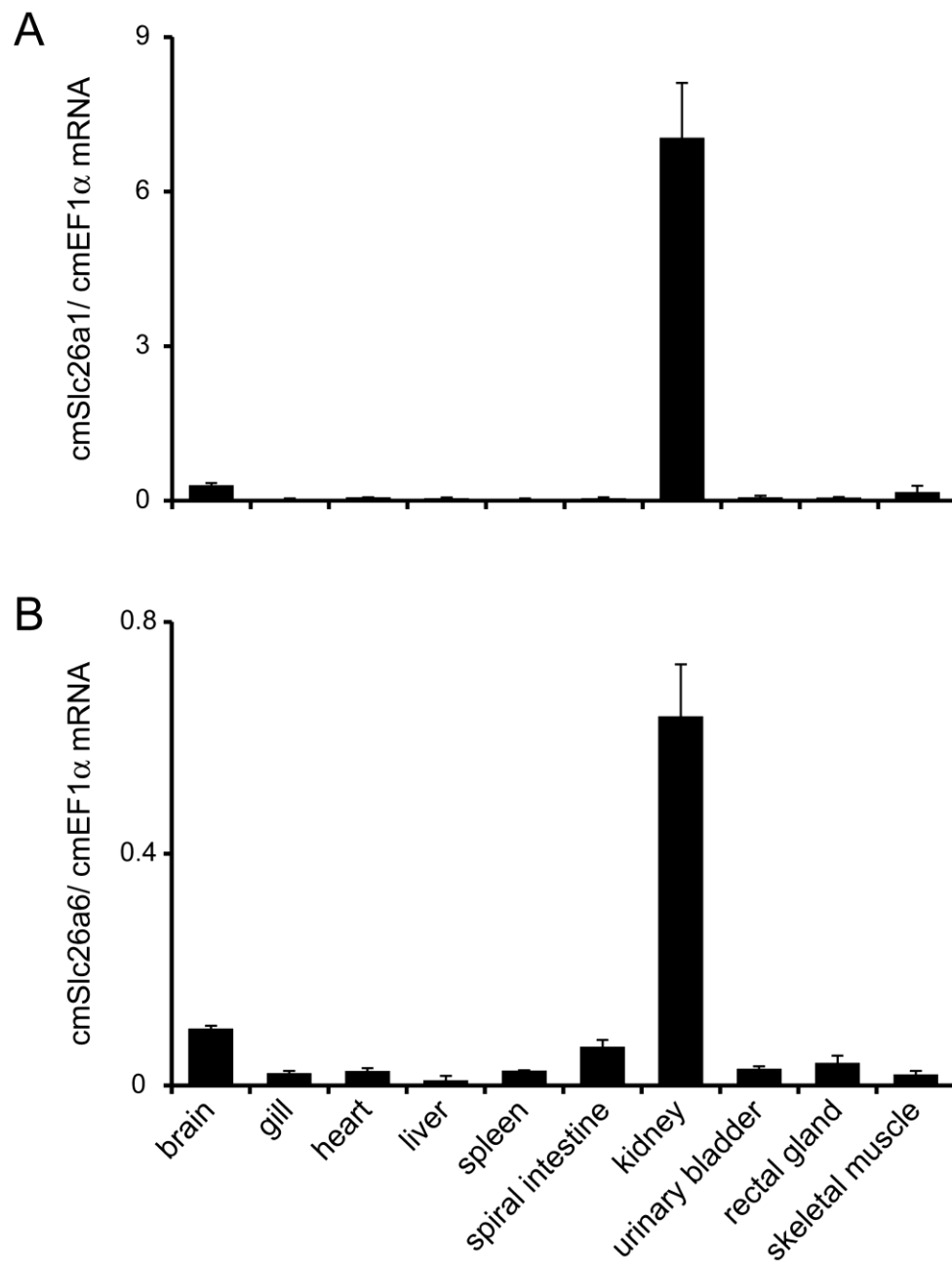
Fig. 1-7. Embryonic tissue distribution of mRNAs. RNAs encoding (A) cmSlc26a1 and (B) cmSlc26a6 were detected stage 36 embryos. The mRNA expression values were normalized against those of cmEF1α mRNA. Data are presented as means ± SEM (n = 6).
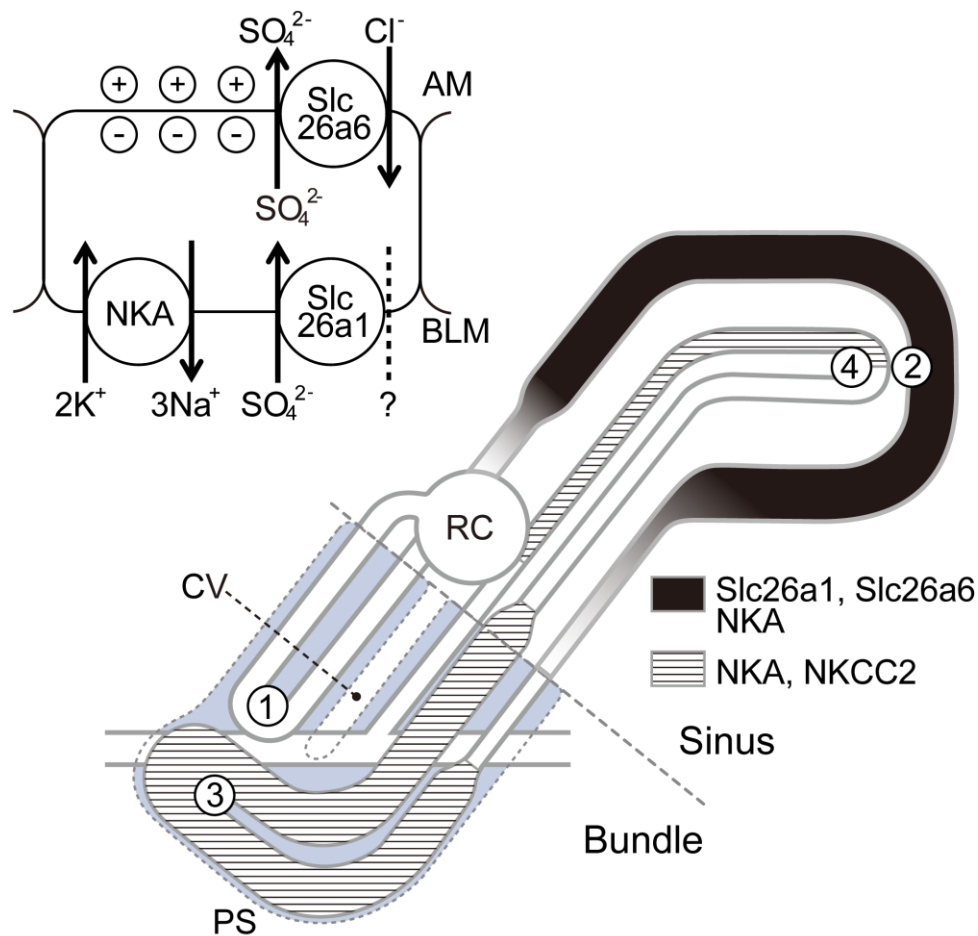
Fig. 1-8. Schematic diagrams showing the elephant fish nephron and PII sulfate secretion. Localization of Slc26a1, Slc26a6, NKA, and NKCC2 is indicated in the diagram of elephant fish nephron. Upper left panel showed a hypothetical model for epithelial SO_4^{2-} secretion in the PII segment. cmSlc26a6 is an electrogenic Cl^-/SO_4^{2-} exchanger localized on the apical membrane. The negative membrane potential and high concentration of Cl^- in the filtered urine most probably drives SO_4^{2-} secretion into the filtrate via Slc26a6. The intracellular SO_4^{2-} is supplied via basolaterally-located cmSlc26a1 (electroneutral SO_4^{2-} transporter) from the blood sinus. The dashed line means that we have no direct evidence for SO_4^{2-}/anion exchange or SO_4^{2-}-cation cotransport for cmSlc26a1. The encircled numbers represent the number of loops. AM, apical membrane; BLM, basolateral membrane; CV, central vessel; RC, renal corpuscle; PS, peritubular sheath.

Chapter 2

Identification of the water reabsorption segments in the bundle zone of elephant fish kidney

Abstract

Marine cartilaginous fishes (sharks, rays and chimaeras) retain a high concentration of urea (350-400 mM) for adaptation to high-salinity marine environment. Urea is freely filtered by the glomerulus, and more than 90% of filtered urea is reabsorbed in the marine cartilaginous fish kidney. However, the mechanism of urea reabsorption still remains largely unsolved. Urea is reabsorbed via facilitative urea transporter. I predicted that a low-urea environment exists in the kidney for passive reabsorption of urea, and that segment(s) for water reabsorption present in their nephron. In this chapter, localization aquaporins (AQPs) that are water channels was investigated in the kidney of elephant fish (*Callorhinchus milii*). Eleven putative AQPs were found in the elephant fish genome database; five AQPs (AQP1, 3-1, 3-2, 4 and 10-1) were abundantly expressed in the kidney. Among them, elephant fish (cm) AQP4 mRNA was highly expressed in tubules. The 3-D reconstruction of the cmAQP4-immunoreactive tubules revealed that cmAQP4 is intensely localized in the basolateral membranes of the descending and ascending limbs of the first loop, and weakly expressed in the collecting tubule. *In vitro* expression analyses using *Xenopus* oocytes revealed that cmAQP4 is a mercury insensitive, functional water channel. These results implied that the first loop and the collecting tubule are segments for water reabsorption, which create a low-urea environment around the collecting tubule. An updated model for urea reabsorption is discussed.

Introduction

Marine cartilaginous fishes (sharks, rays and chimaeras) has adopt a ureotelic osmoregulatory strategy for adaptation to the high-salinity marine environment. They retain a high concentration of urea (350-400 mM) to maintain their plasma slightly hyperosmotic to the surrounding seawater (Smith 1936), and thus cartilaginous fishes do not dehydrate even in the marine environment. To maintain a high concentration of urea in the body, both production and retention of urea are essential. Urea is produced by the ornithine urea cycle in the liver, muscle and several other organs (Anderson 1980; Kajimura et al. 2006; Takagi et al. 2012; Tam et al. 2003). On the other hand, the urea efflux across the shark gill is considerably lower than that of teleost, which favors urea retention in the body (Boylan et al. 1967; Fines et al. 2001). In the kidney, although urea is freely filtered by the glomerulus, more than 90% of filtered urea is reabsorbed from primary urine to the circulation (Clarke and Smith 1932; Kempton 1953). A yet unsolved question is how elasmobranchs reabsorb urea from the primary urine in the kidney.

The concentration of urea in urine is lower than that in plasma (Smith 1929; Smith 1931; Burger 1967; Read 1971), suggesting a specific mechanism for the uphill transport of urea from the primary urine to the circulation. The involvement of an unidentified sodium-coupled urea cotransporter and/or antiporter has been considered for the urea reabsorption in elasmobranch kidney (Walsh and Smith 2001). Several urea transporter(s) (UTs) have been identified in several cartilaginous fish species (Smith and Wright 1999; Janech et al. 2003; Morgan et al. 2003; Hyodo et al. 2004; Kakumura et al. 2009). The UTs of cartilaginous fishes are phloretin-sensitive facilitative transporter, and shared high sequence similarity to the mammalian UT-A2. In houndshark (*Triakis scyllium*) (Hyodo et al. 2004) and elephant fish (*Callorhinchus milii*) (Kakumura et al. 2015), the UT is localized in the collecting tubule, the final segment of the nephron, where Na^+/K^+-ATPase signal was scarcely detected. These results suggested that transport (reabsorption) of urea

in the collecting tubule occurs transcellularly by facilitated diffusion (Hyodo et al. 2004; Kakumura et al. 2015).

Instead of the active urea reabsorption model with unidentified transporter(s), our laboratory group proposed a urea reabsorption model based on the morphological features of cartilaginous fish nephron and the localization of various transporters including UT (Hyodo et al. 2014). In the bundle zone, the collecting tubule is wrapped by an impermeable peritubular sheath together with the four other nephron segments. Urea could be reabsorbed from the collecting tubule, if the urea concentration of interstitial fluid inside the peritubular sheath is lower than that of luminal fluid of the collecting tubule. Our group predicted the presence of a water reabsorption segment in the tubular bundle to generate this concentration gradient of urea.

In vertebrates, aquaporins (AQPs) are categorized into three subfamilies: classical AQPs, aquaglyceroporins, and unorthodox AQPs (Ishibashi et al. 2011). Classical AQPs such as AQP1, AQP2, and AQP4 only allow water to pass through. In addition to water, aquaglyceroporins such as AQP3, AQP7, AQP9, and AQP10 allow small uncharged solutes, such as glycerol and urea to pass through (Rojek et al. 2008). In the elephant fish kidney, Kakumura (2013) found that two types of AQP3 were co-expressed in the anterior half of the late distal tubule. In spiny dogfish (*Squalus acanthias*), immunoreactive AQP4 was localized in many tubules both in the sinus and bundle zones in the kidney (Cutler et al. 2012a). However, little is known about distribution of AQPs in the bundle zone of cartilaginous fish kidney.

In chapter 2, a comprehensive search of AQP genes was initially performed in elephant fish genome database. Among five AQP mRNAs that were strongly expressed in the elephant fish kidney, only AQP4 was expressed intensely in segments in the tubular bundle. I determined that the AQP4-expressing segments are the first loop and the collecting tubule, and proposed an updated model for urea reabsorption in the elephant fish kidney.

Materials and methods

Fish

Elephant fish were maintained and sampled as described in the Materials and Methods of Chapter 1. For mRNA and protein localization, tissues were fixed with Bouin's solution without acetic acid at 4°C for 2 days, and then washed in 70% ethanol, and stored at 4°C.

Tissue distribution and cDNA cloning

Amino acid sequences of frog (*Xenopus tropicalis* and *X. laevis*) and human aquaporins (AQPs) were used as BLAST queries to search for candidate genes in the Elephant Shark Genome Database (http://esharkgenome.imcb.a-star.edu.sg/). Sets of specific primers were designed to amplify the transcripts of elephant fish (cm) AQP genes (Table 2-1), and tissue distribution of cmAQP mRNAs was examined by RT-PCR using the cDNA set described in Chapter 1. RT-PCR was performed with KAPA Taq EXtra (Kapa Biosystems, Boston, MA, USA) for 36 cycles for cmAQP1, cmAQP3-1, cmAQP3-2, cmAQP4, cmAQP9, cmAQP10-1, cmAQP10-2 and cmAQP12 mRNAs, while 40 cycles for cmAQP14 and cmAQP15. Amplified PCR products were electrophoresed on 1% agarose gel and visualized by ethidium bromide fluorescence.

cDNAs encoding the entire open reading frame (ORF) of cmAQP1, cmAQP4 and cmAQP10-1 were amplified with specific primers and high-fidelity KOD-Plus DNA polymerase (Toyobo, Osaka, Japan). For cmAQP1, nucleotide sequence of 3'-noncoding region was initially determined by 3'-RACE methods using the SMARTer RACE cDNA Amplification Kit (Clontech, Mountain View, CA, USA), according to the manufacturer's instructions. The amplified cDNAs were then ligated into pGEMHE, and the nucleotide sequence was determined by an automated DNA sequencer (3130*xl* Genetic Analyzer; Life Technologies) and BigDye® Terminator v3.1 Cycle Sequencing Kit (Applied Biosystems, Foster City, CA, USA). All primers used are listed in Table 2-1.

Molecular phylogenetic analysis

The translated amino acid sequences of cmAQP1, cmAQP4, and cmAQP10-1 were aligned with those of other vertebrate AQP proteins using Clustal W 2.1 program (Thompson et al. 1994). The sequences of AQP family proteins were obtained from the DDBJ and Ensembl databases. Molecular phylogenetic trees were constructed by a Bayesian Metropolis coupled Markov chain Monte Carlo method in the MrBayes 3.1.2 program (http://mrbayes.sourceforge.net/). I ran four separate Marcov chains for 1,500,000 generations and sampled them every 100 generations to create a posterior probability distribution of 15,000 trees. The first 3,750 trees were discarded as burn-in before stabilization, and then a 50% majority-rule tree was constructed from the subsequent trees. The reliability of the generated tree was shown by posterior probabilities in the Bayesian analysis.

In situ **hybridization**

Kidney sections were prepared as described in Chapter 1. The DNA fragments (cmAQP1, 367 bp; cmAQP3-1, 894 bp; cmAQP3-2, 1085 bp; cmAQP4, 460 bp and 482 bp) were amplified using gene-specific primers listed in Table 2-1, and ligated into pGEM T-easy (Promega, Madison, WI, USA). The linearized plasmids were used to synthesize digoxigenin (DIG)-labeled antisense and sense cRNA probes (DIG RNA Labeling Kit; Roche Applied Science, Mannheim, Germany), according to the manufacturer's protocols. *In situ* hybridization of AQPs were performed with the same protocols described in Chapter 1. For cmAQP4, two cRNA probes corresponding to the NH_2- and COOH-halves of cmAQP4, respectively, were prepared, and were used separately or in mixture.

Immunohistochemistry

The polypeptide KSTQPPGGKYVEV+C that corresponded to the COOH-terminal cytoplasmic domain of cmAQP4, was synthesized and coupled *via* cysteine to keyhole

limpet hemocyanin. This conjugated peptide was emulsified with complete Freund's adjuvant and injected into guinea pig for immunization (Protein Purify, Gunma, Japan). For the immunohistochemistry of urea transporter (cmUT1), an established antiserum raised against the COOH-terminal region of cmUT1 was used (Kakumura et al. 2015).

Serial kidney sections at 6 μm were mounted onto MAS-coated slides and incubated with the antisera of cmAQP4 and cmUT1 according to the immunohistochemistry method described in Chapter 1. cmAQP4 (1:40000, 1:20000, or 1:10000) and cmUT1 (1:2000) antisera diluted with PBS-NGS were used in primary incubation and goat anti-guinea pig IgG or goat anti-rabbit IgG were used in secondary incubation

Three dimensional reconstruction of immunoreactive segments

Approximately 100 serial sections were stained with the anti-cmAQP4 antiserum as described above, and were used for 3-D reconstruction of cmAQP4-positive tubules. Slides were scanned with a Compact Digital Slide Scanner TOCO (Claro, Aomori, Japan). The scanned images were displayed using iViewer ver. 5.4.6. In the bundle zone, a cross sectional view of the five tubular segments (the descending and ascending limbs of the first and the third loops, and the collecting tubule) can be identified using the morphological features. The five segments were marked in different colors using Adobe Photoshop Elements 6.0. The marked serial sections were then automatically aligned and stacked using the stackreg and turboreg plugins of ImageJ (Abramoff et al. 2004). Finally, 3D images of the stacked sections were generated using the ImageJ 3D viewer plugin.

Water permeability of oocytes expressing cmAQP4

The entire coding region of cmAQP4 cDNA was inserted onto the pGEMHE expression vector. The construct was linearized with *Nhe* I, and cRNA was transcribed *in vitro* using the T7 mMESSAGE mMACHINE kit (Ambion, Austin, TX, USA). Oocytes were harvested and injected using the protocol described in Chapter 1.

On the day of assay, oocytes were transferred from iso-osmotic (200 mOsm) to hypo-osmotic (40 mOsm) MBS at 20°C. Images of the oocytes were obtained every 10 sec up to 2 min with a digital camera (DS-5Mc-U2, Nikon, Tokyo, Japan) attached to a stereomicroscope (MZ FLIII, Leica Microsystems GmbH), which was controlled by an imaging software NIS-Elements D (ver.2.30, Nikon). The volume of oocyte was calculated by measuring the maximum cross-section area of the oocyte using the imageJ software   (Abramoff et al. 2004).

The osmotic water permeability (Pf) was calculated using the following equation (Preston et al., 1992):

$$Pf = V_0 \times d(\ V\ /\ V_0\ )dt\ [\ S \times V_W \times (\ Osm_{in} - Osm_{out}\ )\ ],$$

where $d(V/V_0)dt$ is the initial rate of increase in relative oocyte volume; V_0 is the initial volume of the oocyte ($V_0 = 9 \times 10^{-4}$ cm^3); S is the initial oocyte surface area ($S = 0.045$ cm^2); V_W is the molar volume of water ($V_W = 18$ cm^3 mol^{-1}).

Effects of mercuric chloride were examined by incubating oocytes in MBS containing 0.3 mM HgCl$_2$ for 10 min before transfer to 40 mOsm of MBS.

Statistical analysis

Data are presented as means ± SEM. Data from the oocyte experiment were analyzed by one-way analysis of variance (ANOVA), followed by Tukey-Kramer's multiple comparison test. P values less than 0.05 were considered as statistically significant.

Results

Database search, cloning, and tissue distribution of AQPs

I found a number of fragments sharing high homology to known AQPs in the genome database, and designated elephant fish (cm) AQP0, 1, 3, 4, 9, 10, 12, 14, and 15, following the nomenclature described by Finn et al. (2014). These cmAQPs included six cmAQPs reported previously (Kakumura 2013). In elephant fish, two subtypes were among AQP3 and AQP10 (cmAQP3-1, 3-2, 10-1 and 10-2). Then, tissue distribution of cmAQP mRNAs was examined by RT-PCR using the gene-specific primer sets. Among the identified cmAQPs, cmAQP1, 3-1, 3-2, 4 and 10-1 mRNAs were abundantly expressed in the elephant fish kidney (Fig. 2-1). I determined the cDNA sequences encoding ORF of cmAQP1, cmAQP4 and cmAQP10-1. The putative cmAQP1, cmAQP4 and cmAQP10-1 possess 295, 349, and 301 amino acid residues, respectively. The cDNA sequences of cmAQP3-1 and 3-2 were previously determined (Kakumura 2013). The newly identified cmAQPs contained six putative membrane spanning domains and two NPA motifs, which are some common signatures of AQP family (Zardoya and Villalba 2001). Molecular phylogenetic analysis of AQP family showed that cmAQP1, cmAQP3-1, cmAQP3-2, cmAQP4, and cmAQP10-1 clustered to the clades of AQP1, AQP3, AQP4, and AQP10, respectively (Fig. 2-2).

Localization of cmAQP mRNAs in the elephant fish kidney

Before detailed analysis, initial localization screening for cmAQP1, cmAQP3-1, cmAQP3-2, cmAQP4, and cmAQP10-1 mRNAs by *in situ* hybridization was performed. Hybridization signals of cmAQP1 mRNA were detected in tubules located in the transitional area between the sinus zone and the bundle zone (arrows in Fig. 2-3A). Weak signals were also observed in some tubules in the bundle zone (arrowheads in inset in Fig. 2-3A). No signals for cmAQP1 mRNA were found in the sinus zone (Fig. 2-3B). As

already reported by Kakumura (2013), both cmAQP3-1 and cmAQP3-2 mRNAs were intensely expressed in the late distal tubule in the sinus zone (Figs. 2-3D and 2-3F), but not in tubules located in the bundle zone (Figs. 2-3C and 2-3E). The late distal tubule is characterized by a relatively small diameter and thin epithelial cells (insets in Figs. 2-3D and 2-3F). cmAQP4 mRNA was abundantly expressed in tubules in the bundle zone (Fig. 2-3G). Signals for cmAQP4 were not detected in the sinus zone (Fig. 2-3H). No signal was observed in the sections incubated with corresponding sense probes (data not shown). Although the RT-PCR revealed that cmAQP10-1 mRNA is expressed in the elephant fish kidney, hybridization signals for cmAQP10-1 mRNA was undetectable by *in situ* hybridization. Based on the above results, I focused on cmAQP4 in the following investigations.

Hybridization signal for cmAQP4 mRNA was observed in the neck segment that originated from the urinary pole of the Bowman's capsule (arrowheads in Figs. 2-4A and 2-4B). The neck segment is characterized by numerous ciliated cells for the propulsion of glomerular filtrate. In the bundle zone, a cross sectional view of five tubules (the first and third loops and the collecting tubule) wrapped with a peritubular sheath was observed (Fig. 2-4C). Intense signals of cmAQP4 mRNA were detected in two of five tubules (arrowheads in Fig. 2-4C) and moderate signals were also detected in another tubular segment (arrow in Fig. 2-4C). Hybridization signals for cmAQP4 were also detected in the collecting duct (Fig. 2-4D).

Identification of segments expressing cmAQP4

In addition to the mRNA signals, localization of cmAQP4 protein was examined with an antiserum raised against a specific synthetic peptide. Observations using adjacent sections showed that the signals of immunohistochemistry and *in situ* hybridization of cmAQP4 were consistent (Figs. 2-4A to H). Preabsorption of the anti-cmAQP4 serum with the specific synthetic polypeptide resulted in the disappearance of the

immunoreactive signals (Figs. 2-4I to L). These results strongly support the specificity of cmAQP4 mRNA and protein signals in the present study. Immunoreactive signals of cmAQP4 was observed in the basolateral plasma membranes of positive tubules (Figs. 2-4E to G). In the collecting duct, only weak immunoreactive signals were detected in the lateral membranes (arrows in Fig. 2-4H).

To identify tubular segments expressing cmAQP4 in the bundle zone, micrographs of serial sections with the cmAQP4 signals were obtained, and the 3-D images of the immunoreactive tubules were generated with the computer assisted 3-D reconstruction software. Similar to the results of *in situ* hybridization, the neck segment, which originated from the urinary pole of the Bowman's capsule, contained intense signals of cmAQP4 (Fig. 2-5A). The neck segment entered into the bundle zone, and was connected to the descending limb of the first loop (the proximal tubule Ia). The descending limb of the first loop was also immunoreactive with cmAQP4 antiserum (the tubule 1 in Fig. 2-5B). In the reconstructed image in figure 2-5C, the neck segment and the descending limb of the first loop were marked in white color. In the shallow area of the tubular bundle (Fig. 2-5B), weak signals were detected in two of five tubules [yellow (the tubule 2) and green (the tubule 5)] (Fig. 2-5C). The early distal tubule was morphologically distinguishable from other four segments in the bundle zone, because it was comprised of the largest columnar cells (the tubule 4 in Fig. 2-5B). The early distal tubule (red) was not immunoreactive, while the other tubules with relatively smaller diameters (blue) (the tubule 3 in Fig. 2-5B) were not immunoreactive.

In the deep area of the tubular bundle (Fig. 2-5D to G), the cmAQP4-positive descending limb of the first loop (the tubule 1; white) formed a loop with another intensely immunoreactive tubule (the tubule 2; yellow), showing that the yellow tubule was the ascending limb of the first loop (Fig. 2-5E and 2-5G). On the other hand, cmAQP4-negative segments [tubules 3 (blue) and 4 (red)] formed another loop in the deep area of the bundle zone. The tubule with weak immunoreactive signals (tubule 5;

green) connected to the collecting duct (Fig. 2-5F). The cmAQP4 signals in the tubule 5 were co-localized with immunoreactive urea transporter (cmUT1) in adjacent sections (Fig. 2-6). Taken together, the green tubule with weak signals is the collecting tubule.

Functional properties

Water permeability through the cmAQP4 protein was evaluated by a swelling assay using *X. laevis* oocytes. After transfer of injected oocytes from iso-osmotic (200 mOsm) to hypo-osmotic (40 mOsm) MBS buffer, the relative volume of the cmAQP4-injected oocytes was markedly increased (Fig. 2-7A) when compared to control oocytes. The water permeability (*P*f value) of cmAQP4-injected oocytes was significantly higher than that in water-injected control oocytes (Fig. 2-7B). The increase in osmotic water permeability was not inhibited by addition of 0.3 mM $HgCl_2$ in cmAQP4-injected oocytes (Figs. 2-7A and 2-7B).

Discussion

It is predicted that water reabsorption in the bundle is involved in urea reabsorption in the hypothetical model (Hyodo et al. 2014). In present study, I found eleven genes encoding aquaporin-family (AQP-family) proteins in the elephant fish genome database. Among them, cmAQP4 was intensely expressed in tubules in the bundle zone in the elephant fish kidney. Using the serial sections stained with the cmAQP4 antiserum, 3-D images of the cmAQP4-positive and -negative tubules were reconstructed. The 3-D reconstruction revealed that cmAQP4 is intensely expressed in the basolateral membranes of the descending and ascending limbs of the first loop and weakly expressed in the collecting tubule. These results suggested that the first loop and collecting tubule are segments for water reabsorption in the tubular bundle.

cmAQP4 is a mercury insensitive water channel located in the bundle zone

The ORF of cmAQP4 contained six transmembrane domains and the NPA box, which are common characteristics of most AQP proteins. The swelling assay using *Xenopus* oocytes revealed that cmAQP4 is a functional water channel. The water permeability of cmAQP4 was insensitive to $HgCl_2$, a well-established inhibitor for AQPs. Similar results have been reported in AQP4s of mammals (Hasegawa et al. 1994; Jung et al. 1994), zebrafish (Tingaud-Sequeira et al. 2010) and spiny dogfish (Cutler et al. 2012b). A cysteine residue in the second extracellular loop of AQPs was considered to be responsible for mercury-induced inhibition of water permeation (Yukutake et al., 2008). In AQP4s of most vertebrates, alanine or serine was found at the same position of this cysteine residue. A serine residue was also found in the corresponding position of cmAQP4, implying that this could be the reason the lack of inhibition by $HgCl_2$.

Although water transport activity of cmAQP4 is similar to that of spiny dogfish AQP4, distribution of AQP4 was considerably different between elephant fish and spiny dogfish.

The cmAQP4 mRNA was strongly expressed in the brain and kidney, and weakly expressed in the rectal gland. In spiny dogfish, the most intense mRNA signal was observed in the rectal gland, while strong expression of AQP4 mRNA was detected in many tissues including the kidney, brain and muscle (Cutler et al. 2012b). Moderate level of expression was also seen in the liver. In the elephant fish kidney, cmAQP4 mRNA and protein were mainly detected in the first loop and the collecting tubule in the bundle zone. On the other hand, in the spiny dogfish kidney, immunoreactive signals for AQP4 were observed in multiple intermediate and distal segments both in the sinus zone and the bundle zone (Cutler et al. 2012a). Currently, I do not know a reason for the discrepancy. AQP4 may contribute to different functions between elephant fish and spiny dogfish. Alternatively, the specificity of antisera used in the spiny dogfish might have some problems as two antisera raised against the spiny dogfish AQP4 were used but results were not consistent between the two antisera (Cutler et al. 2012a).

A possible model for urea reabsorption

The present study revealed that the descending and ascending limbs of the first loop and the collecting tubule are water-permeable segments in the bundle zone. Beginning at the neck segment, the whole descending limb of the first loop abundantly expressed cmAQP4. Regarding the ascending limb of the first loop, on the other hand, the deep portion contained more cmAQP4 than the shallow portion of the bundle zone (Fig. 2-8A). These results suggest that the ascending limb of the first loop can be divided into two functionally different segments. I designates here the segment abundantly expressing cmAQP4 as PIa1, while the shallow portion of the ascending limb of the first loop as PIa2.

Taken together with the previously proposed hypothetical model (Hyodo et al. 2014), I propose an updated model for urea reabsorption, which focuses on the tubular bundle (Fig. 2-8). In this model, three functionally different segments are considered: the water permeable PIa1, the diluting segment in the third loop, and the urea-permeable collecting

tubule (Fig. 2-8A). The first step is an active NaCl reabsorption driven by Na^+/K^+-ATPase (NKA)   (Fig. 2-8B) in the bundle zone, where strong gene expression was demonstrated in the early distal tubule (EDT; the ascending limb of the third loop) of elephant fish (Fig. 2-8A; Kakumura et al. 2015) and houndshark (Hyodo et al. 2004). In the EDT, Na^+-K^+-$2Cl^-$ cotransporter 2 (NKCC2) is co-expressed with NKA, suggesting that Na^+ and Cl^- are actively reabsorbed to inside the sheath through the basolateral NKA and apical NKCC2 (Fig. 2-8B; Kakumura et al. 2015). This idea is supported by the morphological and physiological characteristics of the EDT. The epithelial cells of the EDT have elaborate basolateral infoldings and numerous large mitochondria (Hentschel 1991). Microperfusion results of the EDT demonstrated a high Cl^- absorption rate in spiny dogfish, while furosemide, an inhibitor of NKCC2, abolished the Cl^- absorption (Friedman and Hebert 1990). Electrophysiological properties of the EDT were consistent with those of the mammalian thick ascending limb of the loop of Henle (a diluting segment) (Gamba et al. 1994; Hebert et al. 2004). The reabsorbed Na^+ and Cl^- in the EDT will increase the osmolality of interstitial fluid wrapped by the peritubular sheath (Fig. 2-8B). The raised osmolality in the interstitial fluid increases water absorption through other water-permeable segments, such as the PIa1 (Fig. 2-8C). Low-urea fluid, in which the urea concentration is considerably lower than that in the blood, is thus generated inside the peritubular sheath.

The filtrate diluted in the EDT then flows into the fourth loop of nephron (the late distal tubule; LDT). In the elephant fish kidney, the anterior half of the LDT expresses AQP3-1 and 3-2 (Kakumura 2013), while NKA and NKCC2 are co-expressed in the posterior half of the LDT (Kakumura et al. 2015). Therefore, urea in the filtrate is concentrated in the LDT by reabsorption of water and NaCl to the blood sinuses. The urea-rich filtrate then flows into the collecting tubule in which urea transporter is expressed in the apical and basolateral membranes of the epithelial cells (Fig. 2-8D). Urea is reabsorbed down a concentration gradient to the interstitial fluid via the facilitative urea

transporter (Fig. 2-8E). In the collecting tubule of the elephant fish kidney, cmAQP4 was expressed together with the urea transporter (UT1) (Fig. 2-8A). Co-expression of urea transporter and AQP has also been shown in the mammalian nephron, in which UT-A1 is co-localized with apical AQP2 and basolateral AQP3 and AQP4 in the inner medullary collecting duct (Hasler et al. 2009). In the mammalian inner medullary collecting duct, osmotic influx of water facilitates diffusion of urea through UT-A1, which increase the osmolality of the interstitium to facilitate water reabsorption. The same system might occur in the collecting tubule of elephant fish nephron. In the elephant fish nephron, reabsorption of urea most likely increases osmotic gradient between the interstitial fluid and the filtrate in the collecting tubule, which in turn, facilitates water influx (Fig. 2-8E). Likewise, the resulting influx of water from collecting tubules further facilitates urea reabsorption.

To date, only few studies have examined the capillary system in the bundle zone. Hentschel et al. (1998) described a single lymph capillary-like central vessel, which is different from the mammalian vasa recta. The central vessel originates as a few blind-ending branches at the distal end of the tubular bundle, runs along the entire bundle, and finally merges with the blood sinuses. The central vessel is the only exit of the interstitial fluid inside the peritubular sheath (Fig. 2-8F). Because of high resistance at the peritubular sheath, the increase in interstitial fluid volume may generate a hydrostatic pressure that drives the fluid to flow unidirectionally from the tip of the bundle to the blood sinuses (Fig. 2-8F), and thus an 'uphill' transport of urea from the filtrate to the circulation becomes possible.

In the elephant fish kidney, cmAQP4 was localized only in the basolateral membrane. Currently, no information is available concerning an apical AQP in the first loop and the collecting tubule. In the mammalian inner medullary collecting duct, AQP4 is localized in the basolateral membrane, while vasopressin-responsive AQP2 is localized in the

apical membrane (Fushimi et al. 1993; Nielsen et al. 1993; 2002; Terris et al. 1995). However, AQP2 (and its ancestral molecule, AQP0p) has been found only from sarcopterigians. In the elephant fish kidney, a candidate molecule is cmAQP1. Hybridization signals of cmAQP1 mRNA were detected in tubular segments located in the transitional area between the sinus zone and the bundle zone. In addition, although signal was weak, signals for cmAQP1 mRNA were also detected in the first loop of nephron, together with cmAQP4 mRNA. Currently, immunohistochemical detection has not been succeeded yet for cmAQP1. In the mammalian kidney, AQP1 is localized to both apical and basolateral membrane of the nephron.

Table 2-1. Primer sets used in the present study

Primer sets for tissue distribution analysis of aquaporins		
Gene name	Primer sequence 5' to 3'	
cmAQP1	Sense	GAGAGAGCTGCAGACCAGC
	Antisense	CTTTGGCTTCATCTCGACC
cmAQP3-1	Sense	TGAGCTCGAGTCCCAGATAAA
	Antisense	GCCAGTTTTCTCCAGTTGTCA
cmAQP3-2	Sense	CTCAAAGCCTCGCTGTTCAC
	Antisense	GGGGGAGATATCTGGAGGTT
cmAQP4	Sense	CCTGACTCTGAGCCTGATCC
	Antisense	TGTCGATAACCTGGGAGGTC
cmAQP9	Sense	TCCCAAGAGGAACAATGGAG
	Antisense	TTTTTCTTCGGGGATTGTTG
cmAQP10-1	Sense	ATGAGCCTGACCTCCTTCCT
	Antisense	GGGTGAAACATCCACCTTTG
cmAQP10-2	Sense	CACTTGAACCCAGCCATCTC
	Antisense	ACTGCTCTCTGGATGAACTGTCT
cmAQP12	Sense	GGCTGGACTTAATGTTTCATTTG
	Antisense	CCTCTGCGGTTATTTTCGAG
cmAQP14	Sense	TCTGTTCCAGGATTTGAGGAG
	Antisense	GCTGAGGCCGATGGCTAA
cmAQP15	Sense	CACTGAGTGCCGAGTTCCT
	Antisense	GGCGTCAGGATAAAGCTGTC

Primers for 3'-RACE		
cmAQP1	Sense	GAACGGACAGCTCGAAGATT

Primer sets for cloning		
cmAQP1	Sense	GCGTGTGTTTGAAGGAGACC
	Antisense	AAAAATGGGATTTGAGTCATGT
cmAQP4	Sense	ATCAGGTGGAATGGGAAGG
	Antisense	GGCTCTCTGCTTTCAGTGCT
cmAQP10-1	Sense	GTAGAGTGGAGGCCGTGAAC
	Antisense	GTTTGAGGTTGGGGTTTGG

Primer sets for *in situ* hybridization		
cmAQP1	Sense	TGTAGGGGTCGAGCTAATCG
	Antisense	TTTCTCCAGGTTTCCCTCCT
cmAQP4	Sense	(same with the cloning primer)
	Antisense	GCGTGATGAGGTAGAGGATTC
	Sense	ACTGGGAGTTACCAAGGTAAATAAG

Antisense   (same with the cloning primer)

Primer sets for swelling assay		
cmAQP4	Sense	AAAATCTAGAGCGTTACAATGTTCCCTTC
	Antisense	AAAAAAGCTTTGCTTCTTGCTAGTCATACA

Table 2-2. The accession numbers of genes used in the molecular phylogenetic analysis

Gene name	Accession number
AQPM	BAI62182
anole AQP14	ENSACAP00000023015
catfish AQP7	NM_001201082
chicken AQP0	NM_204266
chicken AQP1	NM_001039453
chicken AQP2	XM_428855
chicken AQP4	NM_001004765
chicken AQP5	XM_001231780
chicken AQP10	XM_004948281
chicken AQP11	XM_003640598
chicken AQP12	NM_001109679
chicken AQP14	ENSGALP00000041082
coelacanth AQP14	ENSLACP00000021646
dogfish AQP4	JF944824
dogfish AQP15	KJ815007
duck AQP9	XM_005011938
eel AQP1b	AB586029
eel AQP3	AB378501
eel AQP10	AB378503
frog AQP0	NM_001097347
frog AQP1	NM_001005829
frog AQP3	NM_001016845
frog AQP5	XM_002935743
frog AQP7	NM_001015726
frog AQP8	NM_001114256
frog AQP9	XM_002937673
frog AQP10-2	ENSXETT00000049658
frog AQP12a	NM_001094650
frog AQP13	NP_001082310
human AQP0	NM_012064
human AQP1	NM_198098
human AQP2	NM_000486
human AQP3	NM_004925
human AQP4	NM_001650
human AQP5	NM_001651
human AQP6	NM_001652
human AQP7	NM_001170
human AQP8	NM_001169

human AQP9	NM_020980
human AQP10	NM_080429
human AQP11	NM_173039
human AQP12a	NM_198998
mummichog AQP0	AF191906
mouse AQP6	NM_175087
platyfish AQP15	XP_005817244
platypus AQP13	XP_001520638
salmon AQP1	NM_001140000
salmon AQP8	NM_001173915
seabass AQP3	DQ647191
smelt AQP9	DQ533629
smelt AQP10b	KM455589
smelt AQP11	BT074912
snake AQP3	HQ377190
stickleback AQP1a2	ENSGACT00000023023
takifugu AQP4	AB610922
takifugu AQP7	AB610919
takifugu AQP8	AB610923
takifugu AQP10a	AB610920
takifugu AQP12	AB610925
tetraodon AQP1a	ENSTNIT00000011493
tetraodon AQP1b	ENSTNIT00000001619
tilapia AQP14	ENSONIP00000021523
tilapia AQP15	XP_003442458
turtle AQP15	ENSPSIP00000010966
zebrafish AQP0-2	DQ003080
zebrafish AQP1a1	NM_207059
zebrafish AQP1a2	NM_001135682
zebrafish AQP3a	NM_213468
zebrafish AQP3b	NM_001166121
zebrafish AQP4	NM_001003749
zebrafish AQP7	NM_199910
zebrafish AQP8	AY732215
zebrafish AQP9a	NM_001033096
zebrafish AQP10a	NM_001002349
zebrafish AQP10b	NM_001083047
zebrafish AQP12	NM_001045862
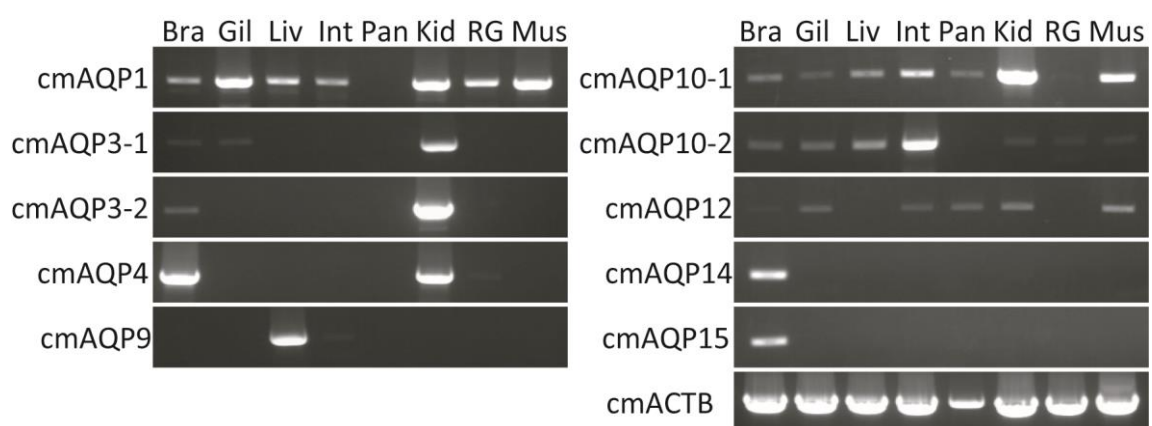
Fig. 2-1. Tissue distribution of AQP mRNAs in adult elephant fish examined by RT-PCR. Bra, brain; Gil, gill; Liv, liver; Int, intestine; Pan, pancreas; Kid, kidney; RG, rectal gland; Mus, muscle.
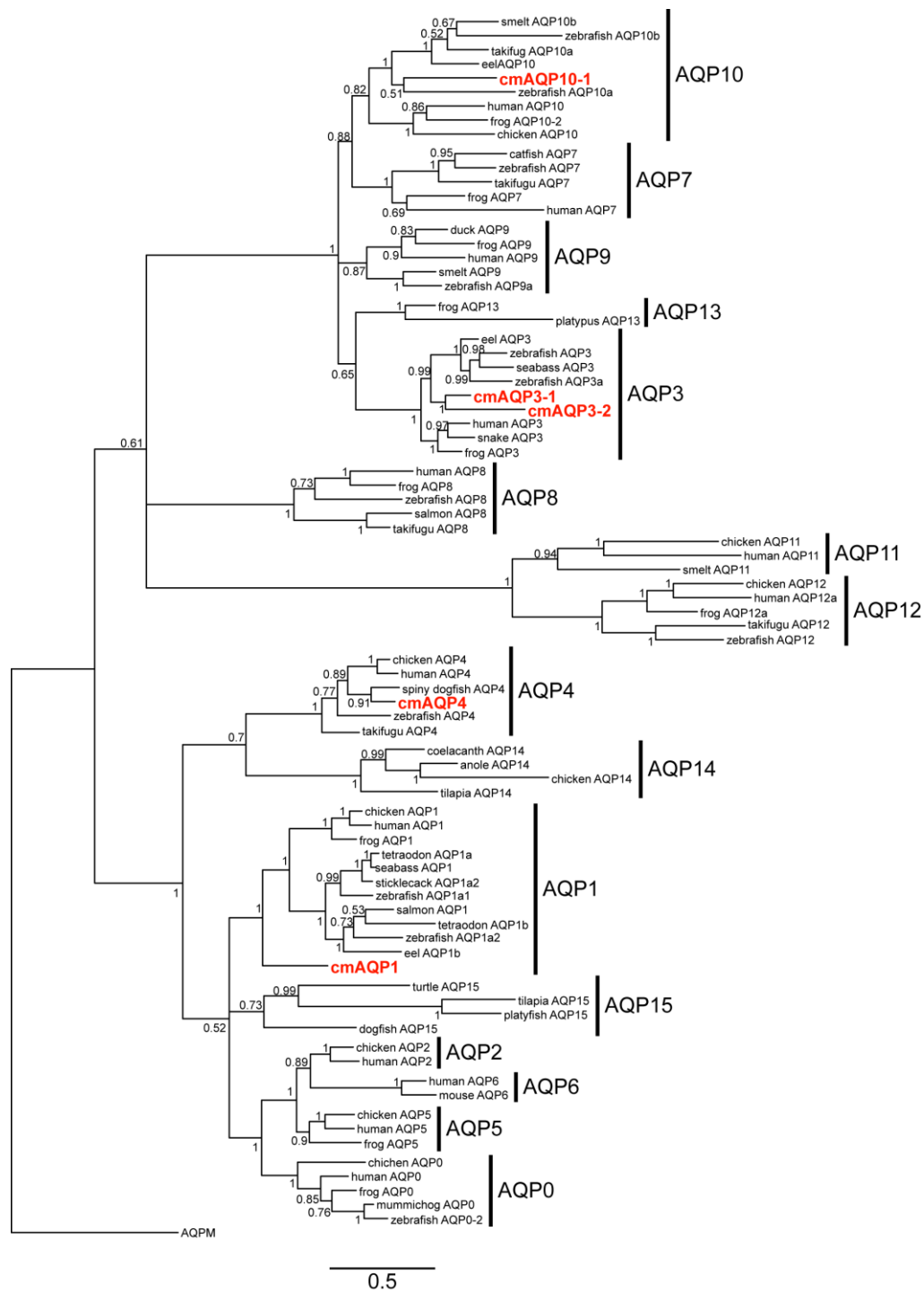
Fig. 2-2. Molecular phylogeny of vertebrate AQP family proteins. The elephant fish (holocephalan) sequences identified in this study are shown in red bold letters with select vertebrates indicated in normal font. The accession numbers of genes and mRNAs used in the analysis are listed in Table 2-2. AQPM (archaeal aquaporin; accession number, BAI62182) sequence was used as outgroup. Numbers at branch nodes represent Bayesian posterior probabilities
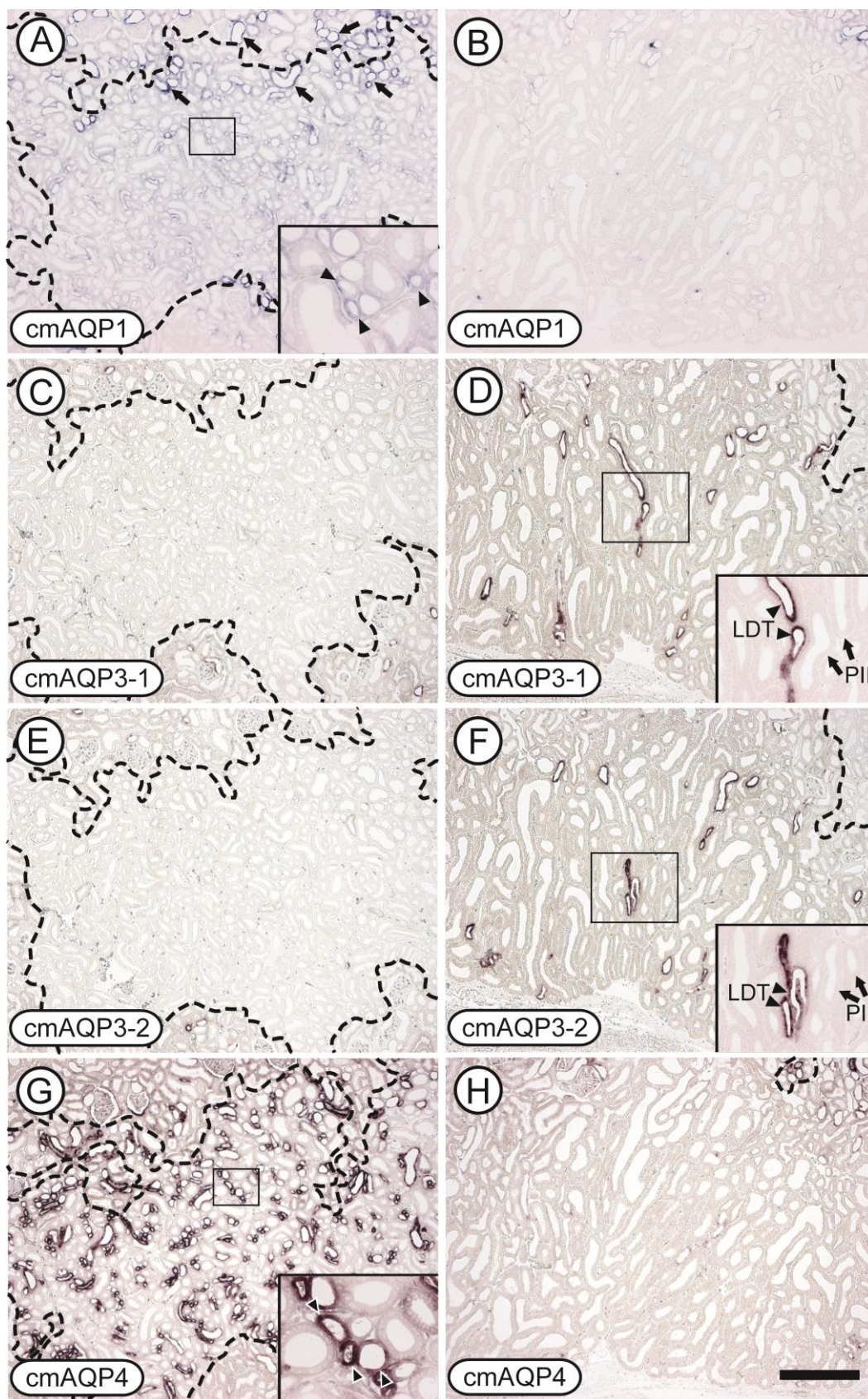
Fig. 2-3. Kidney sections subjected to *in situ* hybridization with cRNA probes for cmAQP1 (A, B), cmAQP3-1 (C, D), cmAQP3-2 (E, F) or cmAQP4 (G, H). The kidney is separated into two zones, a bundle zone (A, C, E and G) and a sinus zone (B, D, E and H). cmAQP1 was expressed in tubules located in the transitional area between the sinus zone and the bundle zone (A), and weakly in bundle zone (inset in A). Signals for cmAQP3-1 (D) and cmAQP3-2 (F) mRNAs were detected in the late distal tubule (LDT) in the sinus zone, but not in the bundle zone (C and E). cmAQP4 mRNA was abundantly expressed in tubules of the bundle zone (G), but not in the sinus zone (H). Dotted lines indicate the borders between the bundle zone and the sinus zone. LDT, late distal tubule; PII, proximal segment II. Scale bar, 400 μm.
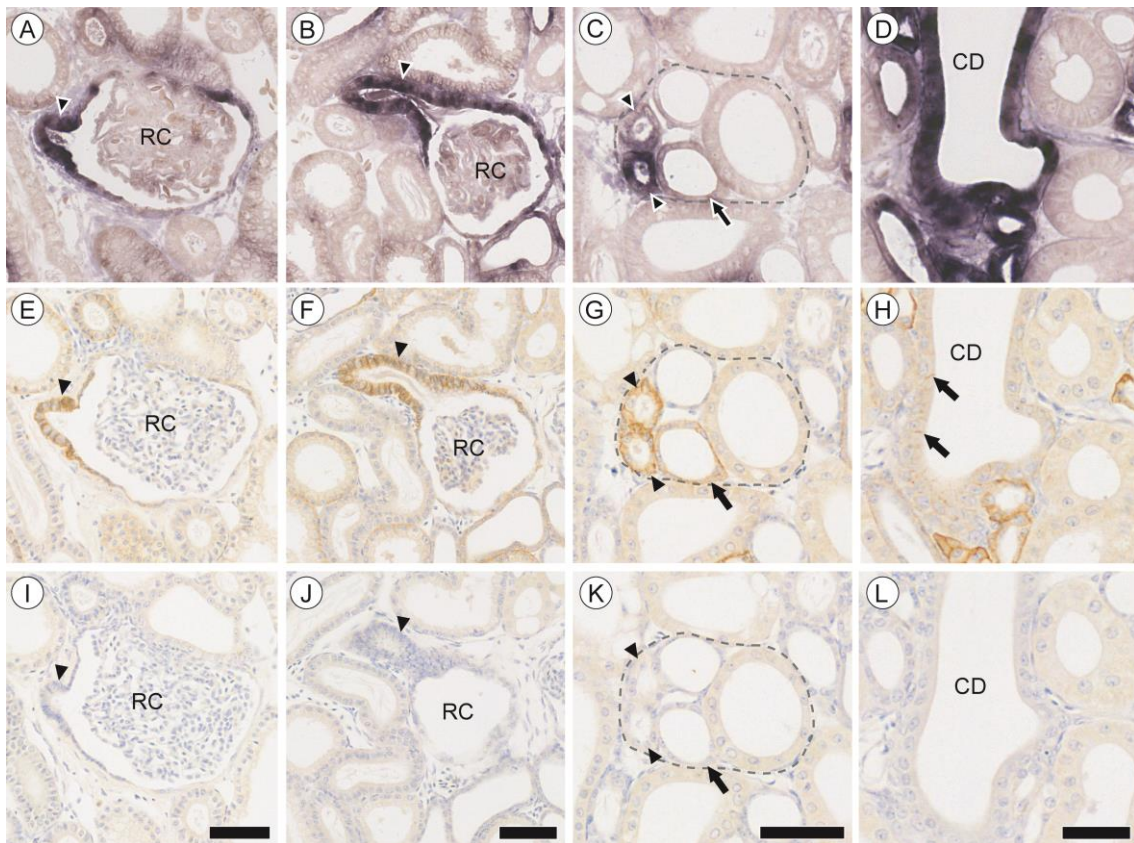
Fig. 2-4. Localization of cmAQP4 mRNA by *in situ* hybridization (A, B, C, and D) and cmAQP4 protein by immunohistochemistry (E, F, G, and H) in the bundle zone. The signals of cmAQP4 mRNA and protein were first detected in the neck segment (arrowheads in A, B, E, and F) that originated from the renal corpuscle (RC). Two of five tubules were also intensely stained with cmAQP4 mRNA and protein in the bundle zone (arrowheads in C and G), while weak signals for cmAQP4 mRNA and protein were detected in one tubule (arrows in C and G). Hybridization signals were intensely observed in the entire collecting duct (D), while immunoreactivity of cmAQP4 was low (arrows in H). Immunoreactive signals were displaced by preabsorption of antibody with the antigen peptide (I, J, K, and L). For immunohistochemistry, sections were counterstained with hematoxylin. RC, renal corpuscle; CD, collecting duct. Scale bars, 50 μm (A, B, C, E, F, G, I, J and K) and 25 μm (D, H and L).
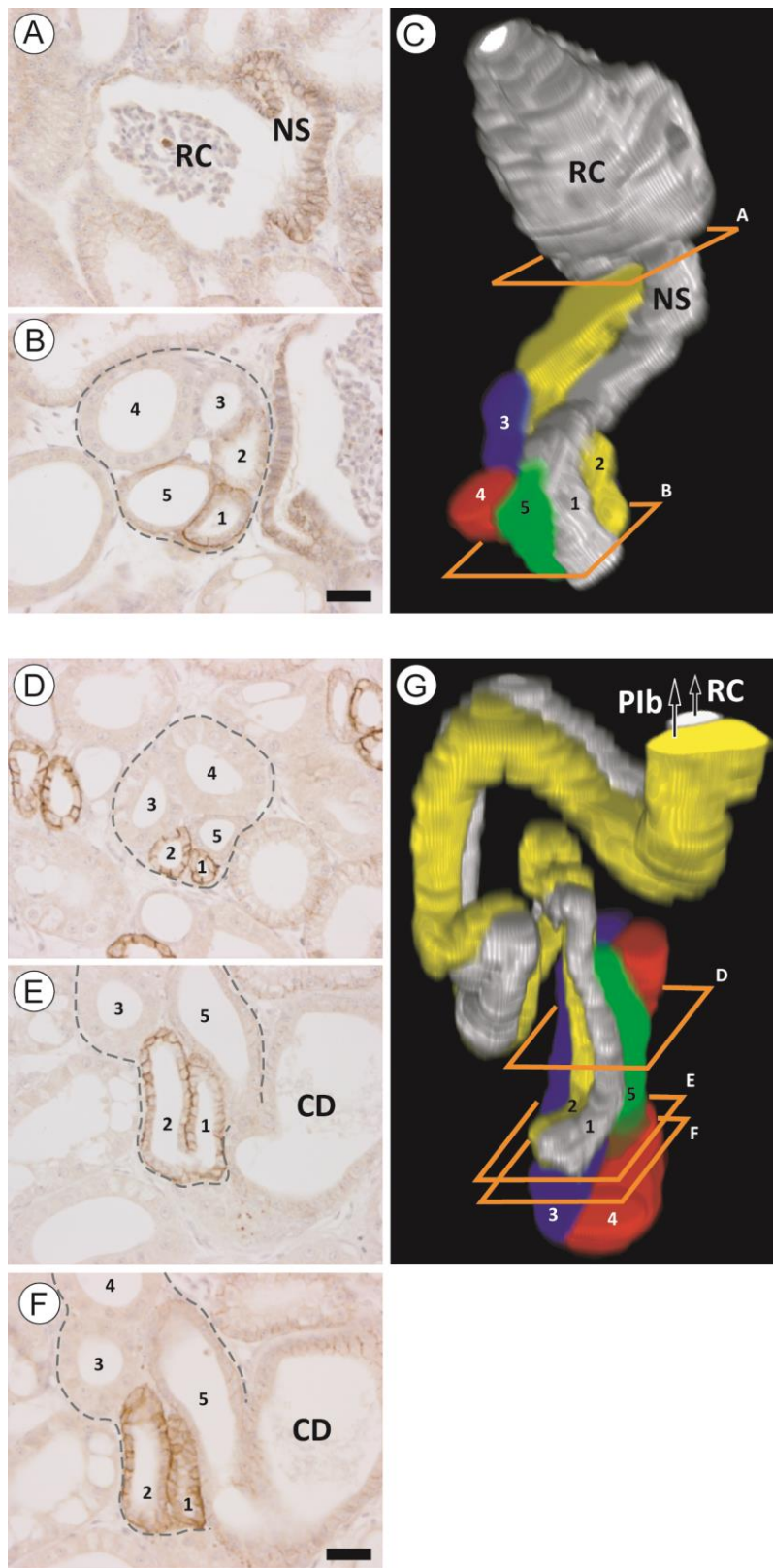
Fig. 2-5. Reconstructed 3-D images using serial sections with immunoreactive signals of cmAQP4. (A, B, D, E and F) representative sections used for the reconstruction. C and G show 3-D images reconstructed using serial sections. (C), shallow portion of the bundle zone; (G) the deep portion of the bundle zone. Orange quadrangles in 3-D images indicate the positions of sections in A, B, D, E and F. cmAQP4 was localized in the neck segment (NS in A) (the tubule marked in white color in C) and the descending limb of the first loop (the tubule 1 in B, and the white colored tubule in C). Two intensely stained tubules formed a loop in the deep area of bundle zone (the tubules 1 and 2 in E, and the white and yellow tubules in G). cmAQP4 was weakly expressed in the collecting tubule (the tubule 5 in F, and the green colored tubule in G). Color code: white, renal corpuscle, the neck segment and the descending limb of the first loop; yellow, the ascending limb of the first loop; blue, the descending limb of the third loop; red, the ascending limb of the third loop; green, the collecting tubule. RC, renal corpuscle; CD, collecting duct; PIb, proximal segment Ib. Scale bars, 25 μm.
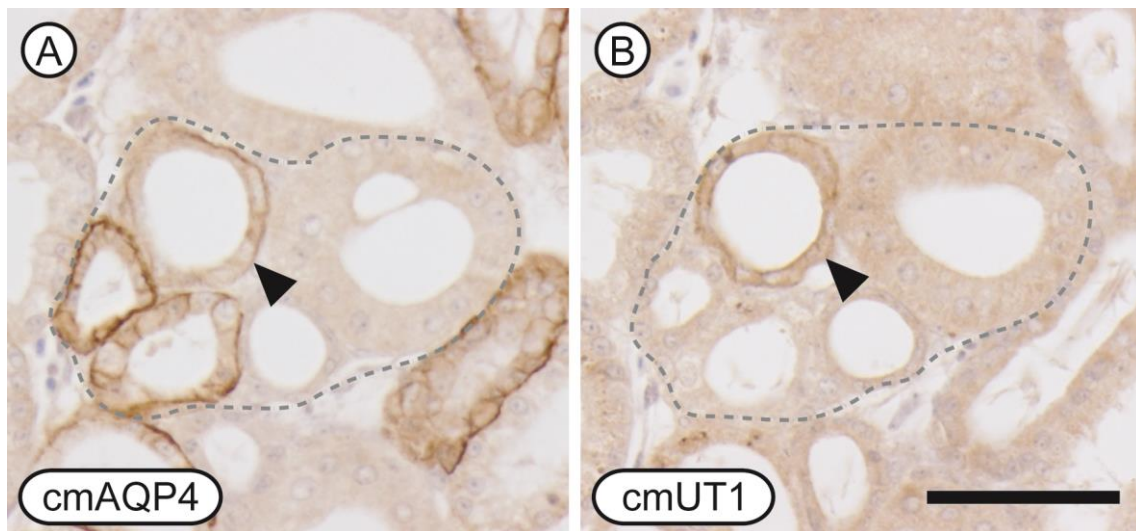
Fig. 2-6. Localization of immunoreactive cmAQP4 and cmUT1. cmAQP4 was weakly stained in the tubule expressing cmUT1 (arrowheads in A and B). Scale bar, 50 μm.
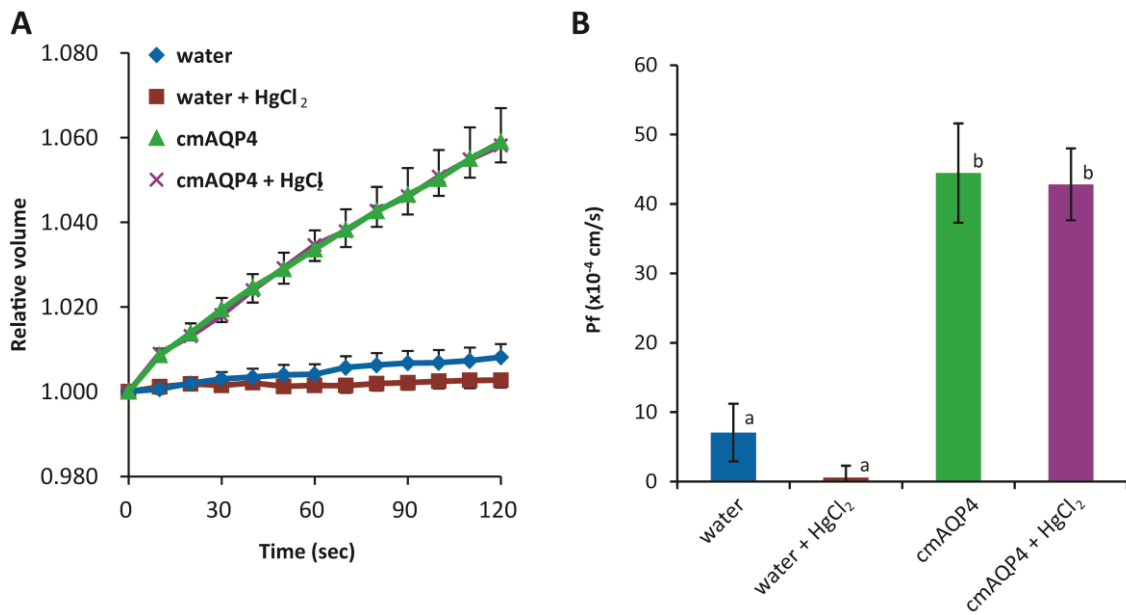
Fig. 2-7. Water transport activity of cmAQP4. Time course of the osmotically-induced swelling of *Xenopus* oocyte by hypotonic stimulation (A). Oocytes were microinjected with water or cmAQP4 cRNA. Some of the oocytes were incubated with 0.3 mM $HgCl_2$. Osmotic water permeability (*Pf*) was calculated from the initial rate of oocyte swelling (B). Various letters indicate significantly different among treatment groups ($p < 0.05$).
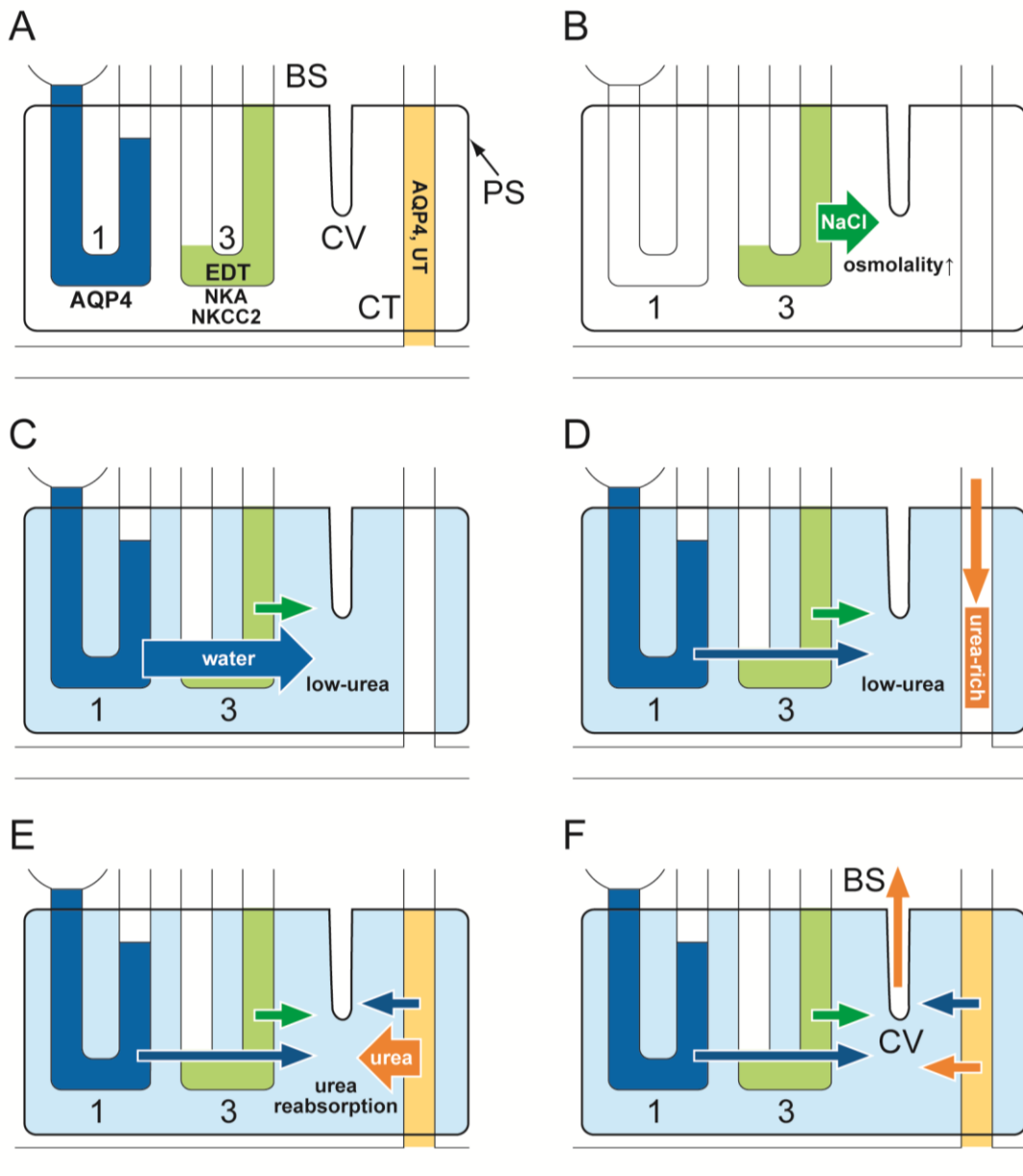
Fig. 2-8. Schematic diagrams showing a model for urea reabsorption in the tubular bundle. (A) localization of transporting molecules. Na^+/K^+-ATPase (NKA) and Na^+-K^+-$2Cl^-$ cotransporter type-2 (NKCC2) are expressed in the early distal tubule (EDT; the third loop). AQP4 is localized in the first loop (PIa1) and the collecting tubule (CT). In the CT, facilitative urea transporter (UT) is also expressed. (B) as the first step, NaCl is actively reabsorbed into the interstitium from the EDT (green arrow) . As a result, osmolality of

interstitial fluid is increased inside the peritubular sheath (PS). (C) the increased osmolality then drives water reabsorption from the PIa1 via cmAQP4 (blue arrow). The reabsorption of water results in the generation of 'low-urea fluid'. (D) On the other hand, the filtrate, in which urea is concentrated, flows into the CT (orange arrow). (E) urea is reabsorbed from the filtrate (high-urea fluid) to the interstitial fluid (low-urea fluid) (orange arrow). (F) because of high resistance at the peritubular sheath, the interstitial fluid flows unidirectionally in the central vessel (CV) to the blood sinuses (BS).

General Discussion

Marine cartilaginous fishes have adopted a unique urea-based osmoregulation. To achieve this, their kidneys contribute importantly, and the nephron of cartilaginous fish shows quite complicated structure among vertebrates (Lacy and Reale 1985; Hentschel et al. 1998; Kakumura et al. 2015). Morphological and physiological investigations have been performed to understand the function of each nephron segment. Microperfusion and electrophysiological studies suggested that the early distal tubule (the third loop) is a segment for NaCl absorption (Friedman and Hebert 1990). However, function of each nephron segment, as well as mechanisms of reabsorption and secretion processes in the nephron, were still largely unknown when I started my PhD study. I addressed this problem by mapping of membrane transporters using the holocephalan elephant fish.

The cartilaginous fish kidney must have numerous functions related to reabsorption of useful materials and secretion of excess materials. In my PhD work, I focused on the SO_4^{2-} secretion (chapter 1) and the urea reabsorption (chapter 2).

The process of SO_4^{2-} secretion

To avoid hypersulfatemia, cartilaginous fish excrete sulfate from the kidney. In chapter 1, I identified two sulfate transporters abundantly expressed in the kidney, cmSlc26a1 and cmSlc26a6. The cmSlc26a1 is a basolateral electroneutral SO_4^{2-} transporter, while the cmSlc26a6 is an apical electrogenic Cl^-/SO_4^{2-} exchanger. Furthermore, the localization of cmSlc26a1 and cmSlc26a6 suggest that the proximal II (PII) segment in the second loop of nephron is the site of SO_4^{2-} secretion. The present result is consistent with that of the previous micropuncture study that demonstrated the secretion of divalent ions in the second loop of the little skate nephron (Stolte et al, 1977). The second loop of cartilaginous fish nephron is composed of multiple segments that are morphologically distinctive: the proximal segment Ib (PIb), PII, and the intermediate segment I in elephant fish nephron (Kakumura et al. 2015). The present results clearly determined that PII segment is the SO_4^{2-} secretory segment in the second loop.

In chapter 1, I proposed a hypothetical model for secretion of SO_4^{2-} in the elephant fish kidney. The driving force of SO_4^{2-} secretion via apically-located cmSlc26a6 is negative membrane potential generated by Na^+-K^+-ATPase (NKA), which is intensely co-localized in the PII segment (Kakumura et al. 2015). In addition, the concentration gradient for Cl^- also contributes to the driving force for SO_4^{2-} secretion via cmSlc26a6. Intense NKA and NaCl transporter signals were not detected in the proximal segment Ia (PIa) and PIb, the preceding nephron segments. In chapter 2, on the other hand, I discovered that the PIa segment is water permeable. Water is reabsorbed in the PIa segment following an osmotic gradient generated in the tubular bundle. Therefore, it is highly probable that, when filtrate flows into the PII segment, the concentration of Cl^- in the filtrate is considerably higher to that in plasma and primary filtrate. In chapter 1, I estimated a driving force using the Cl^- concentration of plasma. Although Cl^- concentration in the filtrate passing through the PII segment should be confirmed in future work, the value of driving force for SO_4^{2-}/Cl^- exchange most likely much higher than the value calculated in chapter 1.

The process of urea reabsorption via facilitative urea transporter

Most of the filtered urea is reabsorbed in the cartilaginous fish nephron. Marine cartilaginous fish kidney shows a number of anatomical features: 1) the kidney consists of multiple lobules and each lobule is separated into sinus zone and bundle zone; 2) a single nephron traverses repeatedly between the two zones and has an elaborate four-loop configuration and 3) in the bundle zone, the five tubules are enclosed in a sac-like peritubular sheath. These features are considered to be important for urea retention but the mechanism of urea reabsorption was largely unknown when I started my PhD study. An existence of secondarily-active transporting system, such as a sodium-coupled urea cotransporter and/or antiporter, was considered for the reabsorption of urea (Walsh and Smith 2001). Nevertheless, in the cartilaginous fish kidney, only facilitative urea

transporters (UT) have been identified (Smith and Wright 1999; Janech et al. 2003; 2006; 2008; Morgan et al. 2003; Hyodo et al. 2004; Kakumura et al. 2009).

In chapter 2, I identified segments of water reabsorption in the bundle tubules, and proposed the urea reabsorption model. In this model, I postulated three functionally separate segments: active NaCl reabsorbing, water permeable, and urea reabsorbing segments. These three segments are wrapped together by the peritubular sheath. The cells composing the sheath are connected to each other by tight junction, suggesting that the sheath acts as a barrier separating the microenvironment inside the sheath from the outside (Lacy and Reale1986). Inside the sheath, NaCl is actively reabsorbed from primary urine to the interstitial fluid, resulting in an increase of osmolality. The increased osmolality then drives reabsorption of water via AQPs from the filtrate to the interstitial fluid. In this way, a low-urea environment is considered to be generated inside the peritubular sheath. The mechanism that enables the 'uphill' transport of urea from the filtrate to the circulation had been a question over a period of years, because high concentration of urea already exists in the circulation. It is reasonable to say that the peritubular sheath and the three functional segments inside the sheath are key structures for urea reabsorption via facilitative UT.

The whole picture of urine production in elephant fish

In my PhD work, I revealed that the PII is the segment for SO_4^{2-} secretion, and that the first loop and the collecting tubule are permeable to water. Taken together with the previous studies, I here describe a whole picture of urine production in the elephant fish kidney. The first step of urine production is the ultrafiltration at the renal corpuscle. The glomerular filtrate flows into the neck segment, where ciliated cells propel the filtrate. The present study suggested that the neck segment is also water permeable but membrane transport in the neck segment remains to be clarified. The filtrate then flows into the proximal segment Ia (PIa) (Fig. IIB) that is comprised of the descending and ascending

limbs of the first loop of the bundle. The shallow portion of the ascending limb of the first loop did not show intense signals for cmAQP4, and I designated this as PIa2 segment, while the segment with intense cmAQP4 was assigned as PIa1. In the PIa1, water is reabsorbed from the filtrate via cmAQP4 to the interstitial fluid. In the mammalian nephron, nutrients are reabsorbed in the proximal tubules. Immunoreaction for Na^+-D-glucose transporter (homologous to sodium-driven, secondarily active glucose transporter 2) was found in the apical membrane of the PIa and PIb segments in the kidney of spiny dogfish (Kipp et al. 1997), suggesting the involvement of these segments in the bulk reabsorption of glucose also in cartilaginous fish. After leaving the bundle zone, the tubular diameter increased (PIb segment). In the PII segment, tubules have the largest tubular diameter with extremely high columnar cells compared to other segments. The PII is the longest segment forming the second loop in the sinus zone, and I suggested that this segment contributes to the secretion of excess SO_4^{2-} (most probably excess divalent ions) (Fig. IIC). Negative membrane potential generated by NKA and high concentration of Cl^- in the filtrate drive SO_4^{2-} secretion.

The filtrate subsequently flows into the bundle zone. The EDT expresses NKA and NKCC2, and works as a segment for active NaCl reabsorption (Fig. IID; Friedman and Hebert 1990; Kakumura et al. 2015). The reabsorbed NaCl most probably contributes to a driving force for the subsequent water reabsorption in the PIa segment. In the elephant fish kidney, the fourth loop (the late distal tubule, LDT) shows unique anatomical and functional features (Kakumura et al. 2015). The LDT run straight near the renal corpuscle, while it is convoluted around the tip of the loop. The ascending and descending limbs of the straight portion are closely opposed to each other and are arranged in a countercurrent fashion. In the anterior half of LDT, cmAQP3-1 and cmAQP3-2 are expressed (Kakumura 2013), while NKA and NKCC2 were expressed again in the posterior half of LDT (Kakumura et al. 2015). Therefore, it is considered that the filtrate diluted in the EDT is concentrated in the anterior part of LDT, and that the concentrated filtrate is then

diluted again in the posterior part of LDT (Fig. IIE). Reabsorbed NaCl from the posterior half of LDT most likely create a hyperosmotic environment that facilitates reabsorption of water in the anterior half of LDT. The filtrate containing high concentration of urea then flows into the collecting tubule. Urea is reabsorbed in the collecting tubule via facilitative urea transporter by the concentration gradient of urea as a driving force (Fig. IIF). Concomitant with the urea reabsorption, water is also reabsorbed in the collecting tubule. The water reabsorption in the collecting tubule results in an increase in concentration gradient of urea between the filtrate and the interstitial fluid, which further facilitates urea influx.

Kidney function in euryhaline elasmobranchs

Euryhaline teleost fishes, such as salmonids and eels, have been widely used for the research on body fluid regulation, since they can shift their body fluid regulation between FW and SW depending on the environmental salinity. However, most of cartilaginous fishes, including elephant fish, are stenohaline marine species. Only several species have been known as euryhaline elasmobranchs, and bull shark (*Carcharhinus leucas*) is a representative species. In SW environment, bull sharks conduct urea-based osmoregulation, as do other marine elasmobranch species (Pillans and Franklin 2004). On the other hand, even after they migrate into FW environment, they maintain high internal NaCl and urea levels and their body-fluid osmolality is over 600 mOsm, which is approximately twice as in FW teleosts (Pillans and Franklin 2004). For acclimation to FW environment, they have to change the function of osmoregulatory organs; in FW environment, they must excrete excess water from the kidney, while they need to absorb and retain ions and urea. Therefore, euryhaline elasmobranchs can be good models for understanding of kidney function in cartilaginous fish.

Recently, our group conducted a FW-transfer experiment of captive bull sharks in collaboration with Churaumi Aquarium, Okinawa. Using the kidney samples of FW-

acclimated and SW-acclimated bull sharks, I. Imaseki is doing comprehensive search of genes that change expression levels between FW and SW condition by the next generation sequencing (NGS). With regard to sulfate regulation, a downregulation of Slc26a1 mRNA expression has been observed (I. Imaseki and S. Hyodo, personal communication). This is reasonable because FW environment is a SO_4^{2-}-deficient habitat. The downregulation of Slc26a1 mRNA expression further imply that Slc26a1 is important for SO_4^{2-} excretion via kidney in SW environment.

In terms of water balance, FW-acclimated bull sharks have to excrete excess water from the kidney, suggesting that water reabsorption in the nephron is considered to be downregulated. Consistent with this idea, the results of NGS demonstrated that expression of AQP3 mRNA decreased after transfer from SW to FW (Imaseki, personal communication). In the elephant fish kidney, AQP3 is expressed in the anterior half of the late distal tubule, and is considered to contribute to urine concentration (Kakumura 2013). On the other hand, expression of AQP4 mRNA was higher in FW-acclimated bull sharks compared to that in SW-acclimated bull sharks (Imaseki, personal communication). Given that bull sharks have to excrete diluted urine in FW environment, the upregulation of AQP4 seems to be strange. In chapter 2, however, I showed that cmAQP4 is localized in the PIa1 segment in the bundle zone, and that cmAQP4 in the PIa1 segment contributes to urea reabsorption process. The water reabsorption from the PIa1 segment generates a low-urea environment in the tubular bundle, which in turn drives urea reabsorption from the collecting tubule. Since the plasma of bull shark contains high concentration of urea even in FW (Pillans and Franklin 2004), the demand of urea reabsorption is most probably very high.

As mentioned above, future investigation on euryhaline bull shark will make a breakthrough in the research of cartilaginous fish kidney function. Stenohaline freshwater stingray (Potamotrygonidae) will also serve as another important model fish. Freshwater stingray does not use urea as an osmolyte, and thus their plasma composition is similar to

those of FW teleosts (Wood et al. 2002). The nephron of freshwater stingray has only two loops and lacks a peritubular sheath (Lacy et al. 1989).

Unity and diversity of nephron structure and function among vertebrates

As mentioned above, cartilaginous fish kidneys have unique features in their structure and function. In the last part of my thesis, I discuss about unity and diversity of nephron structure and function, by comparing nephron of cartilaginous fishes with that of teleosts and mammals.

In teleost fishes, the major role of kidney in SW environment is excretion of divalent ions including SO_4^{2-}; SO_4^{2-} is secreted from the proximal tubule (Hickman and Trump 1969; Renfro et al. 1999; Pelis and Renfro 2004; Marshall and Grosell 2006; Kato et al. 2009). This is common among marine teleosts, irrespective of the ability to tolerate different salinities: euryhaline species (Fig. IIIB), stenohaline species (Fig. IIIC, Dantzler 2003), and stenohaline species having aglomerular nephron (Fig. IIID, Beyenbach 2004). In chapter 1, I identified that the proximal II segment secrete excess SO_4^{2-} in the cartilaginous fish nephron. In the elephant fish nephron, the proximal tubule can be separated into morphologically and functionally different three segments: other proximal segments (PIa and PIb) do not contribute to SO_4^{2-} secretion. Also in the Japanese eel kidney, the proximal tubule was separated into two parts. However, different from the elephant fish nephron, both of two proximal segments are considered to contribute to SO_4^{2-} secretion in the Japanese eel nephron (Watanabe and Takei 2011). These results imply that the site and the process of excess SO_4^{2-} (or divalent ions) secretion are most likely common among marine fishes (Fig. III). The PIa and PIb segments in the cartilaginous fish kidney are considered to be additional proximal segments that are necessary for reabsorption of useful materials unique to cartilaginous fish nephron.

A characteristic of the mammalian nephron is the countercurrent configuration. The countercurrent multiplier system creates an osmotic gradient from the cortex to the inner

medulla; osmolality of interstitial fluid in the inner medulla is considerably higher than that of plasma (Kokko and Tisher 1976). The extremely high osmolality in the inner medulla is critical for water reabsorption (water retention) (Fig. IVB). Meanwhile, as mentioned before, a single nephron of cartilaginous fish has an elaborate four-loop configuration, and in the bundle zone, the resulting five tubules are enclosed in a sac-like peritubular sheath. Therefore, the five tubules in the bundle zone have been considered to comprise a countercurrent system, as do mammalian nephrons, and the countercurrent-like configuration has been considered to be important for urea reabsorption. However, no evidence has been obtained whether countercurrent multiplier and/or exchange systems exist in the cartilaginous fish nephron, and whether there is an osmotic gradient inside the peritubular sheath. Instead of the osmotic gradient inside the sheath, in chapter 2, I proposed the existence of low-urea environment inside the sheath, and the low-urea interstitial fluid drives urea movement via facilitative urea transporter, resulting in "uphill" urea reabsorption (Fig. IVA). The water reabsorption in the mammalian kidney and the urea reabsorption in the cartilaginous fish kidney are both via passive transport system. Although the mechanisms that create driving force for the passive water and urea transports are different between the mammalian kidney and the cartilaginous fish kidney, the concept that the generation of special microenvironment for subsequent passive transport is considered to be similar between the mammalian kidney and the cartilaginous fish kidney.
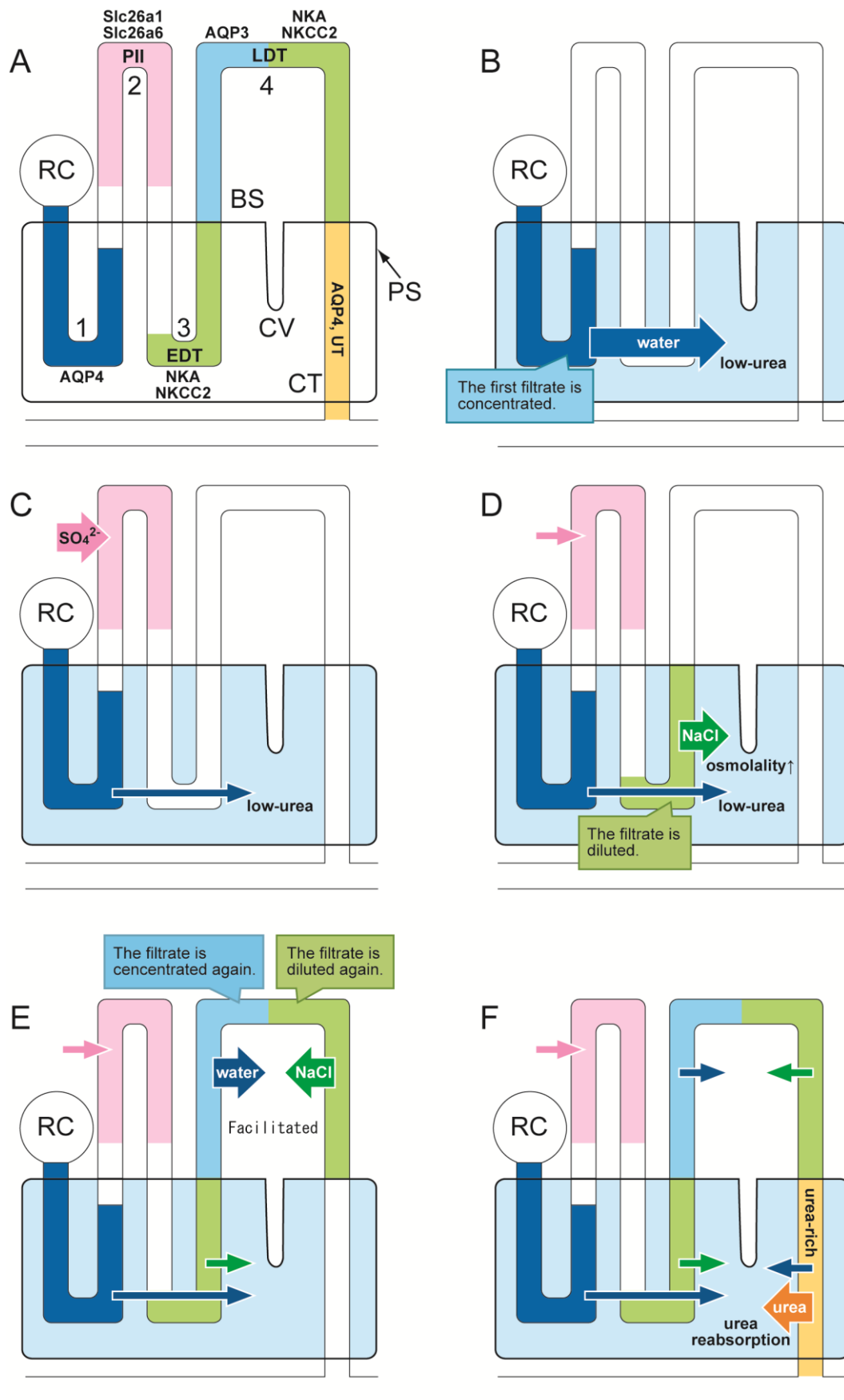
Fig. II. Schematic diagram showing a model for production of urine in elephant fish. (A) Localization of transporting molecules. AQP, aquaporin; NKA, Na^+/K^+-ATPase; NKCC2, Na^+-K^+-$2Cl^-$ cotransporter type-2; facilitative urea transporter; RC, renal corpuscle; PII, proximal II; EDT, early distal tubule; LDT, late distal tubule; CT, collecting tubule; PS, peritubular sheath; CV, central vessel; BS, blood sinuses. (B) as the first step, water is reabsorbed from the primary filtrate via AQP4 (blue arrow). The primary filtrate is concentrated, while fluid in the peritubular sheath is diluted. (C) Sulfate is secreted from the PII segment using concentration gradient of Cl^- as a driving force (pink arrow). (D) NaCl is actively reabsorbed into the interstitium from the EDT (green arrow). Osmolality of interstitial fluid is increased inside the peritubular sheath, while the filtrate is diluted. (E) In the anterior part of LDT, water is reabsorbed from the diluted filtrate (blue arrow). Then, active NaCl reabsorption occurs again in the posterior part of LDT (green arrow). (F) As a result, urea in the filtrate is highly concentrated. Urea is reabsorbed from the urea-rich filtrate to the low-urea interstitial fluid (orange arrow).
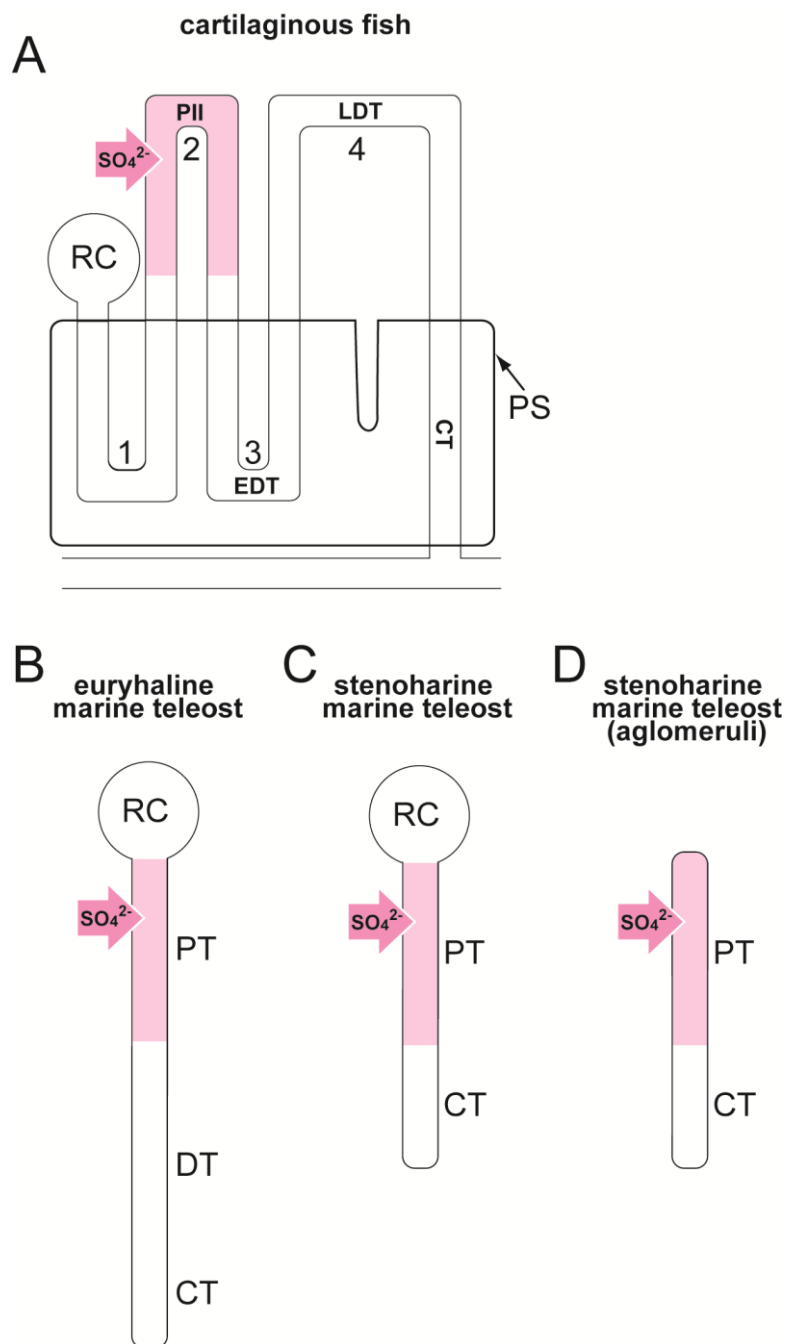
Fig. III. Comparison of the cartilaginous fish nephron with the marine teleost nephrons. Sulfate secretion occurs in the proximal tubule II (PII) in cartilaginous fish (A), while in the proximal tubule (PT) in euryhaline teleosts in SW environment (B), stenohaline marine teleosts (C) and aglomerular nephron in stenohaline marine teleost (D) (pink arrow). RC, renal corpuscle; EDT, early distal tubule; LDT, late distal tubule; PS, peritubular sheath; DT, distal tubule; CT, collecting tubule.
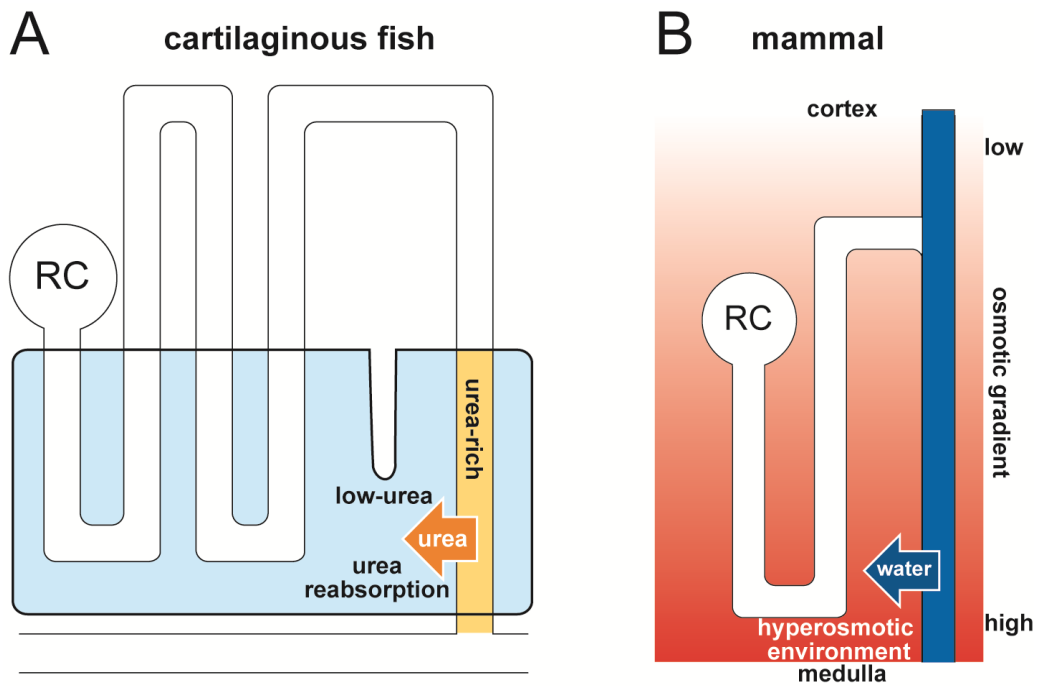
Fig. IV. Comparison of the cartilaginous fish nephron with the mammalian nephron. (A) Cartilaginous fish most likely creates a low-urea environment inside the sheath for urea reabsorption (orange arrow). (B) In mammals, the osmotic gradient exists from the cortex to the inner medulla. The resulting hyperosmotic environment in the inner medulla is required for water reabsorption (blue arrow) from the collecting duct (blue tubule). RC, renal corpuscle.

Acknowledgements

First of all, I would like to express my deepest gratitude to Prof. Susumu Hyodo, my academic supervisor, associate professor of the Laboratory of Physiology in the Atmosphere and Ocean Research Institute (AORI), The University of Tokyo. I deeply appreciate his invaluable supports and warm encouragement during my master's and PhD course. I have learned many important things for science research, including attitude, knowledge and technique, from him. I am proud to be a PhD student of him.

I am sincerely grateful to Prof. Yoshio Takei, the head of the Laboratory of Physiology in the AORI. I appreciate a lot of his valuable comments. I was impressed with his comprehensive knowledge and enthusiasm on research.

I would like to express my sincere gratitude to Mrs. Sanae Ogasawara, who taught me how to measure parameters of body fluid and urine. I really appreciate her kind supports and warm encouragement.

I am grateful to Asst. Prof. Makoto Kusakabe for his supports, valuable comments and warm encouragement.

I am grateful to Prof. Akira Kato for his valuable discussions and support in the functional analysis of sulfate transporters and the scan of slides. I also appreciate his warm encouragement.

I would like to express my gratitude to Prof. John A. Donald, Prof. Tes Toop and Dr. Justin D. Bell for their kind support in sampling adult fish and eggs of elephant fish. Particularly, I deeply thank Dr. Donald for his valuable discussion and comments on my manuscripts and research.

I am grateful to Dr. Taro Watanabe, who taught me how to measure parameters of body fluid and urine, for many technical supports on my study.

I would like to express my gratitude to Prof. Michael F. Romero for his critical

References

Abramoff MD, Magelhaes PJ, Ram SJ. "Image Processing with ImageJ". *Biophotonics Int* 11: 36-42, 2004.

Alper SL, Sharma AK. The SLC26 gene family of anion transporters and channels. *l Aspects Med* 34:494-515, 2013.

Althoff T, Hentschel H, Luig J, Schutz H, Kasch M, Kinne RKH. Na$^+$-D-glucose cotransporter in the kidney of *Squalus acanthias*: molecular identification and intrarenal distribution. *Am J Physiol Regul Integr Comp Physiol* 290: R1094–R1104, 2006.

Anderson PM. Glutamine- and *N*-acetylglutamate-dependent carbamoyl phosphate synthetase in elasmobranchs. *Science* 208:291-293, 1980.

Baustian MD, Beyenbach KW. Natriuretic peptides and the acclimation of aglomerular toadfish to hypo-osmotic media. *J Comp Physiol B* 169:507-14, 1999.

Beyenbach KW, Liu PL. Mechanism of fluid secretion common to aglomerular and glomerular kidneys. *Kidney Int* 49: 1543-1548, 1996.

Beyenbach KW, Petzel DH, Cliff WH. Renal proximal tubules of flounder. I. Physiological properties. *Am J Physiol Regul Integr Comp Physiol* 250:R608-R615, 1986.

Beyenbach KW. Kidneys sans glomeruli. *Am J Physiol Renal Physiol* 286: F811-F827, 2004.

Biemesderfer D, Payne JA, Lytle CY, Forbush B III. Immunocytochemical studies of the Na-K-Cl cotransporter of shark kidney. *Am J Physiol Renal Fluid Electrolyte Physiol* 270:F927-F936, 1996.

Borghese E. Studies on the nephrons of an elasmobranch fish *Scyliorhinus stellaris* (L.). *Z Zellforsch Mikrosk Abat* 72: 88-99, 1966.

Boylan J. Gill permeability in *Squalus acanthias*. In: sharks, skales and rays, edited by

Gilbert PW, Mathewson RF, Rall DP, John Hopkins, 1967, p. 197–206.

Brown EJ, Dantzler WH. Vertebrate renal system. *Handbook of Physiology - Comparative physiology* 1:481-576, 1997.

Burger JW, Hess WN. Function of the rectal gland in the spiny dogfish. *Science* 131: 670-671, 1960.

Burger JW. Problems in the electrolyte economy of the spiny dogfish *Squalus acanthias*. In: sharks, skales and rays, edited by Gilbert PW, Mathewson RF, Rall DP, John Hopkins, 1967, p. 177-185.

Cassola AC, Mollenhauer M, Fromter E. The intracellular chloride activity of rat kidney proximal tubular cells. *Pflügers Arch* 399: 259–265, 1983.

Choe KP, Edwards SL, Claiborne JB, Evans DH. The putative mechanism of Na^+ absorption in euryhaline elasmobranchs exists in the gills of a stenohaline marine elasmobranch, *Squalus acanthias*. *Comp Biochem Physiol A* 146: 155–162, 2007.

Choe KP, Kato A, Hirose S, Plata C, Sindic A, Romero MF, Claiborne JB, Evans DH. NHE3 in an ancestral vertebrate: primary sequence, distribution, localization, and function in gills. *Am J Physiol Regul Integ Comp Physiol* 289:R1520–R1534, 2005.

Clarke RW, Smith HW. Absorption and excretion of water and salts by the elasmobranch fishes III. The use of xylose as a measure of the glomerular filtrate in *Squalus acanthias*. *J Cell Comp Physiol* 1:131–143, 1932.

Crofts DR. The comparative morphology of the caecal gland (rectal gland) of selachian fishes, with some reference to the morphology and physiology of the similar intestinal appendage throughout Ichthyopsida and Sauropsida. *Proc Zool Soc* 95:101-188, 1925.

Cutler CP, Harmon S, Walsh J, Burch K. Characterization of aquaporin4 protein expression and localization in tissues of the dogfish (*Squalus acanthias*). *Front Physiol* 3:21, 2012a.

Cutler CP, MacIver B, Cramb G, Zeidel M. Aquaporin 4 is a ubiquitously expressed isoform in the dogfish (*Squalus acanthias*) shark. *Front Physiol* 2:107, 2012b.

Dantzler WH. Regulation of renal proximal and distal tubule transport: sodium, chloride and organic anions. *Comp Biochem Physiol A Mol Integr Physiol* 136:453-78, 2003.

Deetjen P, Antkowiak D, Boylan JW. Urea reabsorption by the skate nephron: micropuncture of collecting ducts in *Raja erinacea*. *Bull Mt Desert Isl Biol Lab* 12:28-29, 1972.

Didier DA, LeClair EE, Vanbuskirk DR. Embryonic staging and external features of development of the Chimaeroid fish, *Callorhinchus milii* (Holocephali, Callorhinchidae). *J Morphol* 236:25-47, 1998.

Fange R, Fugelli K. The rectal salt gland of elasmobranchs, and osmoregulation in chimaeroid fishes. *Sarsia* 10:27-34, 1963.

Fines GA, Ballantyne JS, Wright PA. Active urea transport and an unusual basolateral membrane composition in the gills of a marine elasmobranch. *Am J Physiol Regul Integr Comp Physiol* 280:R16-R24, 2001.

Finn RN, Chauvigné F, Hlidberg JB, Cutler CP, Cerdà J. The lineage-specific evolution of aquaporin gene clusters facilitated tetrapod terrestrial adaptation. *PLoS One* 26:9, 2014.

Friedman PA, Hebert SC. Diluting segment in kidney of dogfish shark I. Localization and characterization of chloride absorption. *Am J Physiol* 258:R398-R408, 1990.

Friedman PA, Hebert SC. Diluting segment in kidney of dogfish shark I. Localization and characterization of chloride absorption. *Am J Physiol Regul Integr Comp Physiol* 258: R398–R408, 1990.

Fushimi K, Uchida S, Hara Y, Hirata Y, Marumo F, Sasaki S. Cloning and expression of apical membrane water channel of rat kidney collecting tubule. *Nature* 361:549-552, 1993.

Gamba G, Miyanoshita A, Lombardi M, Lytton J, Lee WS, Hediger MA, Hebert SC. Molecular cloning, primary structure, and characterization of two members of the mammalian electroneutral sodium-(potassium)-chloride cotransporter family expressed in kidney. *J Biol Chem* 269:17713-17722, 1994.

Gibson MM, Bagga DA, Miller CG, Maguire ME. Magnesium transport in Salmonella typhimurium: the influence of new mutations conferring Co^{2+} resistance on the CorA Mg^{2+} transport system. *Mol Microbiol* 5: 2753-2762, 1991.

Gordon MS, Schmidt-Nielsen K, Kelly HM. Osmotic Regulation in the Crab-Eating Frog (*Rana Cancrivora*). *J Exp Biol* 38: 659-678, 1961.

Griffith RW, Umminger BL, Grant BF, Pang PK, Pickford GE. Serum composition of the coelacanth, *Latimeria chalumnae* Smith. *J Exp Zool* 187: 87-102, 1974.

Hasegawa H, Ma T, Skach W, Matthay MA, Verkman AS. Molecular cloning of amercurial-insensitive water channel expressed in selected water- transporting tissues. *J Biol Chem* 269:5497-5500, 1994.

Hasler U, Leroy V, Martin PY, Fféraille E. Aquaporin-2 abundance in the renal collecting duct: new insights from cultured cell models. *Am J Physiol Renal Physiol* 297:F8-10, 2009.

Hebert SC, Friedman PA. Diluting segment in kidney of dogfish shark. II. Electrophysiology of apical membranes and cellular resistances. *Am J Physiol Regul Integr Comp Physiol* 258:R409-R417, 1990.

Hebert SC, Mount DB, Gamba G. Molecular physiology of cation-coupled Cl-cotransport: the SLC12 family. *Pflugers Arch* 447:580-593, 2004.

Hentschel H, Storb U, Teckhaus L, Elger M. The central vessel of the renal countercurrent bundles of two marine elasmobranchs-dogfish (*Scyliorhinus caniculus*) and skate (*Raja erinacea*)-as revealed by light and electron microscopy with computer-assisted reconstruction. *Anat Embryol* 198:73-89, 1998.

Hentschel H. Developing nephrons in adolescent dogfish, *Scyliorhinus caniculus* (L.),

with reference to ultrastructure of early stages, histogenesis of the renal countercurrent system, and nephron segmentation in marine elasmobranchs. *Am J Anat* 190:309-333, 1991.

Hickman CP, Trump BF. Fish physiology, Vol I In: *The kidney*, edited by Hoar WS, Randall DJ, Academic Press, New York, pp91:239, 1969.

Hickman CP. Urine composition and kidney tubular function in southern flounder, *Paralichthys lethostigma*, in seawater. *Can J Zool* 46: 439-55, 1968.

Hyodo S, Bell JD, Healy JM, Kaneko T, Hasegawa S, Takei Y, Donald JA, Toop T. Osmoregulation in elephant fish *Callorhinchus milii* (Holocephali), with special reference to the rectal gland. *J Exp Biol* 210:1303-1310, 2007.

Hyodo S, Kakumura K, Takagi W, Hasegawa K, Yamaguchi Y. Morphological and functional characteristics of the kidney of cartilaginous fishes: with special reference to urea reabsorption. *Am J Physiol Regul Integr Comp Physiol* 307:R1381-R1395, 2014.

Hyodo S, Kato F, Kaneko T, Takei Y. A facilitative urea transporter is localized in the renal collecting tubule of the dogfish *Triakis scyllia*. *J Exp Biol* 207:347-356, 2004.

Hyodo S, Tsukada T, Takei Y. Neurohypophysial hormones of dogfish, *Triakis scyllium*: structures and salinity-dependent secretion. *Gen Comp Endocrinol* 138:97-104, 2004.

Ishibashi K, Kondo S, Hara S, Morishita Y. The evolutionary aspects of aquaporin family. *Am J Physiol Regul Integr Comp Physiol* 300:R566-R576, 2011.

Ishibashi K, Sasaki S, Yoshiyama N. Intracellular chloride activity of rabbit proximal straight tubule perfused in vitro. *Am J Physiol Renal Fluid Electrolyte Physiol* 255: F49–F56, 1988.

Islam Z, Hayashi N, Inoue H, Umezawa T, Kimura Y, Doi H, Romero MF, Hirose S, Kato A. Identification and lateral membrane localization of cyclin M3, likely to be involved in renal Mg^{2+} handling in seawater fish. *Am J Physiol Regul Integr*

Comp Physiol 307:R525-R537, 2014.

Islam Z, Hayashi N, Yamamoto Y, Doi H, Romero MF, Hirose S, Kato A. Identification and proximal tubular localization of the Mg^{2+} transporter, Slc41a1, in a seawater fish. *Am J Physiol Regul Integr Comp Physiol* 305:R385-R396, 2013.

Janech MG, Fitzgibbon WR, Chen R, Nowak MW, Miller DH, Paul RV, Ploth DW. Molecular and functional characterization of a urea transporter from the kidney of the Atlantic stingray. *Am J Physiol Renal Physiol* 284: F996–F1005, 2003.

Janech MG, Fitzgibbon WR, Nowark MW, Miller DH, Paul RV, Ploth DW. Cloning and functional characterization of a second urea transporter from the kidney of the Atlantic stingray, *Dasyatis sabina*. *Am J Physiol Regul Integr Comp Physiol* 291: R844–R853, 2006.

Janech MG, Gefroh HA, Cwengros EE, Sulikowski JA, Ploth DW, Fitzgibbon WR. Cloning of urea transporters from the kidneys of two batoid elasmobranchs: evidence for a common elasmobranch urea transporter protein. *Mar Biol* 153: 1173-1179, 2008.

Jones P, Binns D, Chang HY, Fraser M, Li W, McAnulla C, McWilliam H, Maslen J, Mitchell A, Nuka G, Pesseat S, Quinn AF, Sangrador-Vegas A, Scheremetjew M, Yong SY, Lopez R, Hunter S. InterProScan 5: genome-scale protein function classification. *Bioinformatics* 30:1236-1240, 2014.

Jung JS, Bhat RV, Preston GM, Guggino WB, Baraban JM, Agre P. Molecular characterization of an aquaporin cDNA from brain: candidate osmoreceptor and regulator of water balance. *Proc Natl Acad Sci U S A* 91:13052-13056, 1994.

Kajimura M, Walsh PJ, Mommsen TP, Wood CM. The dogfish shark (*Squalus acanthias*) increases both hepatic and extrahepatic ornithine urea cycle enzyme activities for nitrogen conservation after feeding. *Physiol Biochem Zool* 79:602-613, 2006.

Kakumura K, Takabe S, Takagi W, Hasegawa K, Konno N, Bell JD, Toop T,

Donald JA, Kaneko T, Hyodo S. Morphological and molecular investigations of the holocephalan elephant fish nephron: the existence of a countercurrent-like configuration and two separate diluting segments in the distal tubule. *Cell Tissue Res* in press, 2015.

Kakumura K, Watanabe S, Bell JD, Donald JA, Toop T, Kaneko T, Hyodo S. Multiple urea transporter proteins in the kidney of holocephalan elephant fish (*Callorhinchus milii*). *Comp Biochem Physiol B Biochem Mol Biol* 154:239-47, 2009.

Kakumura K. A molecular mechanism for urea reabsorption in the cartilaginous fish kidney. The University of Tokyo. 2013.

Kaneko T, Watanabe S, Lee KM. Functional Morphology of Mitochondrion-Rich Cells in Euryhaline and Stenohaline Teleosts. *Aqua-BioScience Monographs* 1:1-62, 2008.

Karniski LP, Lötscher M, Fucentese M, Hilfiker H, Biber J, Murer H. Immunolocalization of sat-1 sulfate/oxalate/bicarbonate anion exchanger in the rat kidney. *Am J Physiol Renal Physiol* 275:F79-F87, 1998.

Kato A, Chang MH, Kurita Y, Nakada T, Ogoshi M, Nakazato T, Doi H, Hirose S, Romero MF. Identification of renal transporters involved in sulfate excretion in marine teleost fish. *Am J Physiol Regul Integr Comp Physiol* 297:R1647-R1659, 2009.

Katoh F, Tresguerres M, Lee KM, Kaneko T, Aida K, Goss GG. Cloning of rainbow trout SLC26A1: involvement in renal sulfate secretion. *Am J Physiol Regul Integr Comp Physiol* 290:R1468-R1478, 2006.

Kempton RT. Studies on the elasmobranch kidney. II. Reabsorption of urea by the smooth dogfish, *Mustelus canis. Biol Bull* 104:45-56, 1953.

Kipp H, Kinne-Saffran E, Bevan C, Kinne RK. Characteristics of renal Na^+-D-glucose cotransport in the skate (*Raja erinacea*) and shark (*Squalus acanthias*). *Am*

J Physiol Regul Integr Comp Physiol 273: R134– R142, 1997.

Knauf F, Yang CL, Thomson RB, Mentone SA, Giebisch G, Aronson PS. Identification of a chloride-formate exchanger expressed on the brush border membrane of renal proximal tubule cells. *Proc Natl Acad Sci USA* 98:9425-9430, 2001.

Kokko JP, Tisher CC. Water movement across nephron segments involved with the countercurrent multiplication system. *Kidney Int* 10:64-81, 1976.

Krapf R, Berry CA, Verkman AS. Estimation of intracellular chloride activity in isolated perfused rabbit proximal convoluted tubules using a fluorescent indicator. *Biophys J* 53: 955–962, 1988.

Krick W, Schnedler N, Burckhardt G, Burckhardt BC. Ability of sat-1 to transport sulfate, bicarbonate, or oxalate under physiological conditions. *Am J Physiol Renal Physiol* 297:F145-F154, 2009.

Kuo SM, Aronson PS. Oxalate transport via the sulfate/HCO_3 exchanger in rabbit renal basolateral membrane vesicles. *J Biol Chem* 263:9710-9717, 1988.

Lacy ER, Reale E, Grabowski GM, Mackanos LA. Freshwater elasmobranchs do not have a renal counter-current system. Anat Rec 223: 64A, 1989.

Lacy ER, Reale E. The elasmobranch kidney I. Gross anatomy and general distribution of the nephrons. *Anat Embryol* 173:23-34, 1985b.

Lacy ER, Reale E. The elasmobranch kidney II. Sequence and structure of the nephrons. *Anat Embryol* 173:163-186, 1985a.

Lacy ER, Reale E. The elasmobranch kidney. III. Fine structure of the peritubular sheath in the elasmobranch kidney. *Anat Embryol* 173:299-305, 1986.

Lagios M D, Stasko-Concannon S. Ultrastructure and ATPase acrivity of the rectal gland of the chondrichthyean fish *Hydrolagus colliei* (Holocephali). *Cell Tissue Res* 198:287-294, 1979.

Lee A, Beck L, Markovich D. The mouse sulfate anion transporter gene Sat1

(Slc26a1): cloning, tissue distribution, gene structure, functional characterization, and transcriptional regulation thyroid hormone. *DNA Cell Biol* 22:19-31, 2003.

Leydig F. Zur Anatomie und Histologie der Chimaera monstrosa. *Arch Anat Physiol* 18:241-271, 1851.

Li S, Kato A, Takabe S, Chen AP, Romero MF, Umezawa T, Nakada T Hyodo S, Hirose S. Expression of a novel isoform of Na$^+$/H$^+$ exchanger 3 (NHE3) in the kidney and intestine of banded houndshark *Triakis scyllium*. *Am J Physiol Regul Integr Comp Physiol* 304:R865-R876, 2013

Markovich D, Aronson PS. Specificity and regulation of renal sulfate transporters. *Annu Rev Physiol* 69:361-375, 2007.

Markovich D. Physiological roles and regulation of mammalian sulfate transporters. *Physiol Rev* 81:1499-1533, 2001.

Markovich D. Slc13a1 and Slc26a1 KO models reveal physiological roles of anion transporters. *Physiology (Bethesda)* 27: 7-14, 2012.

Marshall WS, Grosell M. Ion transport, osmoregulation, and acid-base balance. In: The physiology of fishes, edited by Evans D and Claiborne JB: CRC Press, 2006, p. 177-230.

McCurley AT, Callard GV. Characterization of housekeeping genes in zebrafish: male-female differences and effects of tissue type, developmental stage and chemical treatment. *BMC Mol Biol* 9: 102, 2008.

Morgan RL, Ballantyne JS, Wright PA. Regulation of a renal urea transporter with reduced salinity in a marine elasmobranch, *Raja erinacea*. *J Exp Biol* 206:3285-3292, 2003.

Nakada T, Westhoff CM, Yamaguchi Y, Hyodo S, Li X, Muro T, Kato A, Nakamura N, Hirose S. Rhesus glycoprotein p2 (Rhp2) is a novel member of the Rh family of ammonia transporters highly expressed in shark kidney. *J Biol Chem* 285: 2653–2664, 2010.

Nakada T, Zandi-Nejad K, Kurita Y, Kudo H, Broumand V, Kwon CY, Mercado A, Mount DB, Hirose S. Roles of Slc13a1 and Slc26a1 sulfate transporters of eel kidney in sulfate homeostasis and osmoregulation in freshwater. *Am J Physiol Regul Integr Comp Physiol* 289:R575-R585, 2005.

Pelis RM, Renfro JL. Role of tubular secretion and carbonic anhydrase in vertebrate renal sulfate excretion. *Am J Physiol Regul Integr Comp Physiol* 287:R491-R501, 2004.

Petrovic S, Ma L, Wang Z, and Soleimani M. Identification of an apical Cl^-/HCO_3^- exchanger in rat kidney proximal tubule. *Am J Physiol Cell Physiol* 285: C608-C617, 2003.

Piermarini PM, Verlander JW, Royaux IE, Evans DH. Pendrin immunoreactivity in the gill epithelium of a euryhaline elasmobranch. *Am J Physiol Regul Integr Comp Physio* 283: R983–R992, 2002.

Pillans RD, Franklin CE. Plasma osmolyte concentrations and rectal gland mass of bull sharks *Carcharhinus leucas*, captured along a salinity gradient. *Comp Biochem Physiol A Mol Integr Physiol* 138: 363-371, 2004.

Preston GM, Carroll TM, Guggino WB, Agre P. Appearance of water channels in *Xenopus* expressing red cell CHIP28 protein. *Science* 256: 385-387, 1992.

Pritchard JB, Renfro JL. Renal sulfate transport at the basolateral membrane is mediated by anion exchange. *Proc Natl Acad Sci USA* 80:2603-2607, 1983.

Pärt P, Wright PA, Wood CM. Urea and water permeability in dogfish (*Squalus acanthias*) gills. *Comp Biochem Physiol* 119A: 117–123, 1998.

Read LJ. Chemical constituents of body fluids and urine of the holocephalan *Hydrolagus colliei*. *Comp Biochem Physiol* A39:185-192, 1971.

Regeer RR, Lee A, Markovich D. Characterization of the human sulfate anion transporter (hsat-1) protein and gene (SAT1; SLC26A1). *DNA Cell Biol* 22: 107-117, 2003.

Renfro JL, Maren TH, Zeien C, and Swenson ER. Renal sulfate secretion is carbonic anhydrase dependent in a marine teleost, *Pleuronectes americanus. Am J Physiol Renal Physiol* 276:F288-F294, 1999.

Rojek A, Praetorius J, Frokiaer J, Nielsen S, Fenton RA. A current view of the mammalian aquaglyceroporins. *Annu Rev Physiol* 70:301-327, 2008.

Romero MF, Fong P, Berger UV, Hediger MA, Boron WF. Cloning and functional expression of rNBC, an electrogenic Na^+-HCO_3^- cotransporter from rat kidney. *Am J Physiol* 274:F425-432, 1998.

Romero MF, Henry D, Nelson S, Harte PJ, Dillon AK, Sciortino CM. Cloning and characterization of a Na^+-driven anion exchanger (NDAE1). A new bicarbonate transporter. *J Biol Chem* 275:24552-24559, 2000.

Satoh H, Susaki M, Shukunami C, Iyama K, Negoro T, and Hiraki Y. Functional analysis of diastrophic dysplasia sulfate transporter. Its involvement in growth regulation of chondrocytes mediated by sulfated proteoglycans. *J Biol Chem* 273: 12307-12315, 1998.

Schmidt-Nielsen B, Truniger B, Rabinowitz L. Sodium-linked urea transport by the renal tubule of the spiny dogfish Squalus acanthias. *Comp Biochem Physiol* 42A: 13-25, 1972.

Schmidt-Nielsen B, Ullrich KJ, Rumrich G, Long WS. Micropuncture study of urea movements across the renal tubules of *Squalus acanthias. Bull Mt Desert Isl Biol Lab* 6:35, 1966.

Schwartz FJ, Maddock MB. Cytogenetics of the elasmobranchs: genome evolution and phylogenetic implications. *Mar Freshwater Res* 53:491-502, 2002.

Shuttleworth TJ. Salt and water balance – Extrarenal mechanisms. In: The Physiology of the Elasmobranch Fishes, edited by Shuttleworth TJ, Boca Raton, FL: CRC Press, 1988, p. 171–199.

Smith CP, Wright PA. Molecular characterization of an elasmobranch urea transporter.

Am J Physiol Regul Integr Comp Physiol 276:R622-R626, 1999.

Smith HW. The absorption and excretion of water and salts by the elasmobranch fishes. II. Marine elasmobranchs. *Am J Physiol* 98: 296-310, 1931.

Smith HW. The composition of the body fluids of elasmobranchs. *J Biol Chem* 81:407-419, 1929.

Smith HW. The retention and physiological role of urea in the Elasmobranchii. *Blot Rev* 11:49-82, 1936.

Stolte H, Galaske RG, Eisenbach GM, Lechene C, Schmidt-Nielsen B, Boylan JW. Renal tubule ion transport and collecting duct function in the elasmobranch little skate, *Raja erinacea*. *J Exp Zool* 199:403-410, 1977.

Stolte H, Galaske RG, Eisenbach GM, Lechene C, Schmidt-Nielsen B, Boylan JW. Renal tubule ion transport and collecting duct function in the elasmobranch little skate, *Raja erinacea*. *J Exp Zool* 199:403-410, 1977.

Swenson ER, Fine AD, Maren TH, Reale E, Lacy ER, Smolka AJ. Physiological and immunocytochemical evidence for a putative H-KATPase in elasmobranch renal acid secretion. *Am J Physiol Renal Fluid Electrolyte Physiol* 267:F639–F645, 1994.

Takabe S, Teranishi K, Takaki S, Kusakabe M, Hirose S, Kaneko T, Hyodo S. Morphological and functional characterization of a novel Na^+/K^+-ATPase-immunoreactive, follicle-like structure on the gill septum of Japanese banded houndshark, *Triakis scyllium*. *Cell Tissue Res* 348:141–153, 2012.

Takagi W, Kajimura M, Bell JD, Toop T, Donald JA, Hyodo S. Hepatic and extrahepatic distribution of ornithine urea cycle enzymes in holocephalan elephant fish (*Callorhinchus milii*). *Comp Biochem Physiol B* 161: 331–340, 2012.

Takagi W, Kajimura M, Tanaka H, Hasegawa K, Bell JD, Toop T, Donald JA, Hyodo S. Urea-based osmoregulation in the developing embryo of oviparous cartilaginous fish (*Callorhinchus milii*): contribution of the extraembryonic yolk sac during the early developmental period. *J Exp Biol* 217:1353-1362, 2014.

Tam WL, Wong WP, Loong AM, Hiong KC, Chew SF, Ballantyne JS, Ip YK. The osmotic response of the Asian freshwater stingray (*Himantura signifer*) to increased salinity: a comparison with marine (*Taeniura lymma*) and Amazonian freshwater (*Potamotrygon motoro*) stingrays. *J. Exp. Biol* 206: 2931-2940, 2003.

Terris J, Ecelbarger CA, Marples D, Knepper MA, Nielsen S. Distribution of aquaporin-4 water channel expression within rat kidney. *Am J Physiol Renal Fluid Electrolyte Physiol* 269:F775-F785, 1995.

Thompson JD, Higgins DG, Gibson TJ. CLUSTAL W: improving the sensitivity of progressive multiple sequence alignment through sequence weighting, position-specific gap penalties and weight matrix choice. *Nucleic Acids Res* 22: 4673-4680, 1994.

Tingaud-Sequeira A, Calusinska M, Finn RN, Chauvigné F, Lozano J, Cerdà J. The zebrafish genome encodes the largest vertebrate repertoire of functional aquaporins with dual paralogy and substrate specificities similar to mammals. *BMC Evol Biol.* 10:38, 2010.

Tresguerres M, Katoh F, Fenton H, Jasinska E, Goss GG. Regulation of branchial V-H$^+$-ATPase Na$^+$/K$^+$-ATPase and NHE2 in response to acid and base infusions in the Pacific spiny dogfish (*Squalus acanthias*). *J Exp Biol* 208:345–354, 2004.

Venkatesh B, Kirkness EF, Loh YH, Halpern AL, Lee AP, Johnson J, Dondona N, Viswanathan LD, Tay A, Venter JC, Strausberg RL, Brenner S. Survey sequencing and comparative analysis of the elephant shark (*Callorhinchus milii*) genome. *PLoS Biol* 5:932-944, 2007.

Venkatesh B, Lee AP, Ravi V, Maurya AK, Lian MM, Swann JB, Ohta Y, Flajnik MF, Sutoh Y, Kasahara M, Hoon S, Gangu V, Roy SW, Irimiya M, Korzh V, Kondrychyn I, Lim ZW, Tay BH, Tohari S, Kong KW, Ho S, Lorente-Galdos B, Quilez J, Marques-Bonet T, Raney BJ, Ingham PW, Tay A, Hillier LW, Minx P, Boehm T, Wilson RK, Brenner S, Warren WC. Elephant shark genome provides

unique insights into gnathostome evolution. *Nature* 505: 174-179, 2014.

Venkatesh B, Tay A, Dandona N, Patil JG, Brenner S. A compact cartilaginous fish model genome. *Curr Biol* 15:R82-R83, 2005.

Walsh PJ, Smith CP. Urea transport. In: *Nitrogen Excretion*, edited by Wright PA, Anderson PM. Academic Press, San Diego/ London, pp.279-307, 2001.

Wang CY, Shi JD, Yang P, Kumar PG, Li QZ, Run QG, Su YC, Scott HS, Kao KJ, She JX. Molecular cloning and characterization of a novel gene family of four ancient conserved domain proteins (ACDP). *Gene* 306:37-44, 2003.

Wang CY, Yang P, Shi JD, Purohit S, Guo D, An H, Gu JG, Ling J, Dong Z, She JX. Molecular cloning and characterization of the mouse Acdp gene family. *BMC Genomics* 5:7, 2004.

Wang Z, Wang T, Petrovic S, Tuo B, Riederer B, Barone S, Lorenz JN, Seidler U, Aronson PS, Soleimani M. Renal and intestinal transport defects in Slc26a6-null mice. *Am J Physiol Cell Physiol* 288: C957-C965, 2005.

Watanabe T, Takei Y. Molecular physiology and functional morphology of SO_4^{2-} xcretion by the kidney of seawater-adapted eels. *J Exp Biol* 214:1783-1790, 2011.

Wood CM, Matsuo AY, Gonzalez RJ, Wilson RW, Patrick ML, Val AL. Mechanisms of ion transport in Potamotrygon, a stenohaline freshwater elasmobranch native to the ion-poor blackwaters of the Rio Negro. *J Exp Biol* 205:3039-3054, 2002.

Wood CM, Pärt P, Wright PA. Ammonia and urea metabolism in relation to gill function and acid–base balance in a marine elasmobranch, the spiny dogfish (*Squalus acanthias*). *J Exp Biol* 198:1545-1558, 1995.

Xie Q, Welch R, Mercado A, Romero MF, Mount DB. Molecular characterization of he murine Slc26a6 anion exchanger: functional comparison with Slc26a1. *Am J hysiol Renal Physiol* 283:F826-F838, 2002.

Yamaguchi Y, Takaki S, Hyodo S. Subcellular distribution of urea transporter in the ollecting tubule of shark kidney is dependent on environmental salinity. *J Exp Zool*

11A:705-718, 2009.

Yukutake Y, Tsuji S, Hirano Y, Adachi T, Takahashi T, Fujihara K, Agre P, Yasui M, Suematsu M. Mercury chloride decreases the water permeability of quaporin-4-reconstituted proteoliposomes. *Biol Cell* 100:355-363, 2008.

Zardoya R, Villalba S. A phylogenetic framework for the aquaporin family in eukaryotes. *J Mol Evol* 52:391-404, 2001.